NASA Supercritical Airfoils

A Matrix of Family-Related Airfoils

Charles D. Harris
*Langley Research Center
Hampton, Virginia*

Summary

A concerted effort within the National Aeronautics and Space Administration (NASA) during the 1960's and 1970's was directed toward developing practical two-dimensional turbulent airfoils with good transonic behavior while retaining acceptable low-speed characteristics and focused on a concept referred to as the supercritical airfoil. This distinctive airfoil shape, based on the concept of local supersonic flow with isentropic recompression, was characterized by a large leading-edge radius, reduced curvature over the middle region of the upper surface, and substantial aft camber.

This report summarizes the supercritical airfoil development program in a chronological fashion, discusses some of the design guidelines, and presents coordinates of a matrix of family-related supercritical airfoils with thicknesses from 2 to 18 percent and design lift coefficients from 0 to 1.0.

Introduction

A concerted effort within the National Aeronautics and Space Administration (NASA) during the 1960's and 1970's was directed toward developing practical airfoils with two-dimensional transonic turbulent flow and improved drag divergence Mach numbers while retaining acceptable low-speed maximum lift and stall characteristics and focused on a concept referred to as the supercritical airfoil. This distinctive airfoil shape, based on the concept of local supersonic flow with isentropic recompression, was characterized by a large leading-edge radius, reduced curvature over the middle region of the upper surface, and substantial aft camber.

The early phase of this effort was successful in significantly extending drag-rise Mach numbers beyond those of conventional airfoils such as the National Advisory Committee for Aeronautics (NACA) 6-series airfoils. These early supercritical airfoils (denoted by the SC(phase 1) prefix), however, experienced a gradual increase in drag at Mach numbers just preceding drag divergence (referred to as drag creep). This gradual buildup of drag was largely associated with an intermediate off-design second velocity peak (an acceleration of the flow over the rear upper-surface portion of the airfoil just before the final recompression at the trailing edge) and relatively weak shock waves above the upper surface.

Improvements to these early, phase 1 airfoils resulted in airfoils with significantly reduced drag creep characteristics. These early, phase 1 airfoils and the improved phase 1 airfoils were developed before adequate theoretical analysis codes were available and resulted from iterative contour modifications during wind-tunnel testing. The process consisted of evaluating experimental pressure distributions at design and off-design conditions and physically altering the airfoil profiles to yield the best drag characteristics over a range of experimental test conditions.

The insight gained and the design guidelines that were recognized during these early phase 1 investigations, together with transonic, viscous, airfoil analysis codes developed during the same time period, resulted in the design of a matrix of family-related supercritical airfoils (denoted by the SC(phase 2) prefix).

The purpose of this report is to summarize the background of the NASA supercritical airfoil development, to discuss some of the airfoil design guidelines, and to present coordinates of a matrix of family-related supercritical airfoils with thicknesses from 2 to 18 percent and design lift coefficients from 0 to 1.0. Much of the discussion pertaining to the fundamental design concepts is taken from reference 1 and unpublished lectures on supercritical technology presented by Richard T. Whitcomb in 1970. Information on the development of supercritical airfoils and earlier publications were originally classified confidential but have since been declassified. Reference 2 discusses potential benefits of applying supercritical airfoil technology to various types of aircraft and flight programs to demonstrate such applications. Table I indicates some of the major milestones in the development of supercritical airfoils.

The high maximum lift and docile stall behavior observed on thick supercritical airfoils generated an interest in developing advanced airfoils for low-speed general aviation application. Starting in the early 1970's, several such airfoils were developed. Emphasis was placed on designing turbulent airfoils with low cruise drag, high climb lift-to-drag ratios, high maximum lift, and predictable, docile stall characteristics.

During the mid 1970's, several medium-speed airfoils were developed that were intended to fill the gap between the low-speed airfoils and the supercritical airfoils for application on light executive-type airplanes. These airfoils provided higher cruise Mach numbers than the low-speed airfoils while retaining good high-lift, low-speed characteristics.

References 3 to 12 document the research effort on NASA low- and medium-speed airfoils.

Symbols

C_p pressure coefficient, $\dfrac{p - p_\infty}{q_\infty}$

$C_{p,\text{sonic}}$ pressure coefficient corresponding to local Mach number of 1.0

c	airfoil chord, distance along reference line from leading edge to trailing edge
c_d	section drag coefficient
c_l	section lift coefficient
c_m	section pitching-moment coefficient about the quarter chord
c_n	section normal-force coefficient
K	curvature of airfoil surfaces, d^2y/dx^2
M	free-stream Mach number
m	slope of airfoil surface, dy/dx
p	pressure, psf
q	dynamic pressure, psf
R_c	Reynolds number based on free-stream conditions and airfoil chord
SC	supercritical
TE	trailing edge
t/c	thickness-to-chord ratio
x	distance along airfoil reference line measured from leading edge
y	distance normal to airfoil reference line
α	angle of attack

Subscripts:

DD	drag divergence
l	lower surface
u	upper surface
∞	free-stream conditions

Airfoil designation:

The airfoil designation is in the form SC(2)-0710, where SC(2) indicates supercritical (phase 2). The next two digits designate the airfoil design lift coefficient in tenths (0.7), and the last two digits designate the airfoil maximum thickness in percent chord (10 percent).

SC(1)-0710   supercritical (phase 1)—0.7 design lift coefficient, 10 percent thick

SC(2)-0710   supercritical (phase 2)—0.7 design lift coefficient, 10 percent thick

SC(3)-0710   supercritical (phase 3)—0.7 design lift coefficient, 10 percent thick

Development of Supercritical Airfoils

Slotted Supercritical Airfoil

In the early 1960's, Richard T. Whitcomb of the Langley Research Center proposed, on the basis of intuitive reasoning and substantiating experimentation, an airfoil shape (fig. 1) with supersonic flow over a major portion of the upper surface and subsonic drag rise well beyond the critical Mach number (ref. 13). The airfoil had a slot between the upper and lower surfaces near the three-quarter chord to energize the boundary layer and delay separation on both surfaces. It incorporated negative camber ahead of the slot with substantial positive camber rearward of the slot. Wind-tunnel results obtained for two-dimensional models of a 13.5-percent-thick airfoil of the slotted shape and a NACA 64A-series airfoil of the same thickness ratio indicated that for a design-section normal-force coefficient of 0.65 the slotted airfoil had a drag-rise Mach number of 0.79 compared with a drag-rise Mach number of 0.67 for the 64A-series airfoil. The drag at a Mach number just less than that of drag rise for the slotted airfoil was due almost entirely to skin friction losses and was approximately 10 percent greater than that for the 64A-series airfoil. The slotted airfoil shape also significantly increased the stall normal-force coefficient at high subsonic speeds. The pitching-moment coefficients for the slotted shape were substantially more negative than those for more conventional airfoils. The rationale leading to the slotted shape was discussed in reference 13. Because the slotted airfoil was designed to operate efficiently at Mach numbers above the "critical" Mach number (the free-stream Mach number at which local sonic velocities develop) with an extensive region of supersonic flow on the upper surface, it was referred to as the "supercritical airfoil." Reference 14 indicated that the gains obtained for this two-dimensional slotted airfoil shape were also realized for a three-dimensional swept wing configuration that incorporated the airfoil shape.

Integral Supercritical Airfoil

It was recognized that the presence of a slot increased skin friction drag and structural complications. Furthermore, both two-dimensional and three-dimensional investigations of the slotted airfoil indicated that the shape of the lower surface just ahead of the slot itself was extremely critical and required very close dimensional tolerances.

Because of these disadvantages, an unslotted or integral supercritical airfoil (fig. 1) was developed in the mid 1960's. The results of the first work on the integral airfoil were given limited distribution in 1967 in a confidential Langley working paper. This paper was later declassified and formed the basis for much of the review of NASA supercritical airfoils presented in reference 1. Except for the elimination of the slot, the general shape of this integral airfoil was similar to that of the slotted airfoil. Proper shaping of the pressure distributions was utilized to control boundary-layer separation rather than a transfer of stream energy from the lower to upper surface through a slot. The maximum thickness-to-chord ratio for the integral supercritical airfoil was 0.11 rather than 0.135 as used for the slotted airfoil. Theoretical boundary-layer calculations indicated that the flow on the lower surface of an integral airfoil with the greater thickness ratio of the slotted airfoil would have separated because of the relatively high adverse pressure gradients at the point of curvature reversal.

The experimental results shown in figure 2 indicated that for a normal-force coefficient of 0.65 the drag-rise Mach number for the integral airfoil was slightly higher than that for the slotted airfoil of reference 13. However, a simplified analysis indicated that the drag rise for a slotted airfoil with the same thickness ratio of the integral airfoil would be roughly 0.81. A rule of thumb is that, all else being equal, there is approximately 0.01 change in drag-rise Mach number for every 0.01 change in thickness ratio. Thus, the integral airfoil was somewhat less effective than the slotted airfoil in delaying drag rise.

For reference, the drag-rise characteristics for a NACA 64_1-212 airfoil, obtained from reference 15, are also presented in figure 2. A comparison of the thickness distribution for this 6-series airfoil with that for the supercritical airfoil suggested that the 11-percent-thick supercritical airfoil was approximately structurally equivalent to the 12-percent-thick 6-series airfoil. Compared with this 6-series airfoil, the integral supercritical airfoil delayed the drag-rise Mach number by an increment somewhat greater than 0.1.

Note the dip in drag coefficient at $M = 0.79$ for the slotted airfoil. There has been much discussion over the years as to whether it is possible to isentropically decelerate a supersonic flow to a subsonic flow without creating a shock wave. At this particular point, the shock wave almost disappeared. There was only a very small glimmer of a wave in schlieren pictures and there did not appear to be much wave energy loss in the wake drag measurements behind the model. It was, for all practical purposes, a shock-free condition. Even though the ideal of a shock-free flow had been accomplished, it was decided that since aircraft must be efficient over a range of operating conditions, a shock-free point-design flow was impractical. It was believed that it was more important to design airfoils that had the lowest possible level of drag up to the cruise point without the shock-free drag dip. The low-speed drag for the integral airfoil was about the same level as for the more conventional 6-series airfoil because the added skin friction of the second component of the slotted airfoil had been eliminated. There was a gradual rise in drag due to wave losses and finally an abrupt rise when the flow finally separated, but no attempt was made to achieve a shock-free condition.

The integral supercritical airfoil also provided a substantial increase in the Mach number and normal-force coefficient at which boundary-layer separation occurred compared with that for the conventional NACA 6-series airfoil of similar thickness (fig. 3). The separation boundary in figure 3 is sometimes called a buffet boundary. In this case, it represents a force boundary, that is, the boundary where the flow over the whole airfoil deteriorated rapidly. Beyond this line, the airfoil experienced large drag increases. The boundary for the 6-series airfoil, indicating a gradual decrease with increasing Mach number, is typical of conventional airfoils. For the supercritical airfoil, the boundary is pushed well out in both Mach number and normal force. This is extremely important for maneuvering aircraft.

In addition, pitching-moment coefficients for the integral supercritical airfoil were reduced compared with the slotted airfoil (fig. 4). It should be noted, however, that the relatively large pitching moments on supercritical airfoils are not as penalizing in their application to swept wings as commonly thought. Tests of three-dimensional aircraft configurations incorporating the supercritical airfoil (ref. 16) have indicated that the optimum twist for supercritical wings designed for higher speeds is greater than for lower speed designs. As the design Mach number approaches 1.0, the magnitude of the optimum twist increases. This large amount of twist substantially reduces or eliminates the trim penalty associated with the greater negative pitching moment for the supercritical airfoil.

A more recent comparison (ref. 17) of the trim drag measurements for a wide-body transonic model with conventional and supercritical wings at a Mach number of 0.82 indicated that the trim drag for the supercritical wing configuration was not significantly higher than that for the conventional wide-body configuration.

The contours of the integral airfoil were such that it could be defined by several equations empirically

fitted to various regions of the airfoil. Since the supercritical airfoil concepts were still in the development stage, however, these equations were never published.

General Design Philosophy

This section discusses the concepts and reasoning at this point in the development of supercritical airfoils that were incorporated into the integral supercritical airfoil.

A comparison of supercritical flow phenomena for a conventional airfoil and the NASA supercritical airfoil is shown in figure 5. As an airfoil approaches the speed of sound, the velocities on the upper surface become supersonic because of the accelerated flow over the upper surface, and there is a local field of supersonic flow extending vertically from the airfoil and immersed in the general subsonic field. On conventional airfoils this pocket of accelerating supersonic flow is terminated near midchord by a more or less pronounced shock wave with attendant wave losses. This shock wave is followed immediately by a decelerating flow to the trailing edge. The pressure rise through the shock wave may, when superimposed on the adverse pressure gradient at the trailing edge, cause separation of the boundary layer with further increases in drag as well as buffeting and stability problems.

The surface pressure distribution and flow field shown at the bottom of figure 5 are representative of those obtained for NASA supercritical airfoils. The upper-surface pressure and related velocity distributions are characterized by a shock location significantly aft of the midchord, an approximately uniform supersonic velocity from about 5 percent chord to the shock, a plateau in the pressure distribution downstream of the shock, a relatively steep pressure recovery on the extreme rearward region, and a trailing-edge pressure slightly more positive than ambient pressure. The lower surface has roughly constant negative pressure coefficients corresponding to subcritical velocities over the forward region and a rapid increase in pressure rearward of the midchord to a substantially positive pressure forward of the trailing edge.

The elimination of the flow acceleration on the upper surface ahead of the shock wave results primarily from reduced curvature over the midchord region of the supercritical airfoil and provides a reduction of the Mach number ahead of the shock for a given lift coefficient with a resulting decrease of the shock strength. The strength and extent of the shock at the design condition could be reduced below that of the pressure distribution shown by shaping the airfoil to provide a gradual deceleration of the supersonic flow

from near the leading edge to the shock wave. The extensive experiments up to this point indicated that the shape associated with the design point pressure distribution shown in figure 5 provided acceptable drag values over a wide Mach number and lift coefficient range.

Figure 6 shows a schematic of what happens in the supersonic flow field above the upper surface of the supercritical airfoil to yield a very weak shock wave and in some cases to eliminate the shock. As mentioned earlier, the local supersonic field is immersed in a subsonic field, and the division between the two fields is called the sonic line. The airfoil produces expansion waves, or waves that tend to reduce pressure and increase velocity starting near the leading edge. If the flow field were a purely supersonic flow, there would be a continual expansion or acceleration of the flow from leading edge to trailing edge. There is actually an infinite series of expansions that move out of this supersonic field, but the effect is illustrated schematically for a single expansion shown as a dashed line. These lines are called characteristic lines. When the flow is mixed, the expansion waves that emanate from the leading edge are reflected back from the sonic line as compression waves that propagate back through the supersonic field to the airfoil surface. Up to this point of contact, all the expansion waves have been accelerating the flow, but as soon as the compression waves get back to the surface, they start to decelerate the flow. These compression waves are then reflected off the solid airfoil surface as more compression waves. So, there are sets of competing waves or disturbances working in the flow that are the key to obtaining good transonic characteristics for airfoils. The idea is to design the shape of the airfoil just right so that these compression or decelerating disturbances tend to balance out the accelerating ones to get an airfoil that has a flat top pressure distribution even though there is continuous curvature over the upper surface. Two primary factors influence the balancing of these expansion and compression waves: the leading edge and the surface over the forward and midchord regions. First, there need to be strong expansions from the leading-edge region so they can be reflected back as compression waves—thus the large leading radius characteristic of supercritical airfoils. The leading edge is substantially larger than for previous airfoils and is more than twice that for a 6-series airfoil of the same thickness-to-chord ratio. Second, the curvature over the midchord region must be kept fairly small so that there is not a very large amount of accelerations being emanated that must be overcome by the reflected compression waves—thus the flattened upper-surface characteristic of supercritical airfoils.

4

Isentropic recompression is thus encouraged and at design conditions an extensive chordwise region of generally constant supersonic flow is maintained over the upper surface and terminated with a very weak shock wave. As noted in reference 18, these two concepts are consistent with the work done by Pearcey (ref. 19) when he demonstrated that the essential geometric feature of sections designed to exploit the isentropic compression due to waves reflected from the sonic line is an abrupt change on the upper surface from the relatively high curvature of the leading edge to a relatively low curvature downstream and that this can be provided with a large leading-edge radius.

Pressure distributions measured on the 11-percent-thick integral airfoil provide a general indication of the flow phenomena associated with NASA supercritical airfoils at design, subcritical, intermediate off-design, and high-lift conditions (fig. 7).

Figure 7(a) shows the nearest experimental pressure distribution to design conditions at a Mach number slightly above the design value. The shock wave location is rearward of that for the design condition with a small acceleration ahead of the shock. This causes a slight increase in shock losses but does not result in boundary-layer separation. Separation would occur when the shock wave moves farther rearward and the pressure plateau is eliminated.

The flow is a little more complex over the aft part of the airfoil. One of the important features of the supercritical airfoil is to keep the flow just behind the shock wave moving at close to the speed of sound (fig. 5). The plateau in the pressure distribution tends to control the forward movement of disturbances associated with the decelerating flow near the trailing edge of the airfoil. This prevents the disturbances from moving forward near the surface and causing the flow to converge into the usual shock wave. However, since the flow at a moderate distance above the surface is subsonic, the disturbances can move forward and downward into the supersonic region to decelerate the flow leading into the shock wave. The combination of these effects significantly reduces the extent and strength of the shock wave. In fact it was a key factor in obtaining the shock-free design condition described in reference 13 for the slotted airfoil.

The pressure plateau behind the shock wave is also necessary to stabilize the boundary layer. When the boundary layer moves through the pressure drop at the shock, it decelerates more than the stream flow because it does not have as much momentum as the stream. If the pressure gradient behind the shock wave is too great, the boundary-layer flow will reverse and result in separated flow. The problem is how to keep the boundary-layer flow from reversing. If the boundary layer has to go through a continuous adverse pressure gradient from ahead of the shock to the trailing edge, boundary-layer theory indicates that it will separate. However, the plateau in the pressure distribution rearward of the shock wave allows a reenergization of the boundary layer by mixing between the shock and the final pressure rise at the trailing edge. As a result, the boundary layer can move through a greater total pressure rise without separating.

Considering another part of the boundary-layer story, the pressure coefficient at the trailing edge on a conventional airfoil is fairly positive. Theoretically it recovers to stagnation pressure, but in reality, because it is impossible for the boundary layer to reach stagnation conditions, it separates locally and the pressure rise is less. On the supercritical airfoil, the intent was to keep the boundary layer attached while it underwent the total pressure rise through the shock wave and the trailing-edge recovery. If the pressures had to rise from the level ahead of the shock to the usual positive pressures at the trailing edge, boundary-layer theory indicates that it would separate even though there is a plateau. Therefore, the supercritical airfoil was designed so that the pressure coefficient at the trailing edge was only slightly positive by making the slope of the lower surface equal to that of the upper surface at the trailing edge. This results in the airfoil having a very sharp and thin trailing edge. The importance of this effect is shown by the experimental data in figure 7(a). The near-ambient pressure at the trailing edge, which results from the small included angle of the trailing edge, reduces to a minimum the total pressure rise the upper-surface boundary layer must traverse and thus minimizes the tendency toward separation.

Turning now to the lower surface, it has been mentioned before that lift is produced by the aft lower-surface cusp, resulting in the type of aft-loaded pressure distribution shown in figure 7(a). There is a severe pressure rise near two-thirds chord to substantially positive pressures in the cusp region. Again referring to boundary-layer theory, boundary layers going into such positive pressures tend to separate much more readily than when going into a pressure rise from less than stream pressure to stream pressure, so that a pressure rise on the lower surface greater than that on the upper surface cannot be tolerated. Therefore, it is important that the velocities on the forward region of the lower surface do not go supersonic. As soon as the flow there goes supersonic, a shock wave pressure rise is superimposed on the pronounced pressure rise leading into the cusp, which increases the tendency for the boundary layer to

separate. In fact, experiments were conducted where the flow on the lower surface went supersonic, and for such cases, the flow did separate.

Attention was also paid to the shape of the pressure rise into the lower-surface cusp as defined by the Stratford criteria of reference 20. There is initially an abrupt rise or steep positive gradient followed by a gradually decreasing gradient into the cusp. This in effect forces the boundary layer right up to the point of separation and then eases off by reducing the rate of pressure rise. In theory, at this point there is zero shear or skin friction, although no decrease in drag that would be associated with this supposedly zero shear was ever measured during supercritical airfoil testing.

In figure 7(b), a subcritical pressure distribution is shown for the same angle of attack. The pressure distribution has a negative peak near the leading edge, followed by a gradual increase in pressure. It is important to keep this peak from becoming so high that the flow will separate. By keeping the velocities down in the middle region (region of low surface curvature) while accelerating the flow over the rear region (region of high surface curvature), the pressure distribution over the mid upper surface is quite flat and has a low level. The lower surface is the same as at supercritical speeds because the lower surface even for the supercritical case is still subcritical.

In figure 7(c), a pressure distribution is shown for an intermediate condition between the design and subcritical points at a Mach number just below the design value. Notice that the front part of the pressure distribution looks quite similar to that of the design point, fairly flat, but the shock location is significantly farther forward than for the design condition. Behind the shock wave the flow experiences a reacceleration because of the increased curvature of the rear part of the airfoil resulting in a second supersonic peak near three-quarter chord. When attempting to design for a minimum shock strength condition, the rearward curvature had to be increased and, as a result, the reacceleration velocity at the intermediate conditions could be sufficiently great to cause a second shock wave. The total pressure rise through this second shock and the immediately following trailing-edge pressure recovery may cause significant boundary-layer separation near the trailing edge.

The pressure distribution shown in figure 7(d) is that measured at the high-lift corner of the variation of normal force with Mach number for separation onset, shown previously in figure 3. The shock wave, associated with a local upstream Mach number of 1.4, causes a very large adverse pressure gradient. However, the trailing-edge pressure recovery and a surface oil flow visualization study indicated that the boundary layer did not completely separate. The bulge in the pressure distribution aft of the shock wave and the surface oil study indicated a very large separation bubble under the shock with flow reattachment near three-quarter chord. For conventional airfoil shapes, the presence of a shock wave associated with an upstream Mach number of 1.4 would cause very severe boundary-layer separation. The key to the greater stability of the boundary layer for the supercritical airfoil was the plateau in the pressure distribution aft of the shock described above. For conventional airfoils, the pressure immediately downstream of the shock wave continues to increase and the higher pressure behind the bubble tends to force the bubble away from the surface. With the plateau on the supercritical airfoil, this adverse effect is eliminated.

Effects of Trailing-Edge Thickness

The design philosophy of the supercritical airfoil required that the trailing-edge slopes of the upper and lower surfaces be equal. This requirement served to retard flow separation by reducing the pressure-recovery gradient on the upper surface so that the pressure coefficients recovered to only slightly positive values at the trailing edge. For an airfoil with a sharp trailing edge, as was the case for early supercritical airfoils, such restrictions resulted in the airfoil being structurally thin over the aft region.

Because of structural problems associated with sharp trailing edges and the potential aerodynamic advantages of thickened trailing edges for transonic airfoils (discussed, for example, in ref. 18), an exploratory investigation was made during the early development phases of the supercritical airfoil to determine the effects on the aerodynamic characteristics of thickening the trailing edge (fig. 8). Figure 9 shows that increasing the trailing-edge thickness of an interim 11-percent-thick supercritical airfoil from 0 to 1.0 percent of the chord resulted in a significant decrease in wave drag at transonic Mach numbers; however, this decrease was achieved at the expense of higher drag at subcritical Mach numbers. Various numbering systems were used during the development of the supercritical airfoils. The 11-percent-thick airfoil with 0-percent-thick trailing edge was referred to as airfoil 4, and the 11-percent-thick airfoil with the 1-percent-thick blunt trailing edge was referred to as airfoil 5. These airfoil numbers had no special meaning with respect to airfoil characteristics but were simply configuration numbers used for identification purposes. Figure 1 summarizes the progression of supercritical airfoil shapes to this point.

Advantages of thick trailing edges at transonic Mach numbers were real and significant, but practical

application appeared to depend on whether the drag penalty at subcritical Mach numbers could be reduced or eliminated. Two questions naturally arose: what would the optimum trailing-edge thickness be for supercritical airfoils, and could the drag penalty at the subcritical Mach numbers due to the thickened trailing edge be reduced by proper shaping of the trailing edge?

In order to investigate more comprehensively the effects of trailing-edge geometry, a refined 10-percent-thick supercritical airfoil was modified (circa 1970) to permit variations in trailing-edge thickness from 0 to 1.5 percent of the chord and inclusion of a cavity in the trailing edge (fig. 10). The refined 10-percent-thick airfoil with the 1-percent-thick blunt trailing edge was identified as airfoil 9, the 1-percent-thick trailing edge with cavity as airfoil 9a, the 1.5-percent-thick trailing edge with cavity as airfoil 10, and the 0.7-percent-thick trailing edge with cavity as airfoil 11. The results, discussed in reference 21 and summarized in figures 11 and 12, suggested several general conclusions: (1) increasing trailing-edge thickness yielded reductions in transonic drag levels with no apparent penalty at subcritical Mach numbers up to a trailing-edge thickness of about 0.7 percent, (2) increases in both subsonic and transonic drag levels appeared with increases in trailing-edge thickness beyond approximately 0.7 percent, (3) small drag reductions through the Mach number range resulted when the 1.0-percent-thick trailing edge was modified to include a cavity in the trailing edge, (4) there appeared to exist some relationship between the optimum airfoil trailing-edge thickness and the boundary-layer displacement thickness over the upper surface of the airfoil (reversal of the favorable effect of increasing trailing-edge thickness appeared to occur when the airfoil trailing-edge thickness exceeded the displacement thickness of the upper-surface boundary layer at the trailing edge), and (5) the general design criterion to realize the full aerodynamic advantage of trailing-edge thickness appeared to be such that the pressure coefficients over the upper surface of the airfoil recover to approximately zero at the trailing edge with the trailing-edge thickness equal to or slightly less than the local upper-surface boundary-layer displacement thickness. The experimental results for airfoil 9a were included in the AGARD experimental data base of reference 22 for computer program assessment.

As a consequence of this investigation, most subsequent experimental development of supercritical airfoils was carried out with cusped trailing edges about 0.7 percent thick. Much later in the supercritical airfoil development program, when the available

ability of analytical codes (discussed in later sections) made it easier to explore variations in trailing-edge geometry, the optimum trailing-edge thickness was found to vary with the maximum thickness of the airfoil and to be somewhat less than 0.7 percent.

Effects of Maximum Thickness

In order to provide a source of systematic experimental data for the early supercritical airfoils, the 11-percent-thick airfoil 5 and the 10-percent-thick airfoil 9 were reported in more detail in reference 23 to compare the aerodynamic characteristics of two airfoils of different maximum thicknesses. As noted above, the trailing edges of both airfoils were blunt and 1 percent thick. Although maximum thickness was the primary variable, dissimilarities between the two airfoils prevented a comparison based on pure thickness. However, general observations concerning the results were made. For the thinner airfoil, the onset of trailing-edge separation began at an approximately 0.1 higher normal-force coefficient at the higher test Mach numbers, and the drag divergence Mach number at a normal-force coefficient of 0.7 was 0.01 higher. Both effects were associated with lower induced velocities over the thinner airfoil.

Effects of Aft Upper-Surface Curvature

The dissimilarities between the 11-percent-thick airfoil 5 and the 10-percent-thick airfoil 9 were in the contours of the rear upper surface. As discussed earlier, the rear upper surface of the supercritical airfoil is shaped to accelerate the flow following the shock wave in order to produce a near-sonic plateau at design conditions. Near the design normal-force coefficient, at intermediate supercritical conditions between the onset of supersonic flow and the design point, the upper-surface shock wave is forward and the rear upper-surface contour necessary to produce the near-sonic plateau at design conditions causes the flow to expand into a second region of supercritical flow in the vicinity of three-quarter chord. Care must be exercised that this second region of supercritical flow is not permitted to expand to such an extent that a second shock wave is formed, which would tend to separate the flow over the rear portion of the airfoil. As part of the systematic wind-tunnel development of the supercritical airfoil, modifications over the rear upper surface of supercritical airfoil 5 were made to evaluate the effect of the magnitude of the off-design second velocity peak on the design point. Surface slopes over the rear upper surface of airfoil 5 were modified as shown in figure 13, and the resultant airfoil was designated as airfoil 6. The modification was accomplished by removing material

over approximately the rear 60 percent of the upper surface without changing the trailing-edge thickness and resulted in an increase in surface curvature around midchord and a decrease in surface curvature over approximately the rearmost 30 percent of the airfoil. (For small values of slope, curvature may be approximated by dm/dx, which is the second derivative of the surface contour d^2y/dx^2.) The evaluation is documented in reference 24.

The results indicated that attempts to reduce the magnitude of the second velocity peak at intermediate off-design conditions in that particular manner had an adverse effect on drag at design conditions. The results suggested, however, that in order to avoid drag penalties associated with the development of the second velocity peak into a second shock system on the upper surface at intermediate off-design conditions, the magnitude of the second peak should be less than that of the leading-edge peak.

Wave losses are approximately proportional to the local Mach number entering the shock and can be minimized by maintaining a region of low curvature and thereby reducing local velocities ahead of the shock. The broad region of relatively low, nearly uniform, upper-surface curvature on the supercritical airfoil extends from slightly rearward of the leading edge to about 70 or 75 percent chord. Reference 25 describes the results of extending this region of low curvature nearer to the trailing edge in an attempt to achieve a more rearward location of the upper-surface shock wave without rapid increases in wave losses and associated separation, thus delaying the drag divergence Mach number at a particular normal-force coefficient or delaying the drag break for a particular Mach number to a higher normal-force coefficient. Extending this low curvature region too near the trailing edge, however, forces a region of relatively high curvature in the vicinity of the trailing edge with increased trailing-edge slope. This high curvature would be expected to produce a more adverse pressure gradient at the trailing edge, where the boundary layer is most sensitive, and would result in a greater tendency toward trailing-edge separation. The degree and chordwise extent of low curvature therefore strongly influences both the strength of the shock wave and the onset of trailing-edge separation, the two principal causes of drag divergence. The results indicated that although simply extending the region of low curvature farther than on earlier supercritical airfoils provided a modest improvement in drag divergence Mach number, it had an unacceptably adverse effect on drag at lower Mach numbers.

An Improved Supercritical Airfoil

During the early development of the two-dimensional supercritical airfoil, emphasis was placed upon developing an airfoil with the highest drag-divergence Mach number attainable at a normal-force coefficient of about 0.7. The normal-force coefficient of 0.7 was chosen as the design goal since, when account was taken of the effects of sweep, it was representative of lift coefficients at which advanced technology near-sonic transports utilizing the supercritical airfoil concept were then expected to cruise.

The resultant airfoil, identified as supercritical airfoil 11, with a ratio of maximum thickness to chord of 0.10 and a ratio of trailing-edge thickness to chord of 0.007, had a drag divergence Mach number of about 0.79 and was reported in reference 21. This airfoil experienced, however, a "creep" or gradual increase in the drag coefficient of about 14 counts (c_d increment of 0.0014) between the subcritical Mach number of 0.60 and the drag divergence Mach number at the design normal-force coefficient. This gradual buildup of drag was largely associated with an intermediate off-design second velocity peak and relatively weak shock waves above the upper surface at these speeds. It was believed that with proper shape refinements, the drag creep could be reduced or eliminated.

Following the development of airfoil 11, design studies of advanced technology transport configurations suggested that cruise Mach number requirements would be somewhat lower than originally anticipated, thereby reducing wing sweep and lift coefficient. Consequently, the design lift coefficient at which the supercritical airfoil was being developed was lowered to about 0.55. The wind-tunnel tests (circa 1972) required for airfoil optimization at the lower normal-force coefficient also provided the opportunity to explore the drag creep problem, thus drag creep was included as a goal and an important factor in the wind-tunnel program. The result (ref. 26) was an airfoil, identified as airfoil 26a, with a slightly smaller leading-edge radius, reduced curvature over the forward and rear upper surface, reduced aft camber, and minor changes over the lower surface. Until this point in the supercritical airfoil development program, the airfoils could more or less still be defined by several empirical equations. In the process of developing airfoil 26a, attempts were made to retain the capability of being able to describe the airfoils with geometric functions, but such efforts were not successful. Airfoil 26a and subsequent airfoils were not, therefore, mathematically described.

Such refinements in the airfoil shape produced improvements in the overall drag characteristics at

normal-force coefficients from about 0.30 to 0.65 compared with earlier supercritical airfoils developed for a normal-force coefficient of 0.70. The drag divergence Mach number of the improved supercritical airfoil 26a varied from approximately 0.82 at a normal-force coefficient of 0.30 to 0.78 at a normal-force coefficient of 0.80 with no drag creep evident up to normal-force coefficients of about 0.65. As discussed in reference 26, these improved drag creep characteristics were largely attributed to a more favorable flow recompression over the forward upper surface and the elimination of a region of overexpansion near three-quarter chord.

Effects of Aft Camber

During the development of the improved 10-percent-thick airfoil 26a, a number of systematic contour modifications were evaluated. These individual modifications were intermediate steps toward a definite design goal but may be organized into small groups of related contour variations. One such grouping showed the effects of variations in surface slope and curvature distributions over the rear portion of the airfoil. Although not approached from the standpoint of camber effects per se, the variations of surface slope and curvature distributions resulted in airfoils with different aft camber and, for convenience, were referred to in this manner. Reference 27 documents the aerodynamic characteristics of these airfoils with different aft camber.

Supercritical Airfoil 31

Emphasis on fuel economy during the early 1970's generated considerable interest in fuel-conserving aircraft envisioned to cruise at Mach numbers near those of then current transports. Such an aircraft could utilize supercritical airfoil technology to achieve weight and drag reductions by permitting the use of thicker wings with higher aspect ratios and less sweep. Because wings with higher aspect ratios would require airfoils with design lift coefficients higher than 0.55, airfoil improvements again centered around developing an airfoil with a design normal-force coefficient of about 0.70 without incurring the troublesome drag creep problem of the earlier airfoil 11.

In order to apply the drag creep improvements incorporated into airfoil 26a, it was used as the starting point in extending the design normal-force coefficient to 0.70. Initially, the location of maximum upper-surface thickness above the reference line was moved forward from $0.40c$ to $0.38c$, and the rear of the airfoil (both upper and lower surfaces) was displaced downward by an amount that varied from $0.0c$ at the new

position of maximum thickness to $0.01c$ at the trailing edge, thereby increasing the aft camber. Moving the position of upper-surface maximum thickness forward by $0.02c$ simply compressed the forward upper surface longitudinally and maintained the same general family resemblance to airfoil 26a.

In addition to the aforementioned changes, several experimental modifications were necessary before arriving at the final configuration: airfoil 31 (circa 1974). These modifications consisted of small curvature variations near the upper-surface leading edge to better control the development of supersonic flow in this region and over the forward lower surface to flatten the forward lower-surface pressure distribution. Geometric characteristics of airfoil 31 are shown in figure 14 and compared with those of airfoil 12. Airfoil 12 differs very little from airfoil 11 (ref. 26) and was selected as a basis of comparison because data were available over a wider range of off-design conditions than for airfoil 11.

The results presented in reference 28 and summarized in figure 15 show that airfoil 31 produced significant improvements in the drag characteristics compared with the earlier supercritical airfoil 12 designed for the same normal-force coefficient ($c_n = 0.7$). Drag creep was practically eliminated at normal-force coefficients between 0.4 and 0.7 and greatly reduced at other normal-force coefficients. Substantial reductions in the drag levels preceding drag divergence were also achieved at all normal-force coefficients. The Mach numbers at which drag diverged were delayed for airfoil 31 at normal-force coefficients up to about 0.6 (by approximately 0.01 and 0.02 at normal-force coefficients of 0.4 and 0.6, respectively) but were slightly lower at higher normal-force coefficients. The trade-off between reduced drag levels preceding drag divergence through the range of normal-force coefficients and reduced drag divergence Mach numbers at the higher normal-force coefficients called attention to the compromises that are sometimes necessary in the design of airfoils for practical applications over a wide range of operating conditions.

Supercritical airfoils through number 31 were developed through intuitive contour modifications in the wind tunnel before adequate theoretical design or analysis codes were available and are referred to as phase 1 airfoils. They resulted from an experimentally iterative process of evaluating experimental pressure distributions at design and off-design conditions and physically altering the airfoil profile to yield the best drag characteristics over a range of test conditions. The models were constructed to provide the capability of on-site (mounted in test section) modifications. They consisted of a metal core with

metal leading and trailing edges that were removable to provide leading- and trailing-edge modifications. The upper and lower surfaces between the steel leading and trailing edges were formed with plastic filler material that could be easily reshaped. Changes to the surface contours could be made by adding or removing fill material. Control and measurement of the contours were provided by templates that rode spanwise on the metal leading and trailing edges. When time permitted and contour variations were known ahead of time, sweep templates were constructed to aid in model changes. When experimental data suggested changes during a tunnel entry, short spanwise strips of the model were first modified and smoothed by hand and then a template cast to that shape was made to aid in getting a uniform contour across the remainder of the span. Using such techniques, it was believed that coordinates could be maintained to an experimental accuracy of about $y/c = 0.0001$ ($y = 0.0025$ in. for a 25-in.-chord model). It was not realistic or practical to believe that the models could be modified and measured on site much better than this.

Theoretically Designed Supercritical Airfoil

The successes in achieving virtually shock-free flow in wind-tunnel tests of two-dimensional airfoils, combined with the evolution of advanced technology aircraft, gave impetus to the development of a practical approach to the theoretical design of transonic lifting airfoils with minimum wave losses. One approach was the complex hodograph method for the design of shockless supercritical airfoils reported in reference 29. This mathematical approach was used by P. R. Garabedian of New York University to design an airfoil to be shock free (isentropic recompression) at a Mach number of 0.78, a lift coefficient of 0.59, and with a maximum thickness-to-chord ratio of about 0.10. The aerodynamic characteristics of this airfoil were then measured in the Langley 8-Foot Transonic Pressure Tunnel to evaluate experimentally the validity of the design technique. Reference 30 presents the results of the experiment and compares them with the aerodynamic characteristics of the improved supercritical airfoil 26a, which was experimentally designed for similar design conditions.

Three major conclusions were reached: (1) except for slight degradation at off-design conditions (drag creep and reduced drag divergence Mach numbers at low c_n), the experimental aerodynamic characteristics of the theoretical airfoil compared well with those of the experimentally designed airfoil; (2) undue emphasis on a single-point shockless design goal would more than likely compromise off-design characteristics—a more realistic design goal would be a minimum wave loss design point that would also provide acceptable off-design characteristics; and (3) the complex hodograph design method could be a valuable design tool if used in conjunction with an adequate analysis program to evaluate off-design characteristics.

Theoretical and experimental results of several other airfoils designed by use of the complex hodograph method of reference 29 are reported in references 31 and 32.

Theoretical Drag Calculations

The airfoil analysis code described in reference 29 gained wide acceptance for the prediction of two-dimensional pressure distributions but was based on a nonconservative form (NCF) of the equation for the velocity potential describing transonic flow. As discussed by Garabedian (refs. 33 and 34), however, the NCF method fell short of giving an adequate prediction of drag-rise Mach numbers because of erroneous positive terms in the artificial viscosity. The shock jumps defined by the NCF method created mass instead of conserving it (see, also, ref. 35), resulting in overprediction of the wave drag, especially in the case of large supersonic zones. A correction was made to this "old" analysis code to account for the mass generated by the NCF method, leading to a more satisfactory evaluation of the wave drag. In addition to the corrected wave drag formulation, an accelerated iteration scheme developed by Jameson (ref. 36) was incorporated to reduce computation time. A comparison between experimental drag characteristics and theoretical drag characteristics derived from the improved "new" analysis code for the interim supercritical airfoil 27 is presented in reference 37. Results (representative results shown in fig. 16) indicate that the "new" version of the analysis code provides more accurate predictions of drag rise and suggest a good cookbook method of applying the new code.

General Design Guidelines

During the experimental development of these phase 1 airfoils, design guidelines were recognized that yielded the best compromises in drag characteristics over a range of test conditions.

The first guideline, referred to as the sonic plateau, is that at some incremental normal-force coefficient and Mach number below the design conditions the pressure distribution on the upper and lower surfaces be flat with the upper-surface pressures just below the sonic value. A generalized off-design sonic-plateau pressure distribution on a representative supercritical airfoil is presented in figure 17. The increment in normal-force coefficient was

a function of the design normal-force coefficient and appeared to be about -0.25 to -0.30 for $c_n = 0.70$. The increment in Mach number was just enough to reduce the upper-surface pressures to below sonic velocity. This "sonic plateau" was an off-design condition that was observed to be consistent with the best compromise between design and off-design drag characteristics over a wide range of conditions. Whenever off-design drag characteristics were sacrificed in order to enhance the design drag characteristics, deviation from a flat, sonic plateau was observed. Toward the end of the experimental phase 1 airfoil development effort, judgments as to the suitability of various model modifications were generally made on the basis of two experimental data points—the design condition and the off-design sonic-plateau condition.

On the upper surface the sonic plateau extends from near the leading edge to the start of the aft pressure recovery and on the lower surface from near the leading edge to the recompression region entering into the cusp. The rearward extent of the upper-surface plateau is determined by a second design guideline that requires the gradient of the aft pressure recovery be gradual enough to avoid local separation problems near the trailing edge for lift coefficients and Mach numbers up to the design point. Consequently, the rearward extent of the upper-surface plateau would depend on thickness ratio since the thicker the airfoil, the higher the induced velocities from which the flow must recover and, therefore, the farther forward the aft pressure recovery must begin.

A third design guideline requires that the airfoil have sufficient aft camber so that at design conditions the angle of attack be about zero. This prevents the location of the upper-surface crest (position of zero slope) from being too far forward with the negative pressure coefficients over the midchord acting over a rearward-facing surface. Both experiments and theoretical analyses have indicated that an increase in angle of attack to positive values results in an abrupt increase in wave drag. A generalized design pressure distribution on a representative supercritical airfoil is presented in figure 18.

The aft camber results in a concave region near the trailing edge on the lower surface with positive pressures, producing negative pitching moments and increased hinge moments, while the physical concavity reduces the structural depth of the flap or aileron. As noted in reference 38, however, both experimental and calculated results have indicated that these positive pressures are important in achieving a high drag-rise Mach number. The depth of the concavity must, therefore, be a compromise based on a number of considerations.

A fourth design guideline specifies a gradually decreasing velocity in the supercritical flow region over the upper surface. This usually results in the highest drag-rise Mach number for a given design lift coefficient. Also, the highest usable drag rise or lift coefficient is generally obtained with a weak shock wave at the end of the supercritical region (ref. 38). Permitting a weak shock rather than trying to design for a shock-free design point also reduces the off-design penalties usually associated with "point design" airfoils.

Analytically Designed Supercritical Airfoils

Based on the general design guidelines discussed above, two supercritical airfoils (fig. 19) were designed (circa 1975)—the 10-percent-thick airfoil 33 reported in reference 39 and the 14-percent-thick airfoil reported in reference 40. The design normal-force coefficient was 0.7 for both airfoils. An iterative computational design process was used that consisted of altering the airfoil coordinates until the viscous airfoil analysis program of reference 29 indicated that the aforementioned design criteria had been satisfied. Until this point in the development of supercritical airfoils, design had been totally dependent on experimental methods and was extremely tedious, time consuming, and expensive. The design of these two airfoils by using the numerical code and the experimental verification of the results was intended to demonstrate that airfoils could be reliably designed by computational methods, thus reducing the cost and wind-tunnel time of developing supercritical airfoils.

Figure 20 presents sketches of the experimentally developed airfoil 31 and the analytically designed airfoil 33, and figures 21 and 22 compare the experimental pressure distributions nearest to the off-design sonic-plateau and design conditions for the two airfoils. To obtain airfoil 33, the ordinates of airfoil 31 were modified over the forward upper and lower surfaces, decreased over the rear upper surfaces, and increased in the vicinity of 80 percent chord on the lower surface. Referring to the experimental pressure distributions that approach the off-design sonic-plateau criterion (fig. 21), the alterations over the upper surface and forward lower surface were necessary to obtain the desired plateau pressure distribution and to reduce the upper-surface aft pressure recovery gradient. The ordinates on the rear lower surface were increased, with the maximum increase at 80 percent, to provide increased depth for control surface and flap structural requirements. Subtracting from the upper surface and adding to the lower surface over the aft portion of the airfoil in this manner reduced the aft camber and, therefore, increased the

angle of attack required to achieve a given normal-force coefficient. The modifications also had to assure that the angle-of-attack design guideline had been met, that is, that the angle of attack required for the design normal-force coefficient of 0.7 remain near 0°.

Since the best drag-rise characteristics are often obtained on airfoils with a small amount of upper-surface trailing-edge separation and since theoretical treatments of the flow at trailing-edge regions are generally unreliable, theoretically predicted flow separation at 98 percent chord was accepted during the design process. Attempts to achieve a more rearward location of theoretical separation by reducing the aft pressure recovery gradient would have forced the rear terminus of the sonic plateau forward, resulting in higher induced velocities in the plateau region and a probable reduction in drag-rise Mach number. Relaxing the separation requirements in this manner during the design process proved to be reasonable since the computational results generally overpredicted separation and separation was not observed in the experimental data. The upper-surface sonic plateau extended from approximately 3 to 80 percent chord on the 10-percent-thick airfoil and from approximately 5 to 66 percent chord on the 14-percent-thick airfoil.

The experimental results (refs. 39 and 40) showed that the 10-percent-thick airfoil 33 and the 14-percent-thick airfoil had good drag-rise characteristics over a wide range of normal-force coefficients with no measurable shock losses up to the Mach numbers at which drag divergence occurred for normal-force coefficients up to 0.7. The drag-rise characteristics of the computationally designed, 10-percent-thick airfoil 33 are compared with those of the earlier experimentally designed airfoil 31 in figure 23 and with those of the analytically designed 14-percent-thick airfoil in figure 24.

Reference 41 documents the low-speed characteristics of the 14-percent-thick airfoil obtained in the Langley Low-Turbulence Pressure Tunnel. This airfoil demonstrated excellent low-speed qualities and achieved unflapped $c_{l,max} = 2.22$ at $R_c = 12 \times 10^6$.

Reference 42, which discusses the status of NASA's airfoil research program in 1975, includes information on the status of supercritical airfoils during that time period.

Matrix of Phase 2 Supercritical Airfoils

The experimental verification of the design guidelines or "target pressure distributions" and the success with which two airfoils were designed using computational methods prompted the design of a matrix of family-related airfoils, all based on the guidelines described above and referred to as the supercritical phase 2 airfoils.

Figures 25 and 26 show the matrix of the airfoils that were designed and indicate the various applications to which they may be applied. The solid symbols indicate the airfoils that have been tested. The 10- and 14-percent-thick airfoils, as discussed above, were tested in the Langley 8-Foot Transonic Pressure Tunnel and reported in references 39 and 40. The three 6-percent-thick airfoils were tested in the Langley 6- by 28-Inch Transonic Tunnel. The results of the 6-percent-thick airfoils also verified the analytical design process but are unpublished. Airfoil coordinates, along with sketches of the airfoils, are presented in tables II through XXII. Even though the codes would have permitted definition of coordinates to more decimal places than shown in these tables, it was felt that the development program was still essentially an experimental process, and, except for the thinner airfoils, no attempt was made to define the vertical coordinates to less than $y/c = 0.0001$. Attention is called to the fact that the coordinates are not presented relative to conventional chord lines. To simplify comparisons between supercritical airfoils, it was the custom to present coordinates relative to a common reference line rather than the standard method of defining airfoils relative to a reference chordline connecting the leading and trailing edges.

Design conditions for each airfoil were established by specifying maximum thickness and lift coefficient and letting the Mach number "float" to assume whatever value was required to achieve the generalized design and off-design pressure distributions shown in figures 17 and 18. Figures 27 and 28 show representative off-design sonic-plateau pressure distributions for some of the airfoils and indicate the design lift coefficient and the Mach numbers at which the sonic plateaus occurred. Figure 29 shows the analytical drag divergence Mach numbers and includes the measured drag divergence Mach numbers for the 10- and 14-percent-thick airfoils designed for $c_l = 0.70$ discussed above. Drag divergence Mach number was defined as the point where the slope of the curve of section drag coefficient as a function of Mach number equals 0.1, $dc_d/dM = 0.1$. Figure 30 shows how the leading-edge radius of the airfoils varies with maximum thickness and indicates the variation to be parabolic in nature.

All airfoils were assumed to be fully turbulent during the design process with transition at 3 percent chord. For airfoils less than 6 percent thick, chord Reynolds number was specified to be 10×10^6. For airfoils 6 percent thick or more, chord Reynolds number was specified to be 30×10^6. These Reynolds

numbers were felt to be representative of the probable applications for the airfoils.

If airfoils with thickness ratios intermediate to those presented in tables II to XXII are desired, and changes in thickness ratios are not more than 1 or 2 percent, the ordinates can be linearly scaled or interpolated from these tables without seriously altering the gradients of the theoretical pressure distributions. The two symmetrical airfoils shown in the matrix were developed by wrapping the thickness distribution of the least-cambered airfoil of each thickness ratio around the reference line, filling in the resultant upper and lower rear cusped surfaces so that the surfaces were straight lines from about 65 percent chord to the trailing edge, and making small modifications to the coordinates to make sure that both surfaces satisfied the upper-surface sonic-plateau guideline at zero angle of attack. The 12-percent-thick symmetrical airfoil, SC(2)-0012, was tested at high Reynolds numbers in the Langley 0.3-Meter Transonic Cryogenic Tunnel, and the results were reported in reference 43. The 14-percent-thick airfoil cambered for 0.7 lift coefficient was also tested at high Reynolds numbers and reported in references 44 and 45.

Phase 3 Supercritical Airfoils

There appeared to be some concern that the leading-edge radii of the supercritical airfoils were too large to be compatible with good low-speed characteristics, that the airfoils had nose down pitching moments that were too large, and that there was not enough structural depth over the rear cusp region where flaps would normally be located. After the design of the matrix of phase 2 airfoils was completed, an attempt was made to address these concerns during the late 1970's. The airfoils studied during these investigations were referred to as supercritical phase 3 airfoils.

Studies (using the same iterative computation techniques as used in the design of the phase 2 airfoils) indicated that reductions in pitching moments could be achieved by thickening the airfoil in the vicinity of the rear lower surface and undercutting the forward lower surface without significantly degrading the airfoil performance at design conditions. Undercutting the forward lower surface also resulted in an effectively smaller leading-edge radius.

Figure 31 compares sketches of the original 12-percent-thick phase 2 supercritical airfoil designed for 0.7 lift coefficient and the same airfoil with the forward lower surface undercut. Figure 32 indicates that the upper surface was relatively unaffected at design conditions by this modification. The curvatures over the lower surface where the undercut surface fairs back into the original airfoil are increased, resulting in higher velocities in the midchord region and slightly reduced pitching moments at a more negative angle of attack. Removing material in this manner increases curvature at the ends of the removal area and decreases curvature in the middle of the area and has a "water bed" effect on the velocities: velocities go up in one place but go down somewhere else.

Thickening the aft region of the airfoil by about 9 percent of the original thickness at 80 percent chord (fig. 33) to approximately the same thickness as a NACA 65-series airfoil by filling in the lower-surface cusp also resulted in a small decrease in pitching moment (fig. 34) but required a slightly higher angle of attack to achieve the same lift coefficient. More recent studies (ref. 46, for example) have indicated that substantial thickening of supercritical-type airfoils in the vicinity of 80 percent chord would be possible without sacrificing transonic performance.

In order to evaluate such modifications experimentally, the existing 14-percent-thick model used in the low-speed evaluation of SC(2)-0714 was modified and tested at low speeds in the Langley Low-Turbulence Pressure Tunnel. Figure 35 shows sketches of the two airfoils and figures 36 and 37 compare the theoretical pressure distributions at the design and sonic-plateau conditions. The experimental results (unpublished) indicated that small reductions in leading-edge pressure peaks were achieved with the smaller leading-edge radius but that low-speed stall occurred a couple of degrees earlier and the maximum lift attained decreased from about 2.2 to 2.1. Subsequent tests of the NASA SC(3)-0714 in the Langley 0.3-Meter Transonic Cryogenic Tunnel are reported in references 47 and 48.

The effort to incorporate these phase 3 modifications into the entire matrix of phase 2 supercritical airfoils was abandoned, however, when on the thinner 6-percent-thick airfoils the increased curvature on the lower surfaces caused the lower-surface velocities to become supersonic and depart from the design guidelines that had been established.

Concluding Remarks

A concerted effort within the National Aeronautics and Space Administration (NASA) during the 1960's and 1970's was directed toward developing practical two-dimensional turbulent airfoils with good transonic behavior while retaining acceptable low-speed characteristics and focused on a concept referred to as the supercritical airfoil. This distinctive airfoil shape, based on local supersonic flow with isentropic recompression, was characterized by a large leading-edge radius, reduced curvature over

the middle region of the upper surface, and substantial aft camber.

This report has summarized the NASA supercritical airfoil development program in a chronological fashion, discussed some of the airfoil design guidelines, and presented coordinates of a matrix of family-related supercritical airfoils with thicknesses of 2 to 18 percent and design lift coefficients from 0 to 1.0.

NASA Langley Research Center
Hampton, VA 23665-5225
January 16, 1990

References

1. Whitcomb, Richard T.: Review of NASA Supercritical Airfoils. ICAS Paper No. 74-10, Aug. 1974.

2. Ayers, Theodore G.: Supercritical Aerodynamics: Worthwhile Over a Range of Speeds. *Astronaut. & Aeronaut.*, vol. 10, no. 8, Aug. 1972, pp. 32–36.

3. McGhee, Robert J.; and Beasley, William D.: *Low-Speed Aerodynamic Characteristics of a 17-Percent-Thick Airfoil Section Designed for General Aviation Applications.* NASA TN D-7428, 1973.

4. McGhee, Robert J.; Beasley, William D.; and Somers, Dan M.: *Low-Speed Aerodynamic Characteristics of a 13-Percent-Thick Airfoil Section Designed for General Aviation Applications.* NASA TM X-72697, 1975.

5. McGhee, Robert J.; and Beasley, William D.: *Effects of Thickness on the Aerodynamic Characteristics of an Initial Low-Speed Family of Airfoils for General Aviation Applications.* NASA TM X-72843, 1976.

6. McGhee, Robert J.; and Beasley, William D.: *Low-Speed Wind-Tunnel Results for a Modified 13-Percent-Thick Airfoil.* NASA TM X-74018, 1977.

7. McGhee, Robert J.; and Beasley, William D.: *Wind-Tunnel Results for an Improved 21-Percent-Thick Low-Speed Airfoil Section.* NASA TM-78650, 1978.

8. McGhee, Robert J.; Beasley, William D.; and Whitcomb, Richard T.: *NASA Low- and Medium-Speed Airfoil Development.* NASA TM-78709, 1979.

9. McGhee, Robert J.; and Beasley, William D.: *Low-Speed Aerodynamic Characteristics of a 13-Percent-Thick Medium-Speed Airfoil Designed for General Aviation Applications.* NASA TP-1498, 1979.

10. McGhee, Robert J.; and Beasley, William D.: *Low-Speed Aerodynamic Characteristics of a 17-Percent-Thick Medium-Speed Airfoil Designed for General Aviation Applications.* NASA TP-1786, 1980.

11. McGhee, Robert J.; and Beasley, William D.: *Wind-Tunnel Results for a Modified 17-Percent-Thick Low-Speed Airfoil Section.* NASA TP-1919, 1981.

12. Ferris, James D.; McGhee, Robert J.; and Barnwell, Richard W.: *Low-Speed Wind-Tunnel Results for Symmetrical NASA LS(1)-0013 Airfoil.* NASA TM-4003, 1987.

13. Whitcomb, Richard T.; and Clark, Larry R.: *An Airfoil Shape for Efficient Flight at Supercritical Mach Numbers.* NASA TM X-1109, 1965.

14. Whitcomb, Richard T.; and Blackwell, James A., Jr.: Status of Research on a Supercritical Wing. *Conference on Aircraft Aerodynamics,* NASA SP-124, 1966, pp. 367–381.

15. Van Dyke, Milton D.; and Wibbert, Gordon A.: *High-Speed Aerodynamic Characteristics of 12 Thin NACA 6-Series Airfoils.* NACA MR A5F27, Army Air Forces, 1945.

16. Whitcomb, Richard T.: The NASA Supercritical Airfoil and Its Application to Swept Wings. *Supercritical Wing Technology—A Progress Report on Flight Evaluations,* NASA SP-301, 1972, pp. 1–11.

17. Jacobs, Peter F.: *Experimental Trim Drag Values and Flow-Field Measurements for a Wide-Body Transport Model With Conventional and Supercritical Wings.* NASA TP-2071, 1982.

18. Holder, D. W.: The Transonic Flow Past Two-Dimensional Aerofoils. *J. Royal Aeronaut. Soc.,* vol. 68, no. 644, Aug. 1964, pp. 501–516.

19. Pearcey, H. H.: The Aerodynamic Design of Section Shapes for Swept Wings. *Advances in Aeronautical Sciences,* Volume 3, Macmillan Co., c.1962, pp. 277–322.

20. Stratford, B. S.: The Prediction of Separation of the Turbulent Boundary Layer. *J. Fluid Mech.,* vol. 5, pt. 1, Jan. 1959, pp. 1–16.

21. Harris, Charles D.: *Wind-Tunnel Investigation of Effects of Trailing-Edge Geometry on a NASA Supercritical Airfoil Section.* NASA TM X-2336, 1971.

22. Harris, Charles D.: Experimental Investigation of a 10 Percent Thick NASA Supercritical Airfoil Section. *Experimental Data Base for Computer Program Assessment,* AGARD-AR-138, May 1979, pp. A9-1–A9-16.

23. Harris, Charles D.: *Aerodynamic Characteristics of Two NASA Supercritical Airfoils With Different Maximum Thicknesses.* NASA TM X-2532, 1972.

24. Harris, Charles D.; and Blackwell, James A., Jr.: *Wind-Tunnel Investigation of Effects of Rear Upper Surface Modification on an NASA Supercritical Airfoil.* NASA TM X-2454, 1972.

25. Harris, Charles D.: *Aerodynamic Characteristics of Two 10-Percent-Thick NASA Supercritical Airfoils With Different Upper Surface Curvature Distributions.* NASA TM X-2977, 1974.

26. Harris, Charles D.: *Aerodynamic Characteristics of an Improved 10-Percent-Thick NASA Supercritical Airfoil.* NASA TM X-2978, 1974.

27. Harris, Charles D.: *Aerodynamic Characteristics of 10-Percent-Thick NASA Supercritical Airfoils With Different Aft Camber.* NASA TM X-72007, 1975.

28. Harris, Charles D.: *Transonic Aerodynamic Characteristics of the 10-Percent-Thick NASA Supercritical Airfoil 31.* NASA TM X-3203, 1975.

29. Bauer, Frances; Garabedian, Paul; Korn, David; and Jameson, Antony: *Supercritical Wing Sections II.* Volume 108 of Lecture Notes in Economics and Mathematical Systems, M. Beckmann and H. P. Kuenzi, eds., Springer-Verlag, 1975.

30. Harris, Charles D.: *Comparison of the Experimental Aerodynamic Characteristics of Theoretically and Experimentally Designed Supercritical Airfoils.* NASA TM X-3082, 1974.

31. Kacprzynski, J. J.; Ohman, L. H.; Garabedian, P. R.; and Korn, D. G.: *Analysis of the Flow Past a Shockless Lifting Airfoil in Design and Off-Design Conditions.* LR-554 (NRC No. 12315), National Research Council of Canada (Ottawa), Nov. 1971. (Also available as AIAA Paper No. 71-567.)

32. Ohman, Lars H.; Kacprzynski, J. J.; and Brown, D.: Some Results From Tests in the NAE High Reynolds Number Two-Dimensional Test Facility on "Shockless" and Other Airfoils. ICAS Paper No. 72-33, Aug.–Sept. 1972.

33. Garabedian, P. R.: Computation of Wave Drag for Transonic Flow. *J. Anal. Math.,* vol. 30, 1976, pp. 164–171.

34. Garabedian, P. R.: Transonic Flow Theory of Airfoils and Wings. *Advances in Engineering Science,* Volume 4, NASA CP-2001, [1976], pp. 1349–1358.

35. Newman, Perry A.; and South, Jerry C., Jr.: *Conservative Versus Nonconservative Differencing: Transonic Streamline Shape Effects.* NASA TM X-72827, 1976.

36. Jameson, Antony: *Accelerated Iteration Schemes for Transonic Flow Calculations Using Fast Poisson Solvers.* NASA CR-143431, 1975.

37. Harris, Charles D.; and Allison, Dennis O.: *Comparison of Experimental and Theoretical Drag Characteristics for a 10-Percent-Thick Supercritical Airfoil Using a New Version of an Analysis Code.* NASA TM X-74041, [1977].

38. Whitcomb, Richard T.: Transonic Airfoil Development. *Special Course on Subsonic/Transonic Aerodynamic Interference for Aircraft,* AGARD-R-712, July 1983, pp. 5-1–5-9.

39. Harris, Charles D.: *Aerodynamic Characteristics of the 10-Percent-Thick NASA Supercritical Airfoil 33 Designed for a Normal-Force Coefficient of 0.7.* NASA TM X-72711, 1975.

40. Harris, Charles D.: *Aerodynamic Characteristics of a 14-Percent-Thick NASA Supercritical Airfoil Designed for a Normal-Force Coefficient of 0.7.* NASA TM X-72712, 1975.

41. Harris, Charles D.; McGhee, Robert J.; and Allison, Dennis O.: *Low-Speed Aerodynamic Characteristics of a 14-Percent-Thick NASA Phase 2 Supercritical Airfoil Designed for a Lift Coefficient of 0.7.* NASA TM-81912, 1980.

42. Pierpont, P. Kenneth: Bringing Wings of Change. *Astronaut. & Aeronaut.,* vol. 13, no. 10, Oct. 1975, pp. 20–27.

43. Mineck, Raymond E.; and Lawing, Pierce L.: *High Reynolds Number Tests of the NASA SC(2)-0012 Airfoil in the Langley 0.3-Meter Transonic Cryogenic Tunnel.* NASA TM-89102, 1987.

44. Jenkins, Renaldo V.; Hill, Acquilla S.; and Ray, Edward J.: *Aerodynamic Performance and Pressure Distributions for a NASA SC(2)-0714 Airfoil Tested in the Langley 0.3-Meter Transonic Cryogenic Tunnel.* NASA TM-4044, 1988.

45. Jenkins, Renaldo V.: *NASA SC(2)-0714 Airfoil Data Corrected for Sidewall Boundary-Layer Effects in the Langley 0.3-Meter Transonic Cryogenic Tunnel.* NASA TP-2890, 1989.

46. Taylor, A. B.: *Development of Selected Advanced Aerodynamics and Active Control Concepts for Commercial Transport Aircraft.* NASA CR-3781, 1984.

47. Johnson, William G., Jr.; Hill, Acquilla S.; and Eichmann, Otto: *Pressure Distributions From High Reynolds Number Tests of a NASA SC(3)-0712(B) Airfoil in the Langley 0.3-Meter Transonic Cryogenic Tunnel.* NASA TM-86370, 1985.

48. Johnson, William G., Jr.; Hill, Acquilla S.; and Eichmann, Otto: *High Reynolds Number Tests of a NASA SC(3)0712(B) Airfoil in the Langley 0.3-Meter Transonic Cryogenic Tunnel.* NASA TM-86371, 1985.

Table I. Major Milestones in the Development of NASA Supercritical Airfoils

Milestone	Date	Reference
Experimentally designed slotted SC airfoil	1964	13 (TM X-1109)
Experimentally designed integral SC airfoil	1966	
Thickened-trailing-edge experiments	1970	21 (TM X-2336)
Improved SC airfoil 26a	1972	26 (TM X-2978)
Theoretically designed SC airfoil	1973	30 (TM X-3082)
Experimentally designed SC airfoil 31	1974	28 (TM X-3203)
Analytically designed 10-percent-thick SC airfoil 33	1975	39 (TM X-72711)
Analytically designed 14-percent-thick SC airfoil	1975	40 (TM X-72712)
Matrix of phase 2 SC airfoils	1976–1978	
Phase 3 SC airfoils	1979	

Table II. Coordinates of 2-Percent-Thick Supercritical Airfoil SC(2)-0402 Designed for 0.4 Lift Coefficient

x/c	$(y/c)_u$	$(y/c)_l$	x/c	$(y/c)_u$	$(y/c)_l$
0.000	0.00000	0.00000	.500	.00970	-.00915
.002	.00135	-.00135	.510	.00965	-.00900
.005	.00205	-.00205	.520	.00960	-.00885
.010	.00280	-.00280	.530	.00955	-.00870
.020	.00375	-.00375	.540	.00950	-.00855
.030	.00445	-.00445	.550	.00940	-.00840
.040	.00500	-.00500	.560	.00930	-.00820
.050	.00550	-.00550	.570	.00920	-.00800
.060	.00590	-.00590	.580	.00910	-.00780
.070	.00625	-.00625	.590	.00900	-.00760
.080	.00660	-.00660	.600	.00890	-.00735
.090	.00690	-.00690	.610	.00880	-.00710
.100	.00720	-.00720	.620	.00870	-.00685
.110	.00745	-.00745	.630	.00860	-.00660
.120	.00770	-.00770	.640	.00845	-.00635
.130	.00790	-.00790	.650	.00830	-.00610
.140	.00810	-.00810	.660	.00815	-.00585
.150	.00830	-.00830	.670	.00800	-.00560
.160	.00845	-.00845	.680	.00785	-.00535
.170	.00860	-.00860	.690	.00770	-.00510
.180	.00875	-.00875	.700	.00755	-.00485
.190	.00890	-.00890	.710	.00740	-.00460
.200	.00900	-.00900	.720	.00720	-.00435
.210	.00910	-.00910	.730	.00700	-.00410
.220	.00920	-.00920	.740	.00680	-.00385
.230	.00930	-.00930	.750	.00660	-.00360
.240	.00940	-.00940	.760	.00640	-.00335
.250	.00950	-.00950	.770	.00620	-.00310
.260	.00960	-.00960	.780	.00600	-.00285
.270	.00965	-.00965	.790	.00580	-.00260
.280	.00970	-.00970	.800	.00555	-.00240
.290	.00975	-.00975	.810	.00530	-.00220
.300	.00980	-.00980	.820	.00505	-.00200
.310	.00985	-.00985	.830	.00480	-.00180
.320	.00990	-.00990	.840	.00455	-.00165
.330	.00995	-.00995	.850	.00425	-.00155
.340	.01000	-.00995	.860	.00395	-.00145
.350	.01000	-.00995	.870	.00365	-.00140
.360	.01000	-.00995	.880	.00330	-.00140
.370	.01000	-.00995	.890	.00295	-.00140
.380	.01000	-.00995	.900	.00255	-.00150
.390	.01000	-.00995	.910	.00215	-.00160
.400	.01000	-.00995	.920	.00170	-.00175
.410	.01000	-.00990	.930	.00120	-.00195
.420	.01000	-.00985	.940	.00070	-.00220
.430	.01000	-.00980	.950	.00015	-.00250
.440	.01000	-.00975	.960	-.00045	-.00290
.450	.00995	-.00965	.970	-.00110	-.00340
.460	.00990	-.00955	.980	-.00180	-.00400
.470	.00985	-.00945	.990	-.00265	-.00470
.480	.00980	-.00935	1.000	-.00360	-.00550
.490	.00975	-.00925			

## Table III. Coordinates of 3-Percent-Thick Supercritical Airfoil SC(2)-0403 Designed for 0.4 Lift Coefficient
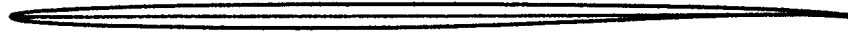
x/c	$(y/c)_u$	$(y/c)_l$	x/c	$(y/c)_u$	$(y/c)_l$
0.000	0.00000	0.00000	.500	.01465	-.01330
.002	.00210	-.00210	.510	.01460	-.01310
.005	.00320	-.00320	.520	.01450	-.01280
.010	.00440	-.00440	.530	.01440	-.01250
.020	.00590	-.00590	.540	.01430	-.01220
.030	.00700	-.00700	.550	.01420	-.01190
.040	.00780	-.00780	.560	.01410	-.01160
.050	.00850	-.00850	.570	.01400	-.01130
.060	.00910	-.00910	.580	.01390	-.01100
.070	.00960	-.00960	.590	.01380	-.01060
.080	.01010	-.01010	.600	.01365	-.01020
.090	.01050	-.01050	.610	.01350	-.00980
.100	.01090	-.01090	.620	.01335	-.00940
.110	.01130	-.01130	.630	.01320	-.00900
.120	.01160	-.01170	.640	.01305	-.00860
.130	.01190	-.01200	.650	.01290	-.00820
.140	.01220	-.01230	.660	.01275	-.00780
.150	.01250	-.01260	.670	.01260	-.00740
.160	.01270	-.01290	.680	.01240	-.00700
.170	.01290	-.01310	.690	.01220	-.00660
.180	.01310	-.01330	.700	.01200	-.00620
.190	.01330	-.01350	.710	.01180	-.00580
.200	.01350	-.01370	.720	.01160	-.00540
.210	.01365	-.01390	.730	.01140	-.00500
.220	.01380	-.01410	.740	.01120	-.00460
.230	.01395	-.01430	.750	.01100	-.00420
.240	.01410	-.01440	.760	.01075	-.00380
.250	.01420	-.01450	.770	.01050	-.00340
.260	.01430	-.01460	.780	.01025	-.00300
.270	.01440	-.01470	.790	.01000	-.00260
.280	.01450	-.01480	.800	.00975	-.00220
.290	.01460	-.01490	.810	.00950	-.00180
.300	.01470	-.01500	.820	.00920	-.00150
.310	.01475	-.01500	.830	.00890	-.00120
.320	.01480	-.01500	.840	.00860	-.00090
.330	.01485	-.01500	.850	.00830	-.00060
.340	.01490	-.01500	.860	.00790	-.00040
.350	.01495	-.01500	.870	.00750	-.00020
.360	.01500	-.01500	.880	.00710	.00000
.370	.01500	-.01500	.890	.00670	.00010
.380	.01500	-.01500	.900	.00620	.00020
.390	.01500	-.01490	.910	.00570	.00020
.400	.01500	-.01480	.920	.00510	.00010
.410	.01500	-.01470	.930	.00450	.00000
.420	.01500	-.01460	.940	.00380	-.00020
.430	.01500	-.01450	.950	.00310	-.00050
.440	.01495	-.01440	.960	.00230	-.00090
.450	.01490	-.01430	.970	.00150	-.00140
.460	.01485	-.01410	.980	.00060	-.00200
.470	.01480	-.01390	.990	-.00030	-.00280
.480	.01475	-.01370	1.000	-.00130	-.00370
.490	.01470	-.01350			

Table IV. Coordinates of 3-Percent-Thick Supercritical Airfoil SC(2)-0503
Designed for 0.5 Lift Coefficient

x/c	$(y/c)_u$	$(y/c)_l$	x/c	$(y/c)_u$	$(y/c)_l$
0.000	0.00000	0.00000	.500	.01430	-.01380
.002	.00210	-.00210	.510	.01420	-.01360
.005	.00320	-.00320	.520	.01410	-.01340
.010	.00430	-.00430	.530	.01400	-.01320
.020	.00570	-.00570	.540	.01390	-.01300
.030	.00680	-.00680	.550	.01375	-.01270
.040	.00760	-.00760	.560	.01360	-.01240
.050	.00830	-.00830	.570	.01345	-.01210
.060	.00890	-.00890	.580	.01330	-.01180
.070	.00950	-.00950	.590	.01315	-.01150
.080	.01000	-.01000	.600	.01300	-.01120
.090	.01050	-.01050	.610	.01280	-.01090
.100	.01090	-.01090	.620	.01260	-.01060
.110	.01130	-.01130	.630	.01240	-.01030
.120	.01170	-.01170	.640	.01220	-.00990
.130	.01200	-.01200	.650	.01200	-.00950
.140	.01230	-.01230	.660	.01180	-.00910
.150	.01260	-.01260	.670	.01160	-.00870
.160	.01285	-.01290	.680	.01140	-.00830
.170	.01310	-.01310	.690	.01115	-.00790
.180	.01330	-.01330	.700	.01090	-.00750
.190	.01350	-.01350	.710	.01065	-.00710
.200	.01370	-.01370	.720	.01040	-.00670
.210	.01390	-.01390	.730	.01015	-.00630
.220	.01405	-.01410	.740	.00990	-.00590
.230	.01420	-.01430	.750	.00960	-.00550
.240	.01435	-.01440	.760	.00930	-.00510
.250	.01450	-.01450	.770	.00900	-.00480
.260	.01460	-.01460	.780	.00870	-.00450
.270	.01470	-.01470	.790	.00840	-.00420
.280	.01480	-.01480	.800	.00810	-.00390
.290	.01485	-.01490	.810	.00770	-.00360
.300	.01490	-.01500	.820	.00730	-.00330
.310	.01495	-.01510	.830	.00690	-.00310
.320	.01500	-.01510	.840	.00650	-.00290
.330	.01500	-.01510	.850	.00610	-.00270
.340	.01500	-.01510	.860	.00560	-.00260
.350	.01500	-.01510	.870	.00510	-.00250
.360	.01500	-.01510	.880	.00460	-.00250
.370	.01500	-.01510	.890	.00400	-.00250
.380	.01500	-.01510	.900	.00340	-.00260
.390	.01500	-.01510	.910	.00270	-.00280
.400	.01495	-.01510	.920	.00200	-.00300
.410	.01490	-.01500	.930	.00120	-.00330
.420	.01485	-.01490	.940	.00040	-.00370
.430	.01480	-.01480	.950	-.00050	-.00420
.440	.01475	-.01470	.960	-.00150	-.00480
.450	.01470	-.01460	.970	-.00250	-.00550
.460	.01465	-.01450	.980	-.00360	-.00630
.470	.01460	-.01440	.990	-.00470	-.00720
.480	.01450	-.01420	1.000	-.00590	-.00830
.490	.01440	-.01400			

Table V. Coordinates of 4-Percent-Thick Supercritical Airfoil SC(2)-0404
Designed for 0.4 Lift Coefficient
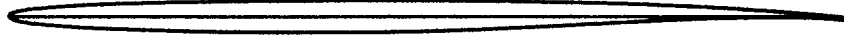
x/c	$(y/c)_u$	$(y/c)_l$	x/c	$(y/c)_u$	$(y/c)_l$
0.000	0.00000	0.00000	.500	.01970	-.01790
.002	.00280	-.00280	.510	.01960	-.01760
.005	.00430	-.00430	.520	.01950	-.01730
.010	.00590	-.00590	.530	.01940	-.01695
.020	.00800	-.00800	.540	.01930	-.01655
.030	.00950	-.00950	.550	.01920	-.01615
.040	.01060	-.01060	.560	.01905	-.01575
.050	.01155	-.01155	.570	.01890	-.01530
.060	.01235	-.01235	.580	.01875	-.01485
.070	.01305	-.01305	.590	.01860	-.01440
.080	.01365	-.01365	.600	.01845	-.01390
.090	.01425	-.01425	.610	.01830	-.01340
.100	.01475	-.01475	.620	.01810	-.01290
.110	.01520	-.01525	.630	.01790	-.01240
.120	.01560	-.01570	.640	.01770	-.01185
.130	.01600	-.01610	.650	.01750	-.01130
.140	.01635	-.01650	.660	.01730	-.01075
.150	.01670	-.01690	.670	.01705	-.01020
.160	.01700	-.01720	.680	.01680	-.00965
.170	.01730	-.01750	.690	.01655	-.00910
.180	.01755	-.01780	.700	.01630	-.00855
.190	.01780	-.01810	.710	.01600	-.00800
.200	.01805	-.01840	.720	.01570	-.00745
.210	.01825	-.01860	.730	.01540	-.00690
.220	.01845	-.01880	.740	.01505	-.00635
.230	.01865	-.01900	.750	.01470	-.00580
.240	.01885	-.01920	.760	.01435	-.00525
.250	.01900	-.01940	.770	.01395	-.00470
.260	.01915	-.01950	.780	.01355	-.00420
.270	.01930	-.01960	.790	.01315	-.00370
.280	.01945	-.01970	.800	.01270	-.00325
.290	.01955	-.01980	.810	.01225	-.00280
.300	.01965	-.01990	.820	.01175	-.00240
.310	.01975	-.02000	.830	.01125	-.00200
.320	.01985	-.02000	.840	.01070	-.00165
.330	.01990	-.02000	.850	.01015	-.00135
.340	.01995	-.02000	.860	.00955	-.00110
.350	.02000	-.02000	.870	.00895	-.00085
.360	.02005	-.02000	.880	.00830	-.00065
.370	.02010	-.02000	.890	.00765	-.00050
.380	.02010	-.02000	.900	.00695	-.00040
.390	.02010	-.01990	.910	.00625	-.00040
.400	.02010	-.01980	.920	.00550	-.00045
.410	.02010	-.01970	.930	.00475	-.00055
.420	.02010	-.01960	.940	.00395	-.00075
.430	.02010	-.01950	.950	.00310	-.00105
.440	.02005	-.01930	.960	.00225	-.00145
.450	.02000	-.01910	.970	.00135	-.00200
.460	.01995	-.01890	.980	.00045	-.00265
.470	.01990	-.01870	.990	-.00050	-.00345
.480	.01985	-.01850	1.000	-.00150	-.00435
.490	.01980	-.01820			

## Table VI. Coordinates of 6-Percent-Thick Supercritical Airfoil SC(2)-0406 Designed for 0.4 Lift Coefficient
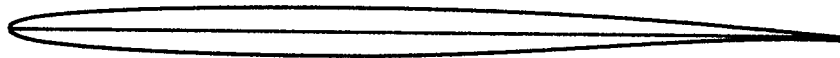
x/c	$(y/c)_u$	$(y/c)_l$	x/c	$(y/c)_u$	$(y/c)_l$
0.000	0.0000	0.0000	.500	.0290	-.0271
.002	.0043	-.0043	.510	.0288	-.0267
.005	.0064	-.0064	.520	.0286	-.0263
.010	.0089	-.0089	.530	.0284	-.0258
.020	.0122	-.0122	.540	.0282	-.0253
.030	.0144	-.0144	.550	.0279	-.0248
.040	.0161	-.0161	.560	.0276	-.0243
.050	.0175	-.0175	.570	.0273	-.0237
.060	.0187	-.0187	.580	.0270	-.0231
.070	.0198	-.0197	.590	.0267	-.0225
.080	.0207	-.0206	.600	.0263	-.0219
.090	.0215	-.0215	.610	.0259	-.0213
.100	.0223	-.0223	.620	.0255	-.0207
.110	.0230	-.0230	.630	.0251	-.0201
.120	.0236	-.0237	.640	.0247	-.0195
.130	.0242	-.0243	.650	.0242	-.0188
.140	.0248	-.0249	.660	.0237	-.0181
.150	.0253	-.0254	.670	.0232	-.0174
.160	.0258	-.0259	.680	.0227	-.0167
.170	.0262	-.0264	.690	.0222	-.0160
.180	.0266	-.0268	.700	.0217	-.0153
.190	.0270	-.0272	.710	.0211	-.0146
.200	.0273	-.0276	.720	.0205	-.0139
.210	.0276	-.0279	.730	.0199	-.0132
.220	.0279	-.0282	.740	.0193	-.0125
.230	.0282	-.0285	.750	.0187	-.0118
.240	.0285	-.0288	.760	.0181	-.0111
.250	.0287	-.0290	.770	.0174	-.0104
.260	.0289	-.0292	.780	.0167	-.0097
.270	.0291	-.0294	.790	.0160	-.0090
.280	.0293	-.0296	.800	.0153	-.0084
.290	.0295	-.0297	.810	.0146	-.0078
.300	.0296	-.0298	.820	.0139	-.0072
.310	.0297	-.0299	.830	.0132	-.0066
.320	.0298	-.0300	.840	.0124	-.0060
.330	.0299	-.0301	.850	.0116	-.0055
.340	.0300	-.0301	.860	.0108	-.0050
.350	.0301	-.0301	.870	.0100	-.0045
.360	.0301	-.0301	.880	.0092	-.0041
.370	.0301	-.0301	.890	.0084	-.0037
.380	.0301	-.0300	.900	.0076	-.0034
.390	.0301	-.0299	.910	.0068	-.0031
.400	.0301	-.0298	.920	.0059	-.0029
.410	.0301	-.0297	.930	.0050	-.0028
.420	.0300	-.0295	.940	.0041	-.0028
.430	.0299	-.0293	.950	.0032	-.0029
.440	.0298	-.0291	.960	.0023	-.0031
.450	.0297	-.0288	.970	.0014	-.0034
.460	.0296	-.0285	.980	.0004	-.0039
.470	.0295	-.0282	.990	-.0006	-.0046
.480	.0294	-.0279	1.000	-.0016	-.0055
.490	.0292	-.0275			

Table VII. Coordinates of 6-Percent-Thick Supercritical Airfoil SC(2)-0606 Designed for 0.6 Lift Coefficient
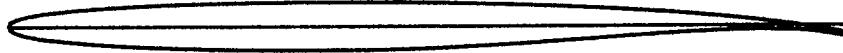
x/c	$(y/c)_u$	$(y/c)_l$	x/c	$(y/c)_u$	$(y/c)_l$
0.000	0.0000	0.0000	.500	.0288	-.0270
.002	.0043	-.0043	.510	.0286	-.0266
.005	.0065	-.0065	.520	.0284	-.0262
.010	.0088	-.0088	.530	.0282	-.0257
.020	.0119	-.0119	.540	.0280	-.0252
.030	.0140	-.0140	.550	.0277	-.0247
.040	.0157	-.0157	.560	.0274	-.0241
.050	.0171	-.0171	.570	.0271	-.0235
.060	.0183	-.0183	.580	.0268	-.0229
.070	.0194	-.0194	.590	.0265	-.0223
.080	.0204	-.0204	.600	.0262	-.0217
.090	.0213	-.0213	.610	.0259	-.0211
.100	.0221	-.0221	.620	.0255	-.0205
.110	.0228	-.0229	.630	.0251	-.0199
.120	.0235	-.0236	.640	.0247	-.0192
.130	.0241	-.0242	.650	.0243	-.0185
.140	.0247	-.0248	.660	.0239	-.0178
.150	.0252	-.0253	.670	.0234	-.0171
.160	.0257	-.0258	.680	.0229	-.0164
.170	.0262	-.0263	.690	.0224	-.0157
.180	.0266	-.0267	.700	.0219	-.0150
.190	.0270	-.0271	.710	.0213	-.0143
.200	.0274	-.0275	.720	.0207	-.0136
.210	.0277	-.0278	.730	.0201	-.0129
.220	.0280	-.0281	.740	.0195	-.0122
.230	.0283	-.0284	.750	.0189	-.0115
.240	.0286	-.0287	.760	.0182	-.0108
.250	.0288	-.0289	.770	.0175	-.0101
.260	.0290	-.0291	.780	.0168	-.0094
.270	.0292	-.0293	.790	.0161	-.0088
.280	.0294	-.0295	.800	.0153	-.0082
.290	.0295	-.0296	.810	.0145	-.0076
.300	.0296	-.0297	.820	.0137	-.0071
.310	.0297	-.0298	.830	.0128	-.0066
.320	.0298	-.0299	.840	.0119	-.0061
.330	.0299	-.0300	.850	.0110	-.0057
.340	.0300	-.0300	.860	.0100	-.0053
.350	.0300	-.0300	.870	.0090	-.0050
.360	.0300	-.0300	.880	.0079	-.0048
.370	.0300	-.0300	.890	.0068	-.0047
.380	.0300	-.0299	.900	.0056	-.0047
.390	.0300	-.0298	.910	.0044	-.0048
.400	.0300	-.0297	.920	.0031	-.0050
.410	.0300	-.0296	.930	.0018	-.0054
.420	.0299	-.0294	.940	.0004	-.0059
.430	.0298	-.0292	.950	-.0010	-.0066
.440	.0297	-.0290	.960	-.0025	-.0076
.450	.0296	-.0287	.970	-.0041	-.0088
.460	.0295	-.0284	.980	-.0059	-.0103
.470	.0294	-.0281	.990	-.0078	-.0120
.480	.0292	-.0278	1.000	-.0098	-.0139
.490	.0290	-.0274			

Table VIII. Coordinates of 6-Percent-Thick Supercritical Airfoil SC(2)-0706
Designed for 0.7 Lift Coefficient
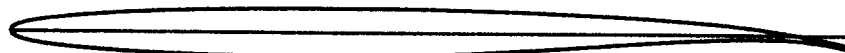
x/c	$(y/c)_u$	$(y/c)_l$	x/c	$(y/c)_u$	$(y/c)_l$
0.000	0.0000	0.0000	.500	.0287	-.0270
.002	.0043	-.0043	.510	.0285	-.0266
.005	.0065	-.0065	.520	.0283	-.0261
.010	.0088	-.0088	.530	.0281	-.0256
.020	.0117	-.0117	.540	.0278	-.0251
.030	.0138	-.0138	.550	.0275	-.0246
.040	.0155	-.0155	.560	.0272	-.0240
.050	.0169	-.0169	.570	.0269	-.0234
.060	.0181	-.0181	.580	.0266	-.0228
.070	.0192	-.0192	.590	.0263	-.0222
.080	.0202	-.0202	.600	.0260	-.0216
.090	.0211	-.0211	.610	.0256	-.0210
.100	.0219	-.0219	.620	.0252	-.0204
.110	.0227	-.0227	.630	.0248	-.0197
.120	.0234	-.0234	.640	.0244	-.0190
.130	.0240	-.0240	.650	.0240	-.0183
.140	.0246	-.0246	.660	.0236	-.0176
.150	.0252	-.0251	.670	.0231	-.0169
.160	.0257	-.0256	.680	.0226	-.0162
.170	.0262	-.0261	.690	.0221	-.0155
.180	.0266	-.0265	.700	.0216	-.0148
.190	.0270	-.0269	.710	.0211	-.0141
.200	.0274	-.0273	.720	.0206	-.0134
.210	.0277	-.0277	.730	.0200	-.0127
.220	.0280	-.0280	.740	.0194	-.0120
.230	.0283	-.0283	.750	.0188	-.0113
.240	.0286	-.0286	.760	.0182	-.0106
.250	.0288	-.0288	.770	.0175	-.0099
.260	.0290	-.0290	.780	.0168	-.0093
.270	.0292	-.0292	.790	.0161	-.0087
.280	.0294	-.0294	.800	.0154	-.0081
.290	.0295	-.0296	.810	.0146	-.0075
.300	.0296	-.0297	.820	.0138	-.0070
.310	.0297	-.0298	.830	.0129	-.0065
.320	.0298	-.0299	.840	.0120	-.0061
.330	.0299	-.0300	.850	.0110	-.0057
.340	.0300	-.0300	.860	.0100	-.0054
.350	.0300	-.0300	.870	.0089	-.0052
.360	.0300	-.0300	.880	.0077	-.0051
.370	.0300	-.0300	.890	.0064	-.0051
.380	.0300	-.0299	.900	.0051	-.0052
.390	.0300	-.0298	.910	.0037	-.0054
.400	.0300	-.0297	.920	.0022	-.0058
.410	.0299	-.0296	.930	.0006	-.0064
.420	.0298	-.0294	.940	-.0011	-.0072
.430	.0297	-.0292	.950	-.0029	-.0082
.440	.0296	-.0290	.960	-.0048	-.0095
.450	.0295	-.0287	.970	-.0068	-.0111
.460	.0294	-.0284	.980	-.0089	-.0130
.470	.0293	-.0281	.990	-.0112	-.0152
.480	.0291	-.0278	1.000	-.0138	-.0177
.490	.0289	-.0274			

## Table IX. Coordinates of 6-Percent-Thick Supercritical Airfoil SC(2)-1006 Designed for 1.0 Lift Coefficient

x/c	$(y/c)_u$	$(y/c)_l$	x/c	$(y/c)_u$	$(y/c)_l$
0.000	0.0000	0.0000	.500	.0254	-.0281
.002	.0042	-.0042	.510	.0249	-.0279
.005	.0064	-.0064	.520	.0244	-.0277
.010	.0087	-.0087	.530	.0239	-.0275
.020	.0117	-.0117	.540	.0234	-.0273
.030	.0140	-.0140	.550	.0229	-.0271
.040	.0158	-.0158	.560	.0223	-.0269
.050	.0174	-.0174	.570	.0217	-.0267
.060	.0188	-.0187	.580	.0211	-.0265
.070	.0200	-.0199	.590	.0205	-.0263
.080	.0211	-.0209	.600	.0198	-.0261
.090	.0221	-.0218	.610	.0191	-.0259
.100	.0230	-.0226	.620	.0184	-.0257
.110	.0238	-.0234	.630	.0177	-.0255
.120	.0245	-.0241	.640	.0169	-.0253
.130	.0252	-.0247	.650	.0161	-.0251
.140	.0258	-.0253	.660	.0153	-.0249
.150	.0264	-.0259	.670	.0144	-.0247
.160	.0269	-.0264	.680	.0135	-.0245
.170	.0274	-.0269	.690	.0126	-.0243
.180	.0278	-.0273	.700	.0117	-.0241
.190	.0282	-.0277	.710	.0107	-.0239
.200	.0285	-.0281	.720	.0097	-.0237
.210	.0288	-.0284	.730	.0087	-.0236
.220	.0291	-.0287	.740	.0076	-.0235
.230	.0293	-.0290	.750	.0065	-.0234
.240	.0295	-.0292	.760	.0053	-.0233
.250	.0297	-.0294	.770	.0041	-.0233
.260	.0298	-.0296	.780	.0028	-.0233
.270	.0299	-.0297	.790	.0015	-.0233
.280	.0300	-.0298	.800	.0001	-.0234
.290	.0300	-.0299	.810	-.0014	-.0235
.300	.0300	-.0300	.820	-.0030	-.0237
.310	.0300	-.0300	.830	-.0046	-.0239
.320	.0300	-.0300	.840	-.0063	-.0242
.330	.0299	-.0300	.850	-.0081	-.0246
.340	.0298	-.0300	.860	-.0100	-.0251
.350	.0297	-.0300	.870	-.0120	-.0257
.360	.0296	-.0299	.880	-.0141	-.0264
.370	.0294	-.0298	.890	-.0162	-.0272
.380	.0292	-.0297	.900	-.0184	-.0281
.390	.0290	-.0296	.910	-.0206	-.0292
.400	.0288	-.0295	.920	-.0229	-.0305
.410	.0286	-.0294	.930	-.0253	-.0320
.420	.0283	-.0293	.940	-.0277	-.0337
.430	.0280	-.0292	.950	-.0302	-.0356
.440	.0277	-.0291	.960	-.0328	-.0377
.450	.0274	-.0290	.970	-.0355	-.0400
.460	.0270	-.0289	.980	-.0383	-.0425
.470	.0266	-.0287	.990	-.0412	-.0452
.480	.0262	-.0285	1.000	-.0443	-.0482
.490	.0258	-.0283			

Table X. Coordinates of 10-Percent-Thick Symmetrical Supercritical Airfoil SC(2)-0010

x/c	$(y/c)_u$	$(y/c)_l$	x/c	$(y/c)_u$	$(y/c)_l$
0.000	0.00000	0.00000	.500	.04840	-.04840
.002	.00760	-.00760	.510	.04810	-.04810
.005	.01160	-.01160	.520	.04780	-.04780
.010	.01550	-.01550	.530	.04740	-.04740
.020	.02070	-.02070	.540	.04700	-.04700
.030	.02430	-.02430	.550	.04650	-.04650
.040	.02700	-.02700	.560	.04600	-.04600
.050	.02920	-.02920	.570	.04550	-.04550
.060	.03110	-.03110	.580	.04490	-.04490
.070	.03280	-.03280	.590	.04430	-.04430
.080	.03430	-.03430	.600	.04360	-.04360
.090	.03570	-.03570	.610	.04280	-.04280
.100	.03690	-.03690	.620	.04200	-.04200
.110	.03800	-.03800	.630	.04110	-.04110
.120	.03900	-.03900	.640	.04020	-.04020
.130	.04000	-.04000	.650	.03920	-.03920
.140	.04090	-.04090	.660	.03820	-.03820
.150	.04170	-.04170	.670	.03715	-.03715
.160	.04250	-.04250	.680	.03610	-.03610
.170	.04320	-.04320	.690	.03505	-.03505
.180	.04390	-.04390	.700	.03400	-.03400
.190	.04450	-.04450	.710	.03295	-.03295
.200	.04510	-.04510	.720	.03190	-.03190
.210	.04560	-.04560	.730	.03085	-.03085
.220	.04610	-.04610	.740	.02980	-.02980
.230	.04660	-.04660	.750	.02875	-.02875
.240	.04700	-.04700	.760	.02770	-.02770
.250	.04740	-.04740	.770	.02665	-.02665
.260	.04780	-.04780	.780	.02560	-.02560
.270	.04810	-.04810	.790	.02455	-.02455
.280	.04840	-.04840	.800	.02350	-.02350
.290	.04870	-.04870	.810	.02245	-.02245
.300	.04900	-.04900	.820	.02140	-.02140
.310	.04920	-.04920	.830	.02035	-.02035
.320	.04940	-.04940	.840	.01930	-.01930
.330	.04960	-.04960	.850	.01825	-.01825
.340	.04970	-.04970	.860	.01720	-.01720
.350	.04980	-.04980	.870	.01615	-.01615
.360	.04990	-.04990	.880	.01510	-.01510
.370	.05000	-.05000	.890	.01405	-.01405
.380	.05000	-.05000	.900	.01300	-.01300
.390	.05000	-.05000	.910	.01195	-.01195
.400	.05000	-.05000	.920	.01090	-.01090
.410	.05000	-.05000	.930	.00985	-.00985
.420	.04990	-.04990	.940	.00880	-.00880
.430	.04980	-.04980	.950	.00775	-.00775
.440	.04970	-.04970	.960	.00670	-.00670
.450	.04960	-.04960	.970	.00565	-.00565
.460	.04940	-.04940	.980	.00460	-.00460
.470	.04920	-.04920	.990	.00355	-.00355
.480	.04900	-.04900	1.000	.00250	-.00250
.490	.04870	-.04870			

## Table XI. Coordinates of 10-Percent-Thick Supercritical Airfoil SC(2)-0410 Designed for 0.4 Lift Coefficient
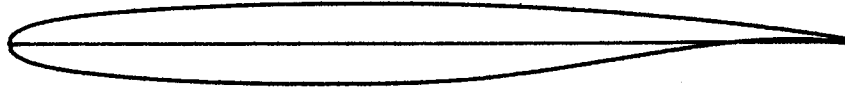
x/c	$(y/c)_u$	$(y/c)_l$	x/c	$(y/c)_u$	$(y/c)_l$
0.000	0.0000	0.0000	.500	.0490	-.0465
.002	.0076	-.0076	.510	.0488	-.0460
.005	.0116	-.0116	.520	.0485	-.0454
.010	.0155	-.0155	.530	.0482	-.0447
.020	.0207	-.0207	.540	.0479	-.0440
.030	.0242	-.0242	.550	.0476	-.0432
.040	.0269	-.0269	.560	.0472	-.0423
.050	.0291	-.0291	.570	.0468	-.0413
.060	.0310	-.0310	.580	.0464	-.0402
.070	.0327	-.0327	.590	.0459	-.0390
.080	.0342	-.0342	.600	.0454	-.0378
.090	.0356	-.0356	.610	.0449	-.0365
.100	.0368	-.0369	.620	.0443	-.0352
.110	.0379	-.0381	.630	.0437	-.0338
.120	.0389	-.0392	.640	.0431	-.0324
.130	.0399	-.0402	.650	.0425	-.0309
.140	.0408	-.0411	.660	.0418	-.0294
.150	.0416	-.0420	.670	.0411	-.0278
.160	.0424	-.0428	.680	.0404	-.0262
.170	.0431	-.0435	.690	.0396	-.0246
.180	.0438	-.0442	.700	.0388	-.0230
.190	.0444	-.0449	.710	.0380	-.0214
.200	.0450	-.0455	.720	.0372	-.0198
.210	.0456	-.0460	.730	.0363	-.0182
.220	.0461	-.0465	.740	.0354	-.0166
.230	.0466	-.0470	.750	.0345	-.0150
.240	.0470	-.0474	.760	.0336	-.0134
.250	.0474	-.0478	.770	.0326	-.0118
.260	.0478	-.0481	.780	.0316	-.0102
.270	.0481	-.0484	.790	.0306	-.0087
.280	.0484	-.0487	.800	.0296	-.0072
.290	.0487	-.0489	.810	.0285	-.0058
.300	.0489	-.0491	.820	.0274	-.0044
.310	.0491	-.0493	.830	.0263	-.0031
.320	.0493	-.0494	.840	.0252	-.0018
.330	.0495	-.0495	.850	.0241	-.0006
.340	.0496	-.0496	.860	.0229	.0005
.350	.0497	-.0497	.870	.0217	.0015
.360	.0498	-.0497	.880	.0205	.0024
.370	.0499	-.0497	.890	.0193	.0031
.380	.0500	-.0497	.900	.0180	.0037
.390	.0500	-.0496	.910	.0167	.0041
.400	.0500	-.0495	.920	.0154	.0043
.410	.0500	-.0494	.930	.0141	.0043
.420	.0500	-.0492	.940	.0127	.0041
.430	.0500	-.0490	.950	.0113	.0037
.440	.0499	-.0488	.960	.0098	.0031
.450	.0498	-.0485	.970	.0083	.0023
.460	.0497	-.0482	.980	.0067	.0012
.470	.0496	-.0478	.990	.0050	-.0001
.480	.0494	-.0474	1.000	.0032	-.0017
.490	.0492	-.0470			

Table XII. Coordinates of 10-Percent-Thick Supercritical Airfoil SC(2)-0610
Designed for 0.6 Lift Coefficient
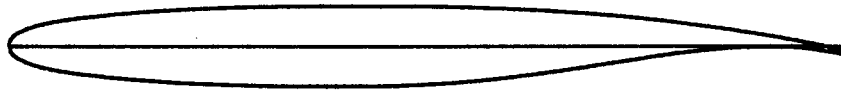
x/c	$(y/c)_u$	$(y/c)_l$	x/c	$(y/c)_u$	$(y/c)_l$
0.000	0.0000	0.0000	.500	.0488	-.0465
.002	.0076	-.0076	.510	.0486	-.0459
.005	.0116	-.0116	.520	.0483	-.0453
.010	.0155	-.0155	.530	.0480	-.0446
.020	.0206	-.0206	.540	.0477	-.0439
.030	.0241	-.0241	.550	.0474	-.0431
.040	.0268	-.0268	.560	.0470	-.0422
.050	.0290	-.0290	.570	.0466	-.0412
.060	.0309	-.0309	.580	.0462	-.0401
.070	.0326	-.0326	.590	.0458	-.0390
.080	.0341	-.0341	.600	.0453	-.0378
.090	.0355	-.0355	.610	.0448	-.0366
.100	.0367	-.0367	.620	.0443	-.0353
.110	.0378	-.0379	.630	.0438	-.0340
.120	.0389	-.0390	.640	.0432	-.0327
.130	.0399	-.0400	.650	.0426	-.0313
.140	.0408	-.0409	.660	.0419	-.0299
.150	.0417	-.0418	.670	.0412	-.0284
.160	.0425	-.0426	.680	.0405	-.0269
.170	.0432	-.0433	.690	.0397	-.0254
.180	.0439	-.0440	.700	.0389	-.0238
.190	.0445	-.0446	.710	.0381	-.0222
.200	.0451	-.0452	.720	.0372	-.0206
.210	.0456	-.0458	.730	.0363	-.0190
.220	.0461	-.0463	.740	.0353	-.0174
.230	.0466	-.0468	.750	.0343	-.0158
.240	.0470	-.0472	.760	.0332	-.0142
.250	.0474	-.0476	.770	.0321	-.0126
.260	.0478	-.0480	.780	.0309	-.0111
.270	.0481	-.0483	.790	.0297	-.0096
.280	.0484	-.0486	.800	.0285	-.0081
.290	.0487	-.0489	.810	.0272	-.0068
.300	.0489	-.0491	.820	.0259	-.0056
.310	.0491	-.0493	.830	.0245	-.0045
.320	.0493	-.0495	.840	.0231	-.0035
.330	.0495	-.0496	.850	.0216	-.0026
.340	.0496	-.0497	.860	.0201	-.0018
.350	.0497	-.0498	.870	.0185	-.0012
.360	.0498	-.0498	.880	.0169	-.0007
.370	.0499	-.0498	.890	.0153	-.0004
.380	.0500	-.0498	.900	.0136	-.0003
.390	.0500	-.0497	.910	.0119	-.0004
.400	.0500	-.0496	.920	.0101	-.0007
.410	.0500	-.0495	.930	.0083	-.0012
.420	.0500	-.0493	.940	.0064	-.0020
.430	.0499	-.0491	.950	.0045	-.0030
.440	.0498	-.0489	.960	.0025	-.0042
.450	.0497	-.0486	.970	.0004	-.0056
.460	.0496	-.0483	.980	-.0018	-.0073
.470	.0494	-.0479	.990	-.0042	-.0093
.480	.0492	-.0475	1.000	-.0067	-.0116
.490	.0490	-.0470			

Table XIII. Coordinates of 10-Percent-Thick Supercritical Airfoil SC(2)-0710 Designed for 0.7 Lift Coefficient
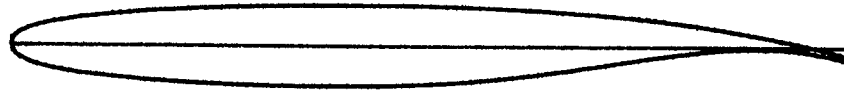
x/c	$(y/c)_u$	$(y/c)_l$	x/c	$(y/c)_u$	$(y/c)_l$
0.000	0.0000	0.0000	.500	.0487	-.0465
.002	.0076	-.0076	.510	.0484	-.0459
.005	.0116	-.0116	.520	.0481	-.0453
.010	.0155	-.0155	.530	.0478	-.0446
.020	.0206	-.0206	.540	.0475	-.0438
.030	.0240	-.0240	.550	.0471	-.0430
.040	.0267	-.0267	.560	.0467	-.0421
.050	.0289	-.0289	.570	.0463	-.0411
.060	.0308	-.0308	.580	.0459	-.0401
.070	.0325	-.0325	.590	.0454	-.0390
.080	.0340	-.0340	.600	.0449	-.0379
.090	.0354	-.0354	.610	.0444	-.0367
.100	.0366	-.0366	.620	.0439	-.0355
.110	.0378	-.0378	.630	.0433	-.0342
.120	.0389	-.0389	.640	.0427	-.0329
.130	.0399	-.0399	.650	.0421	-.0315
.140	.0408	-.0408	.660	.0414	-.0301
.150	.0417	-.0417	.670	.0407	-.0287
.160	.0425	-.0425	.680	.0400	-.0272
.170	.0432	-.0432	.690	.0393	-.0257
.180	.0439	-.0439	.700	.0385	-.0242
.190	.0445	-.0446	.710	.0377	-.0226
.200	.0451	-.0452	.720	.0368	-.0210
.210	.0457	-.0458	.730	.0359	-.0194
.220	.0462	-.0463	.740	.0349	-.0178
.230	.0467	-.0468	.750	.0339	-.0162
.240	.0471	-.0472	.760	.0328	-.0147
.250	.0475	-.0476	.770	.0317	-.0132
.260	.0479	-.0480	.780	.0305	-.0117
.270	.0482	-.0483	.790	.0292	-.0103
.280	.0485	-.0486	.800	.0279	-.0089
.290	.0488	-.0489	.810	.0265	-.0076
.300	.0490	-.0491	.820	.0250	-.0064
.310	.0492	-.0493	.830	.0235	-.0053
.320	.0494	-.0495	.840	.0219	-.0044
.330	.0496	-.0496	.850	.0203	-.0036
.340	.0497	-.0497	.860	.0186	-.0030
.350	.0498	-.0498	.870	.0169	-.0026
.360	.0499	-.0498	.880	.0151	-.0023
.370	.0500	-.0498	.890	.0133	-.0022
.380	.0500	-.0498	.900	.0114	-.0023
.390	.0500	-.0497	.910	.0095	-.0026
.400	.0500	-.0496	.920	.0075	-.0032
.410	.0500	-.0495	.930	.0054	-.0040
.420	.0499	-.0493	.940	.0033	-.0050
.430	.0498	-.0491	.950	.0011	-.0063
.440	.0497	-.0489	.960	-.0012	-.0078
.450	.0496	-.0486	.970	-.0036	-.0096
.460	.0495	-.0483	.980	-.0062	-.0117
.470	.0493	-.0479	.990	-.0090	-.0141
.480	.0491	-.0475	1.000	-.0119	-.0168
.490	.0489	-.0470			

Table XIV. Coordinates of 10-Percent-Thick Supercritical Airfoil SC(2)-1010 Designed for 1.0 Lift Coefficient
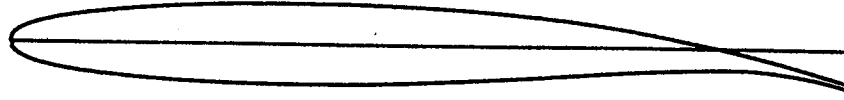
x/c	$(y/c)_u$	$(y/c)_l$	x/c	$(y/c)_u$	$(y/c)_l$
0.000	0.0000	0.0000	.500	.0455	-.0454
.002	.0076	-.0076	.510	.0449	-.0449
.005	.0116	-.0116	.520	.0443	-.0444
.010	.0156	-.0156	.530	.0437	-.0439
.020	.0207	-.0207	.540	.0430	-.0434
.030	.0242	-.0242	.550	.0423	-.0428
.040	.0270	-.0270	.560	.0416	-.0422
.050	.0294	-.0294	.570	.0408	-.0416
.060	.0315	-.0314	.580	.0400	-.0410
.070	.0333	-.0332	.590	.0391	-.0404
.080	.0349	-.0348	.600	.0382	-.0398
.090	.0364	-.0362	.610	.0373	-.0392
.100	.0378	-.0375	.620	.0363	-.0386
.110	.0390	-.0387	.630	.0353	-.0380
.120	.0401	-.0398	.640	.0342	-.0374
.130	.0412	-.0408	.650	.0330	-.0367
.140	.0422	-.0418	.660	.0318	-.0360
.150	.0431	-.0427	.670	.0305	-.0353
.160	.0439	-.0435	.680	.0292	-.0346
.170	.0447	-.0443	.690	.0278	-.0339
.180	.0454	-.0450	.700	.0264	-.0332
.190	.0460	-.0457	.710	.0249	-.0325
.200	.0466	-.0463	.720	.0233	-.0319
.210	.0471	-.0468	.730	.0217	-.0313
.220	.0476	-.0473	.740	.0200	-.0307
.230	.0480	-.0478	.750	.0183	-.0301
.240	.0484	-.0482	.760	.0165	-.0295
.250	.0487	-.0486	.770	.0147	-.0290
.260	.0490	-.0489	.780	.0128	-.0285
.270	.0493	-.0492	.790	.0109	-.0280
.280	.0495	-.0494	.800	.0089	-.0276
.290	.0497	-.0496	.810	.0069	-.0272
.300	.0498	-.0498	.820	.0048	-.0269
.310	.0499	-.0499	.830	.0027	-.0266
.320	.0500	-.0500	.840	.0005	-.0264
.330	.0500	-.0500	.850	-.0017	-.0263
.340	.0500	-.0500	.860	-.0040	-.0264
.350	.0500	-.0500	.870	-.0063	-.0267
.360	.0499	-.0499	.880	-.0087	-.0271
.370	.0498	-.0498	.890	-.0111	-.0277
.380	.0497	-.0496	.900	-.0136	-.0285
.390	.0495	-.0494	.910	-.0161	-.0295
.400	.0493	-.0492	.920	-.0187	-.0307
.410	.0491	-.0489	.930	-.0214	-.0321
.420	.0488	-.0486	.940	-.0241	-.0337
.430	.0485	-.0483	.950	-.0269	-.0355
.440	.0482	-.0480	.960	-.0298	-.0375
.450	.0478	-.0476	.970	-.0327	-.0398
.460	.0474	-.0472	.980	-.0357	-.0423
.470	.0470	-.0468	.990	-.0388	-.0451
.480	.0465	-.0464	1.000	-.0420	-.0481
.490	.0460	-.0459			

Table XV. Coordinates of 12-Percent-Thick Symmetrical Supercritical Airfoil SC(2)-0012
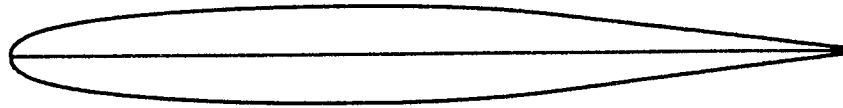
x/c	$(y/c)_u$	$(y/c)_l$	x/c	$(y/c)_u$	$(y/c)_l$
0.000	0.00000	0.00000	.500	.05808	-.05808
.002	.00912	-.00912	.510	.05772	-.05772
.005	.01392	-.01392	.520	.05736	-.05736
.010	.01860	-.01860	.530	.05688	-.05688
.020	.02484	-.02484	.540	.05640	-.05640
.030	.02916	-.02916	.550	.05580	-.05580
.040	.03240	-.03240	.560	.05520	-.05520
.050	.03504	-.03504	.570	.05460	-.05460
.060	.03732	-.03732	.580	.05388	-.05388
.070	.03939	-.03939	.590	.05316	-.05316
.080	.04119	-.04119	.600	.05232	-.05232
.090	.04282	-.04282	.610	.05136	-.05136
.100	.04428	-.04428	.620	.05040	-.05040
.110	.04560	-.04560	.630	.04932	-.04932
.120	.04680	-.04680	.640	.04824	-.04824
.130	.04800	-.04800	.650	.04704	-.04704
.140	.04908	-.04908	.660	.04584	-.04584
.150	.05004	-.05004	.670	.04458	-.04458
.160	.05100	-.05100	.680	.04332	-.04332
.170	.05184	-.05184	.690	.04206	-.04206
.180	.05268	-.05268	.700	.04080	-.04080
.190	.05340	-.05340	.710	.03954	-.03954
.200	.05412	-.05412	.720	.03828	-.03828
.210	.05472	-.05472	.730	.03702	-.03702
.220	.05532	-.05532	.740	.03576	-.03576
.230	.05592	-.05592	.750	.03450	-.03450
.240	.05640	-.05640	.760	.03324	-.03324
.250	.05688	-.05688	.770	.03198	-.03198
.260	.05736	-.05736	.780	.03072	-.03072
.270	.05772	-.05772	.790	.02946	-.02946
.280	.05808	-.05808	.800	.02820	-.02820
.290	.05844	-.05844	.810	.02694	-.02694
.300	.05880	-.05880	.820	.02568	-.02568
.310	.05904	-.05904	.830	.02442	-.02442
.320	.05928	-.05928	.840	.02316	-.02316
.330	.05952	-.05952	.850	.02190	-.02190
.340	.05964	-.05964	.860	.02064	-.02064
.350	.05976	-.05976	.870	.01938	-.01938
.360	.05988	-.05988	.880	.01812	-.01812
.370	.06000	-.06000	.890	.01686	-.01686
.380	.06000	-.06000	.900	.01560	-.01560
.390	.06000	-.06000	.910	.01434	-.01434
.400	.06000	-.06000	.920	.01308	-.01308
.410	.06000	-.06000	.930	.01182	-.01182
.420	.05988	-.05988	.940	.01056	-.01056
.430	.05976	-.05976	.950	.00930	-.00930
.440	.05964	-.05964	.960	.00804	-.00804
.450	.05952	-.05952	.970	.00678	-.00678
.460	.05928	-.05928	.980	.00552	-.00552
.470	.05904	-.05904	.990	.00426	-.00426
.480	.05880	-.05880	1.000	.00300	-.00300
.490	.05844	-.05844			

Table XVI. Coordinates of 12-Percent-Thick Supercritical Airfoil SC(2)-0412 Designed for 0.4 Lift Coefficient
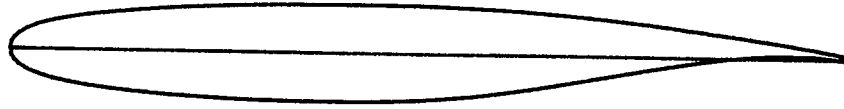
x/c	$(y/c)_u$	$(y/c)_l$	x/c	$(y/c)_u$	$(y/c)_l$
0.000	0.0000	0.0000	.500	.0588	−.0555
.002	.0092	−.0092	.510	.0585	−.0547
.005	.0141	−.0141	.520	.0582	−.0539
.010	.0190	−.0190	.530	.0578	−.0530
.020	.0253	−.0253	.540	.0574	−.0520
.030	.0297	−.0296	.550	.0570	−.0509
.040	.0330	−.0329	.560	.0565	−.0498
.050	.0357	−.0356	.570	.0560	−.0486
.060	.0380	−.0379	.580	.0555	−.0473
.070	.0400	−.0400	.590	.0549	−.0459
.080	.0418	−.0418	.600	.0543	−.0444
.090	.0434	−.0434	.610	.0536	−.0429
.100	.0448	−.0449	.620	.0529	−.0413
.110	.0461	−.0463	.630	.0522	−.0397
.120	.0473	−.0476	.640	.0514	−.0380
.130	.0484	−.0488	.650	.0506	−.0362
.140	.0494	−.0499	.660	.0497	−.0344
.150	.0504	−.0509	.670	.0488	−.0326
.160	.0513	−.0518	.680	.0479	−.0307
.170	.0522	−.0527	.690	.0469	−.0288
.180	.0530	−.0535	.700	.0459	−.0269
.190	.0537	−.0542	.710	.0449	−.0250
.200	.0544	−.0549	.720	.0439	−.0231
.210	.0550	−.0555	.730	.0428	−.0212
.220	.0556	−.0561	.740	.0417	−.0193
.230	.0562	−.0567	.750	.0406	−.0174
.240	.0567	−.0572	.760	.0394	−.0155
.250	.0571	−.0577	.770	.0382	−.0137
.260	.0575	−.0581	.780	.0370	−.0119
.270	.0579	−.0585	.790	.0358	−.0102
.280	.0583	−.0588	.800	.0345	−.0085
.290	.0586	−.0591	.810	.0332	−.0068
.300	.0589	−.0593	.820	.0319	−.0052
.310	.0591	−.0595	.830	.0306	−.0037
.320	.0593	−.0597	.840	.0292	−.0023
.330	.0595	−.0598	.850	.0278	−.0009
.340	.0597	−.0599	.860	.0264	.0003
.350	.0598	−.0600	.870	.0250	.0014
.360	.0599	−.0600	.880	.0235	.0024
.370	.0600	−.0600	.890	.0220	.0032
.380	.0601	−.0599	.900	.0205	.0038
.390	.0601	−.0598	.910	.0190	.0043
.400	.0601	−.0596	.920	.0174	.0045
.410	.0601	−.0594	.930	.0158	.0045
.420	.0601	−.0592	.940	.0142	.0042
.430	.0600	−.0589	.950	.0125	.0038
.440	.0599	−.0586	.960	.0108	.0031
.450	.0598	−.0582	.970	.0090	.0022
.460	.0597	−.0578	.980	.0072	.0010
.470	.0595	−.0573	.990	.0053	−.0005
.480	.0593	−.0568	1.000	.0033	−.0022
.490	.0591	−.0562			

Table XVII. Coordinates of 12-Percent-Thick Supercritical Airfoil SC(2)-0612 Designed for 0.6 Lift Coefficient

x/c	$(y/c)_u$	$(y/c)_l$	x/c	$(y/c)_u$	$(y/c)_l$
0.000	0.0000	0.0000	.500	.0586	-.0554
.002	.0092	-.0092	.510	.0583	-.0546
.005	.0141	-.0141	.520	.0580	-.0538
.010	.0190	-.0190	.530	.0576	-.0529
.020	.0252	-.0252	.540	.0572	-.0519
.030	.0296	-.0296	.550	.0568	-.0509
.040	.0329	-.0329	.560	.0563	-.0497
.050	.0355	-.0355	.570	.0558	-.0485
.060	.0378	-.0378	.580	.0553	-.0472
.070	.0398	-.0398	.590	.0547	-.0458
.080	.0416	-.0416	.600	.0541	-.0444
.090	.0432	-.0432	.610	.0534	-.0429
.100	.0447	-.0447	.620	.0527	-.0414
.110	.0460	-.0460	.630	.0520	-.0398
.120	.0472	-.0473	.640	.0512	-.0382
.130	.0484	-.0485	.650	.0504	-.0365
.140	.0495	-.0496	.660	.0495	-.0348
.150	.0505	-.0506	.670	.0486	-.0330
.160	.0514	-.0515	.680	.0476	-.0312
.170	.0523	-.0524	.690	.0466	-.0294
.180	.0531	-.0532	.700	.0456	-.0276
.190	.0538	-.0540	.710	.0445	-.0258
.200	.0545	-.0547	.720	.0434	-.0240
.210	.0551	-.0554	.730	.0422	-.0222
.220	.0557	-.0560	.740	.0410	-.0204
.230	.0563	-.0565	.750	.0397	-.0186
.240	.0568	-.0570	.760	.0384	-.0168
.250	.0573	-.0575	.770	.0371	-.0150
.260	.0577	-.0579	.780	.0357	-.0133
.270	.0581	-.0583	.790	.0343	-.0117
.280	.0585	-.0586	.800	.0328	-.0102
.290	.0588	-.0589	.810	.0313	-.0087
.300	.0591	-.0592	.820	.0297	-.0073
.310	.0593	-.0594	.830	.0281	-.0060
.320	.0595	-.0595	.840	.0265	-.0048
.330	.0597	-.0596	.850	.0248	-.0037
.340	.0599	-.0597	.860	.0231	-.0028
.350	.0600	-.0598	.870	.0213	-.0021
.360	.0601	-.0598	.880	.0195	-.0016
.370	.0602	-.0598	.890	.0176	-.0012
.380	.0602	-.0598	.900	.0157	-.0010
.390	.0602	-.0597	.910	.0137	-.0010
.400	.0602	-.0596	.920	.0117	-.0013
.410	.0602	-.0594	.930	.0096	-.0018
.420	.0601	-.0592	.940	.0075	-.0025
.430	.0600	-.0589	.950	.0053	-.0035
.440	.0599	-.0586	.960	.0031	-.0048
.450	.0598	-.0582	.970	.0008	-.0063
.460	.0596	-.0578	.980	-.0016	-.0081
.470	.0594	-.0573	.990	-.0041	-.0102
.480	.0592	-.0567	1.000	-.0067	-.0125
.490	.0589	-.0561			

Table XVIII. Coordinates of 12-Percent-Thick Supercritical Airfoil SC(2)-0712 Designed for 0.7 Lift Coefficient
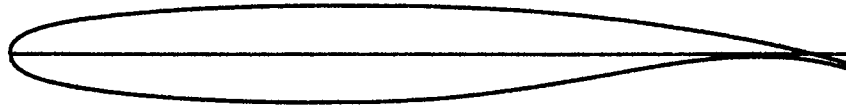
x/c	$(y/c)_u$	$(y/c)_l$	x/c	$(y/c)_u$	$(y/c)_l$
0.000	0.0000	0.0000	.500	.0584	-.0554
.002	.0092	-.0092	.510	.0581	-.0546
.005	.0141	-.0141	.520	.0577	-.0537
.010	.0190	-.0190	.530	.0573	-.0528
.020	.0252	-.0252	.540	.0569	-.0518
.030	.0294	-.0294	.550	.0564	-.0508
.040	.0327	-.0327	.560	.0559	-.0496
.050	.0354	-.0353	.570	.0554	-.0484
.060	.0377	-.0376	.580	.0549	-.0471
.070	.0397	-.0396	.590	.0543	-.0457
.080	.0415	-.0414	.600	.0537	-.0443
.090	.0431	-.0430	.610	.0530	-.0429
.100	.0446	-.0445	.620	.0523	-.0414
.110	.0459	-.0459	.630	.0516	-.0398
.120	.0471	-.0472	.640	.0508	-.0382
.130	.0483	-.0484	.650	.0500	-.0366
.140	.0494	-.0495	.660	.0491	-.0349
.150	.0504	-.0505	.670	.0482	-.0332
.160	.0513	-.0514	.680	.0472	-.0315
.170	.0522	-.0523	.690	.0462	-.0298
.180	.0530	-.0531	.700	.0451	-.0280
.190	.0537	-.0539	.710	.0440	-.0262
.200	.0544	-.0546	.720	.0428	-.0244
.210	.0551	-.0553	.730	.0416	-.0226
.220	.0557	-.0559	.740	.0403	-.0208
.230	.0562	-.0564	.750	.0390	-.0191
.240	.0567	-.0569	.760	.0376	-.0174
.250	.0572	-.0574	.770	.0362	-.0157
.260	.0576	-.0578	.780	.0347	-.0141
.270	.0580	-.0582	.790	.0332	-.0125
.280	.0584	-.0585	.800	.0316	-.0110
.290	.0587	-.0588	.810	.0300	-.0095
.300	.0590	-.0591	.820	.0283	-.0082
.310	.0592	-.0593	.830	.0266	-.0070
.320	.0594	-.0595	.840	.0248	-.0059
.330	.0596	-.0596	.850	.0230	-.0050
.340	.0598	-.0597	.860	.0211	-.0043
.350	.0599	-.0598	.870	.0192	-.0038
.360	.0600	-.0598	.880	.0172	-.0035
.370	.0601	-.0598	.890	.0152	-.0033
.380	.0601	-.0598	.900	.0131	-.0034
.390	.0601	-.0597	.910	.0110	-.0036
.400	.0601	-.0596	.920	.0088	-.0041
.410	.0601	-.0594	.930	.0065	-.0049
.420	.0600	-.0592	.940	.0042	-.0059
.430	.0599	-.0589	.950	.0018	-.0072
.440	.0598	-.0586	.960	-.0007	-.0087
.450	.0596	-.0582	.970	-.0033	-.0105
.460	.0594	-.0578	.980	-.0060	-.0126
.470	.0592	-.0573	.990	-.0088	-.0150
.480	.0590	-.0567	1.000	-.0117	-.0177
.490	.0587	-.0561			

Table XIX. Coordinates of 14-Percent-Thick Supercritical Airfoil SC(2)-0414 Designed for 0.4 Lift Coefficient
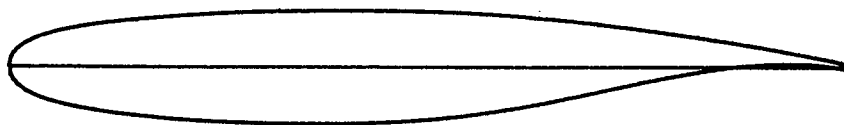
x/c	$(y/c)_u$	$(y/c)_l$	x/c	$(y/c)_u$	$(y/c)_l$
0.000	0.0000	0.0000	.500	.0684	-.0642
.002	.0108	-.0108	.510	.0680	-.0633
.005	.0166	-.0166	.520	.0676	-.0623
.010	.0225	-.0225	.530	.0672	-.0612
.020	.0299	-.0299	.540	.0667	-.0600
.030	.0350	-.0350	.550	.0662	-.0587
.040	.0389	-.0389	.560	.0656	-.0573
.050	.0421	-.0421	.570	.0650	-.0558
.060	.0448	-.0448	.580	.0643	-.0543
.070	.0471	-.0472	.590	.0636	-.0527
.080	.0491	-.0493	.600	.0628	-.0510
.090	.0510	-.0512	.610	.0620	-.0492
.100	.0527	-.0529	.620	.0611	-.0474
.110	.0542	-.0545	.630	.0602	-.0455
.120	.0556	-.0560	.640	.0593	-.0435
.130	.0569	-.0573	.650	.0583	-.0415
.140	.0581	-.0585	.660	.0573	-.0394
.150	.0592	-.0597	.670	.0562	-.0373
.160	.0602	-.0608	.680	.0551	-.0352
.170	.0612	-.0618	.690	.0540	-.0330
.180	.0621	-.0627	.700	.0528	-.0308
.190	.0629	-.0636	.710	.0516	-.0286
.200	.0637	-.0644	.720	.0503	-.0264
.210	.0644	-.0651	.730	.0490	-.0242
.220	.0651	-.0658	.740	.0477	-.0220
.230	.0657	-.0664	.750	.0464	-.0198
.240	.0663	-.0670	.760	.0450	-.0177
.250	.0668	-.0675	.770	.0436	-.0156
.260	.0673	-.0680	.780	.0422	-.0136
.270	.0677	-.0684	.790	.0407	-.0116
.280	.0681	-.0688	.800	.0392	-.0097
.290	.0685	-.0691	.810	.0377	-.0078
.300	.0688	-.0694	.820	.0362	-.0060
.310	.0691	-.0696	.830	.0346	-.0043
.320	.0693	-.0698	.840	.0330	-.0027
.330	.0695	-.0699	.850	.0314	-.0012
.340	.0697	-.0700	.860	.0298	.0001
.350	.0699	-.0700	.870	.0281	.0013
.360	.0700	-.0700	.880	.0264	.0023
.370	.0701	-.0699	.890	.0247	.0032
.380	.0702	-.0698	.900	.0229	.0039
.390	.0702	-.0697	.910	.0211	.0044
.400	.0702	-.0695	.920	.0193	.0046
.410	.0702	-.0693	.930	.0175	.0046
.420	.0701	-.0690	.940	.0156	.0043
.430	.0700	-.0686	.950	.0137	.0038
.440	.0699	-.0682	.960	.0117	.0031
.450	.0697	-.0677	.970	.0097	.0021
.460	.0695	-.0672	.980	.0076	.0008
.470	.0693	-.0666	.990	.0055	-.0008
.480	.0690	-.0659	1.000	.0033	-.0027
.490	.0687	-.0651			

Table XX. Coordinates of 14-Percent-Thick Supercritical Airfoil SC(2)-0614
Designed for 0.6 Lift Coefficient
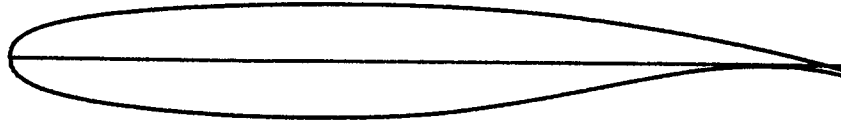
x/c	$(y/c)_u$	$(y/c)_l$	x/c	$(y/c)_u$	$(y/c)_l$
0.000	0.0000	0.0000	.500	.0681	-.0642
.002	.0108	-.0108	.510	.0677	-.0632
.005	.0166	-.0166	.520	.0673	-.0622
.010	.0225	-.0225	.530	.0669	-.0611
.020	.0298	-.0298	.540	.0664	-.0599
.030	.0349	-.0349	.550	.0659	-.0586
.040	.0387	-.0388	.560	.0653	-.0572
.050	.0418	-.0419	.570	.0647	-.0557
.060	.0445	-.0446	.580	.0640	-.0541
.070	.0468	-.0469	.590	.0633	-.0525
.080	.0489	-.0490	.600	.0626	-.0508
.090	.0508	-.0509	.610	.0618	-.0491
.100	.0525	-.0526	.620	.0610	-.0473
.110	.0541	-.0542	.630	.0601	-.0455
.120	.0555	-.0557	.640	.0591	-.0436
.130	.0568	-.0570	.650	.0581	-.0417
.140	.0580	-.0582	.660	.0570	-.0397
.150	.0591	-.0594	.670	.0559	-.0377
.160	.0602	-.0605	.680	.0547	-.0356
.170	.0612	-.0615	.690	.0535	-.0336
.180	.0621	-.0624	.700	.0522	-.0315
.190	.0629	-.0633	.710	.0509	-.0294
.200	.0637	-.0641	.720	.0495	-.0274
.210	.0644	-.0648	.730	.0481	-.0253
.220	.0651	-.0655	.740	.0466	-.0233
.230	.0657	-.0661	.750	.0451	-.0213
.240	.0663	-.0667	.760	.0436	-.0193
.250	.0668	-.0672	.770	.0420	-.0174
.260	.0673	-.0677	.780	.0404	-.0155
.270	.0678	-.0681	.790	.0387	-.0137
.280	.0682	-.0685	.800	.0370	-.0119
.290	.0686	-.0688	.810	.0352	-.0102
.300	.0689	-.0691	.820	.0334	-.0086
.310	.0692	-.0693	.830	.0316	-.0072
.320	.0694	-.0695	.840	.0297	-.0059
.330	.0696	-.0697	.850	.0278	-.0047
.340	.0698	-.0698	.860	.0258	-.0037
.350	.0699	-.0699	.870	.0238	-.0029
.360	.0700	-.0699	.880	.0218	-.0023
.370	.0701	-.0698	.890	.0197	-.0019
.380	.0701	-.0697	.900	.0176	-.0017
.390	.0701	-.0696	.910	.0154	-.0017
.400	.0701	-.0694	.920	.0132	-.0019
.410	.0700	-.0692	.930	.0109	-.0024
.420	.0699	-.0689	.940	.0086	-.0031
.430	.0698	-.0686	.950	.0062	-.0041
.440	.0696	-.0682	.960	.0038	-.0054
.450	.0694	-.0677	.970	.0013	-.0069
.460	.0692	-.0672	.980	-.0013	-.0087
.470	.0690	-.0666	.990	-.0039	-.0108
.480	.0687	-.0659	1.000	-.0066	-.0132
.490	.0684	-.0651			

Table XXI. Coordinates of 14-Percent-Thick Supercritical Airfoil SC(2)-0714 Designed for 0.7 Lift Coefficient
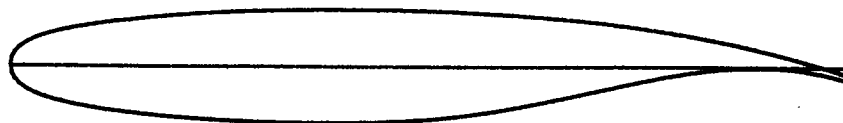
x/c	$(y/c)_u$	$(y/c)_l$	x/c	$(y/c)_u$	$(y/c)_l$
0.000	0.00000	0.00000	.500	.06800	-.06460
.002	.01077	-.01077	.510	.06760	-.06370
.005	.01658	-.01658	.520	.06720	-.06270
.010	.02240	-.02240	.530	.06680	-.06160
.020	.02960	-.02960	.540	.06630	-.06040
.030	.03460	-.03450	.550	.06580	-.05910
.040	.03830	-.03820	.560	.06530	-.05770
.050	.04140	-.04130	.570	.06470	-.05620
.060	.04400	-.04390	.580	.06410	-.05460
.070	.04630	-.04620	.590	.06350	-.05290
.080	.04840	-.04830	.600	.06280	-.05110
.090	.05020	-.05010	.610	.06210	-.04920
.100	.05190	-.05180	.620	.06130	-.04730
.110	.05350	-.05340	.630	.06050	-.04530
.120	.05490	-.05490	.640	.05970	-.04330
.130	.05620	-.05620	.650	.05880	-.04120
.140	.05740	-.05740	.660	.05790	-.03910
.150	.05860	-.05860	.670	.05690	-.03700
.160	.05970	-.05970	.680	.05590	-.03480
.170	.06070	-.06070	.690	.05480	-.03260
.180	.06160	-.06160	.700	.05370	-.03040
.190	.06250	-.06250	.710	.05250	-.02820
.200	.06330	-.06330	.720	.05130	-.02600
.210	.06410	-.06410	.730	.05000	-.02380
.220	.06480	-.06480	.740	.04870	-.02160
.230	.06540	-.06550	.750	.04730	-.01940
.240	.06600	-.06610	.760	.04580	-.01730
.250	.06650	-.06670	.770	.04430	-.01520
.260	.06700	-.06720	.780	.04270	-.01320
.270	.06750	-.06770	.790	.04110	-.01130
.280	.06790	-.06810	.800	.03940	-.00950
.290	.06830	-.06850	.810	.03760	-.00790
.300	.06860	-.06880	.820	.03580	-.00640
.310	.06890	-.06910	.830	.03390	-.00500
.320	.06920	-.06930	.840	.03190	-.00380
.330	.06940	-.06950	.850	.02990	-.00280
.340	.06960	-.06960	.860	.02780	-.00200
.350	.06970	-.06970	.870	.02560	-.00140
.360	.06980	-.06970	.880	.02340	-.00100
.370	.06990	-.06970	.890	.02110	-.00080
.380	.06990	-.06960	.900	.01870	-.00090
.390	.06990	-.06950	.910	.01620	-.00120
.400	.06990	-.06930	.920	.01370	-.00170
.410	.06980	-.06910	.930	.01110	-.00250
.420	.06970	-.06880	.940	.00840	-.00360
.430	.06960	-.06850	.950	.00560	-.00500
.440	.06950	-.06810	.960	.00270	-.00670
.450	.06930	-.06770	.970	-.00020	-.00870
.460	.06910	-.06720	.980	-.00320	-.01100
.470	.06890	-.06670	.990	-.00630	-.01360
.480	.06860	-.06610	1.000	-.00950	-.01650
.490	.06830	-.06540			

Table XXII. Coordinates of 18-Percent-Thick Supercritical Airfoil SC(2)-0518 Designed for 0.5 Lift Coefficient
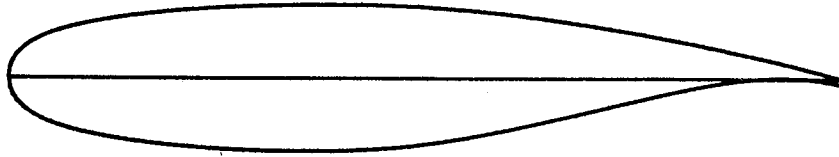
x/c	$(y/c)_u$	$(y/c)_l$	x/c	$(y/c)_u$	$(y/c)_l$
0.000	0.0000	0.0000	.500	.0867	-.0806
.002	.0139	-.0139	.510	.0860	-.0792
.005	.0213	-.0213	.520	.0853	-.0777
.010	.0291	-.0291	.530	.0845	-.0761
.020	.0389	-.0389	.540	.0837	-.0744
.030	.0456	-.0457	.550	.0828	-.0726
.040	.0508	-.0509	.560	.0819	-.0707
.050	.0550	-.0550	.570	.0809	-.0688
.060	.0585	-.0585	.580	.0798	-.0668
.070	.0615	-.0615	.590	.0787	-.0647
.080	.0642	-.0642	.600	.0775	-.0626
.090	.0666	-.0666	.610	.0763	-.0604
.100	.0687	-.0687	.620	.0750	-.0582
.110	.0707	-.0707	.630	.0737	-.0560
.120	.0725	-.0725	.640	.0724	-.0537
.130	.0742	-.0742	.650	.0710	-.0514
.140	.0757	-.0758	.660	.0696	-.0491
.150	.0771	-.0773	.670	.0681	-.0468
.160	.0784	-.0787	.680	.0666	-.0444
.170	.0796	-.0799	.690	.0650	-.0420
.180	.0807	-.0811	.700	.0634	-.0396
.190	.0818	-.0822	.710	.0618	-.0372
.200	.0828	-.0832	.720	.0601	-.0348
.210	.0837	-.0841	.730	.0584	-.0324
.220	.0845	-.0849	.740	.0566	-.0300
.230	.0853	-.0857	.750	.0548	-.0276
.240	.0860	-.0864	.760	.0530	-.0252
.250	.0866	-.0870	.770	.0511	-.0229
.260	.0872	-.0875	.780	.0492	-.0206
.270	.0877	-.0880	.790	.0473	-.0183
.280	.0882	-.0884	.800	.0453	-.0161
.290	.0886	-.0888	.810	.0433	-.0139
.300	.0890	-.0891	.820	.0413	-.0118
.310	.0893	-.0893	.830	.0392	-.0098
.320	.0896	-.0895	.840	.0371	-.0079
.330	.0898	-.0896	.850	.0350	-.0061
.340	.0900	-.0897	.860	.0328	-.0044
.350	.0901	-.0897	.870	.0306	-.0029
.360	.0902	-.0896	.880	.0284	-.0016
.370	.0903	-.0895	.890	.0262	-.0005
.380	.0903	-.0893	.900	.0239	.0003
.390	.0903	-.0890	.910	.0216	.0009
.400	.0902	-.0887	.920	.0193	.0012
.410	.0901	-.0883	.930	.0169	.0012
.420	.0899	-.0878	.940	.0145	.0009
.430	.0897	-.0872	.950	.0120	.0003
.440	.0894	-.0865	.960	.0094	-.0007
.450	.0891	-.0858	.970	.0068	-.0020
.460	.0887	-.0850	.980	.0041	-.0037
.470	.0883	-.0841	.990	.0014	-.0058
.480	.0878	-.0831	1.000	-.0014	-.0083
.490	.0873	-.0819			

Slotted (1964)

Integral (1966)

Integral with thickened trailing edge (1968)

Figure 1. Progression of supercritical airfoil shape.
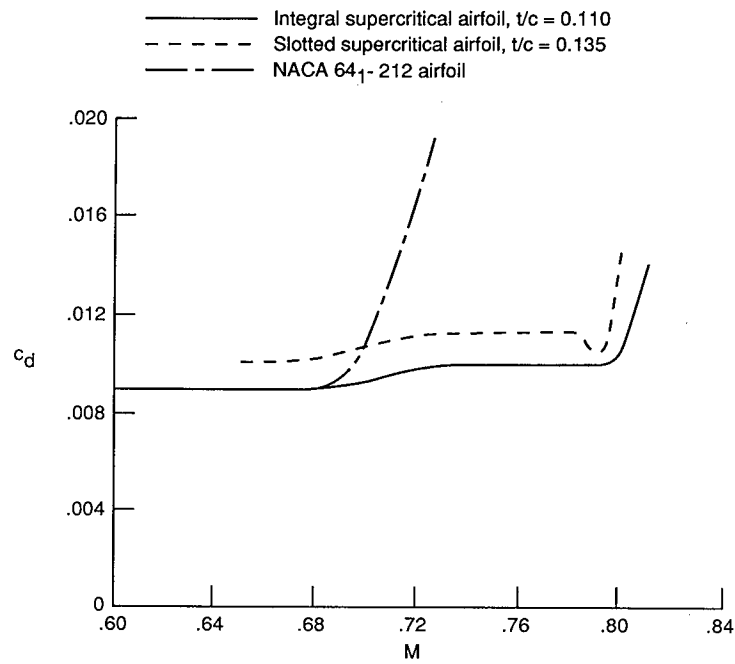
Figure 2. Variation of section drag coefficient with Mach number for section normal-force coefficient of 0.65.
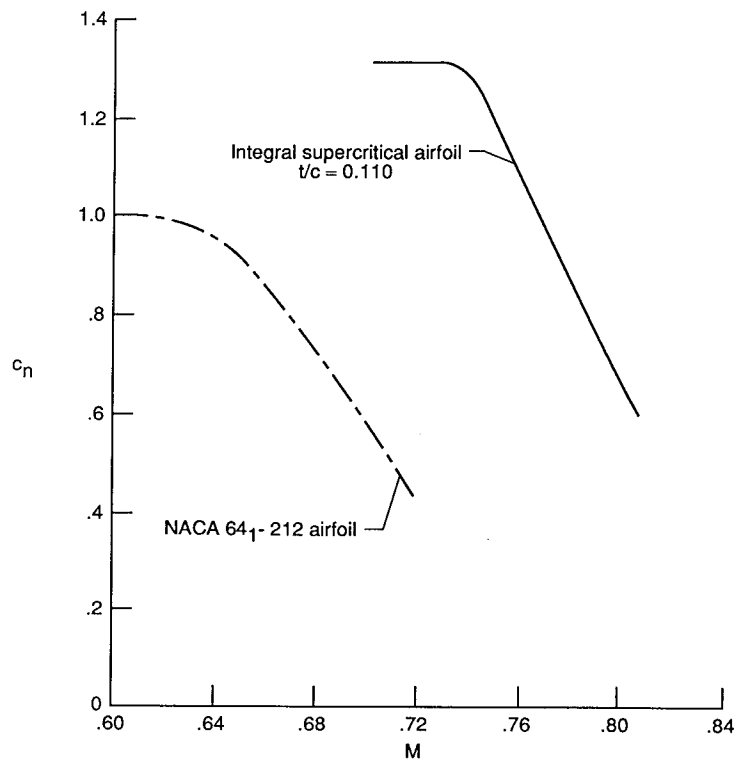
Figure 3. Variation of section normal-force coefficient with Mach number for onset of upper-surface boundary-layer separation.
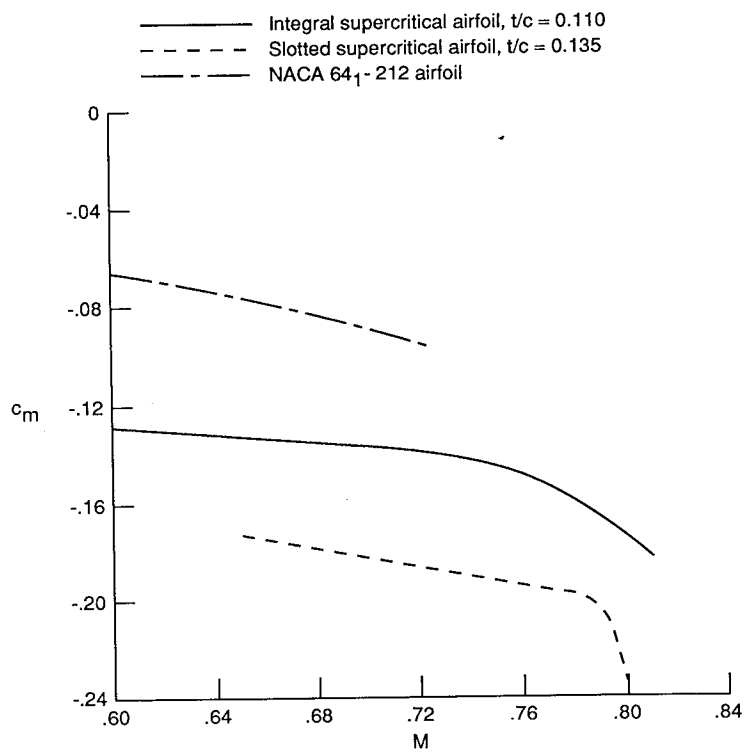
Figure 4. Variation of section pitching-moment coefficient with Mach number for section normal-force coefficient of 0.65.

Flow fields

Supersonic flow

Strong shock wave

Conventional airfoil

Separated boundary layer

Pressure distributions

Upper surface

$C_{p,sonic}$

C_p

−

+

Lower surface

Supercritical airfoil

Weak shock wave

C_p

−

+
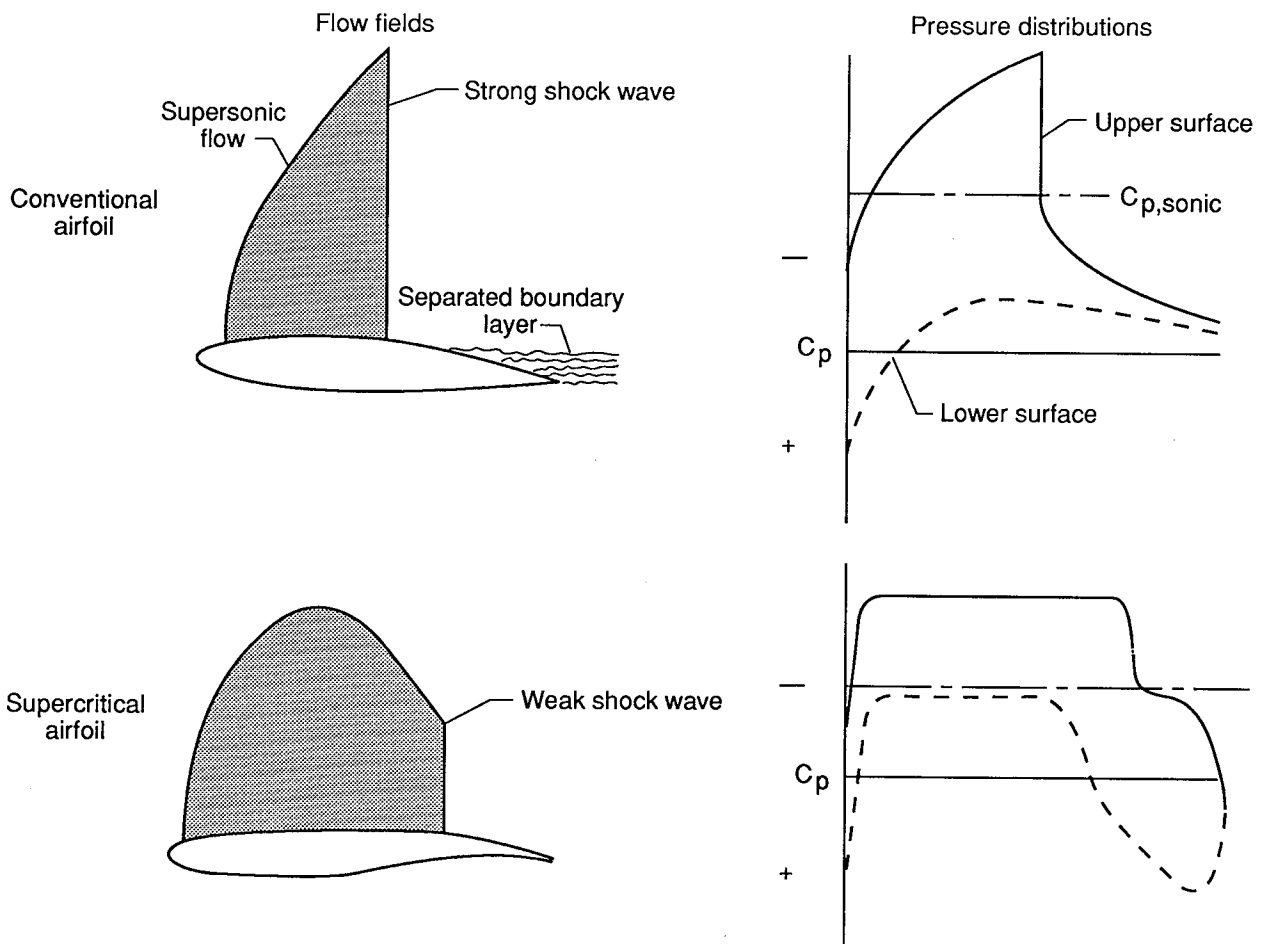
Figure 5. Flow fields around supercritical and conventional airfoils.

41
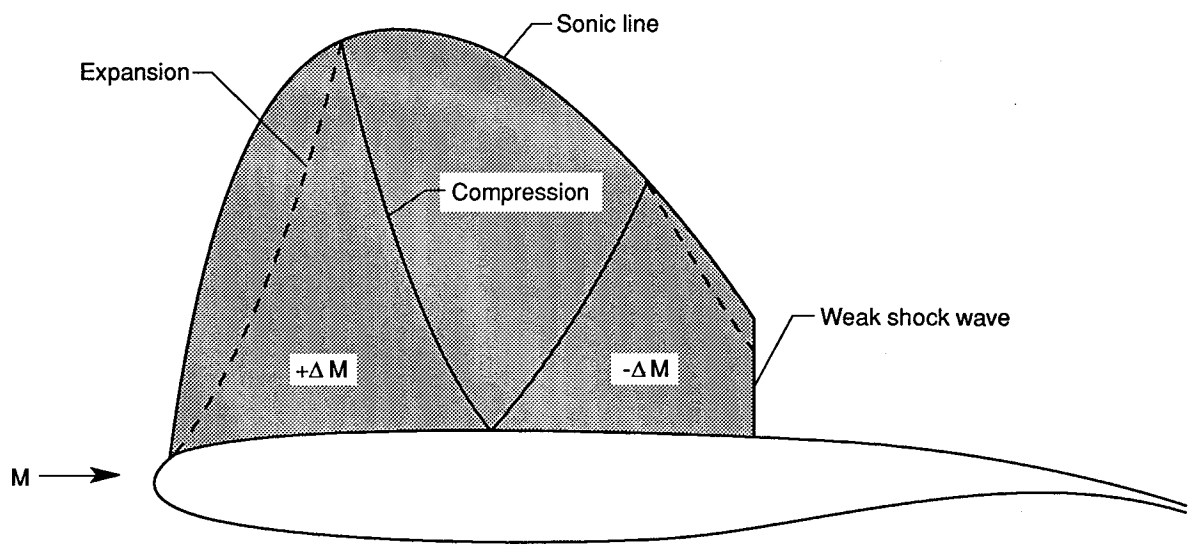
Figure 6. Schematic flow field of supercritical airfoil.
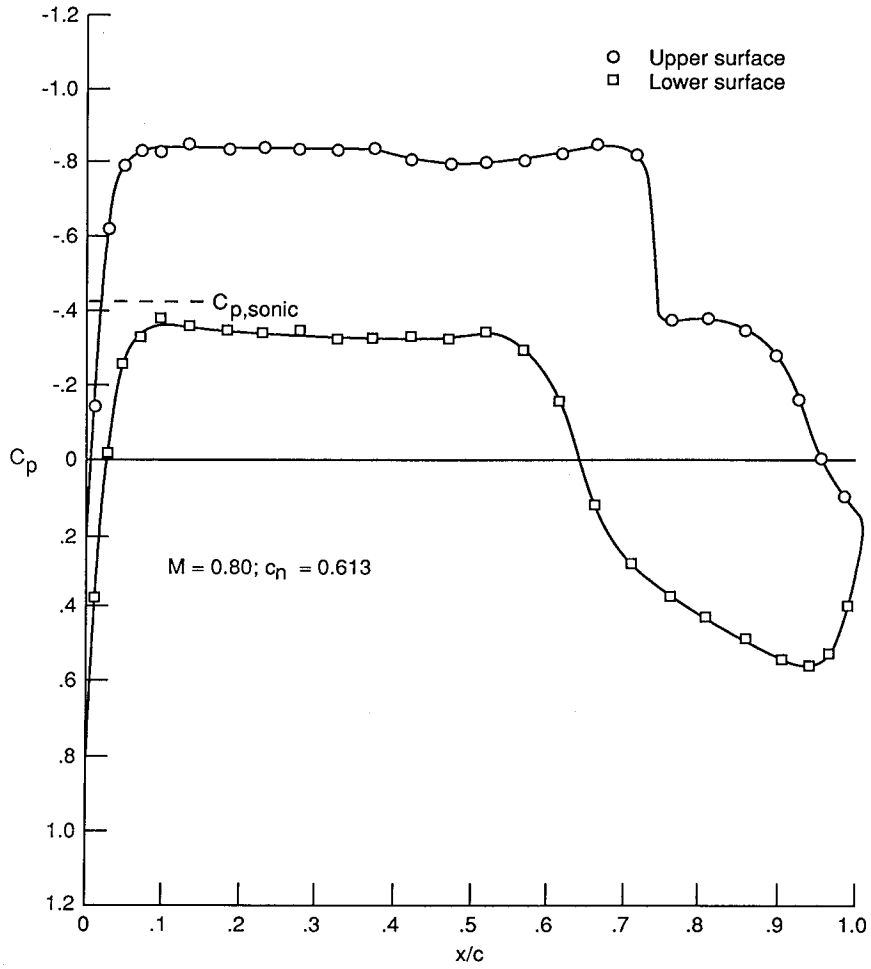
(a) Slightly above design Mach number.

Figure 7. Chordwise pressure distributions on 11-percent-thick integral supercritical airfoil.
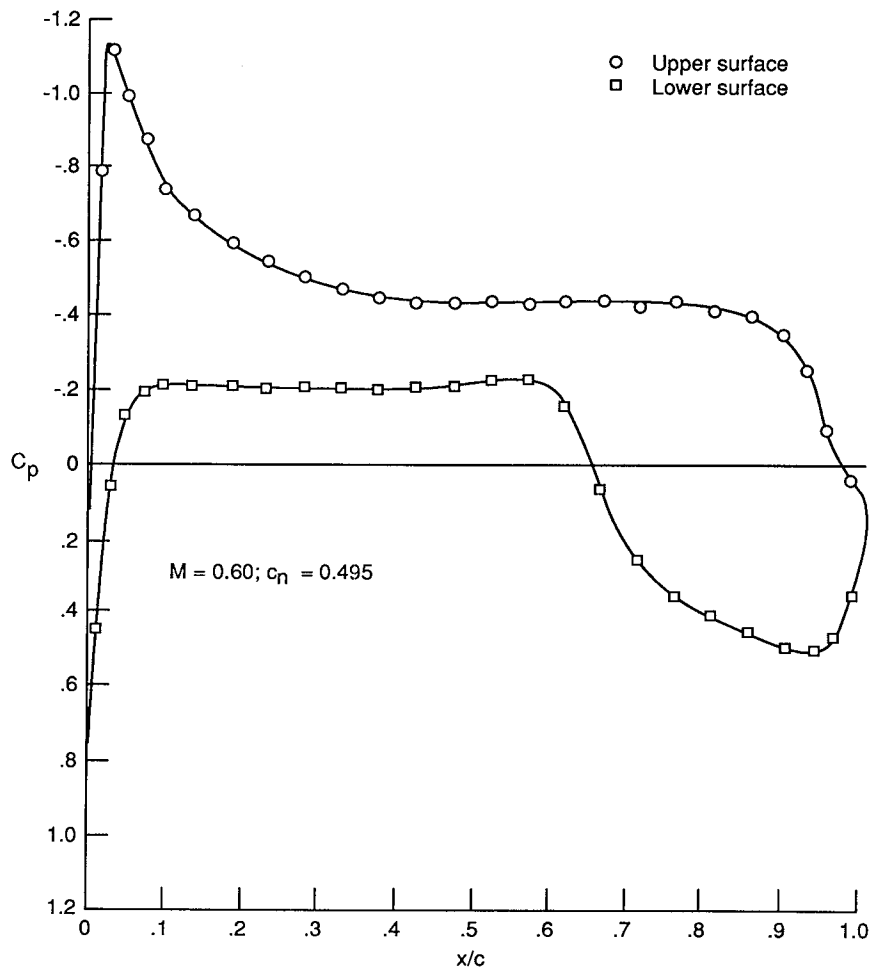
(b) Subcritical conditions.

Figure 7. Continued.
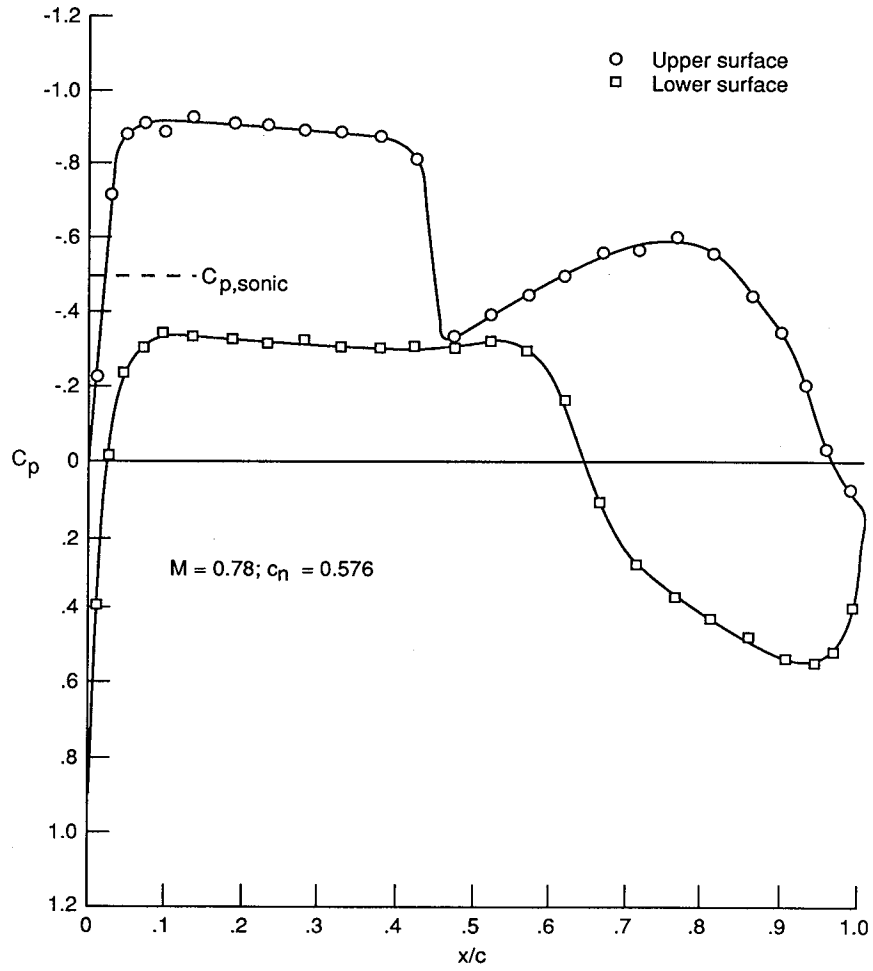
(c) Intermediate off-design conditions.

Figure 7. Continued.
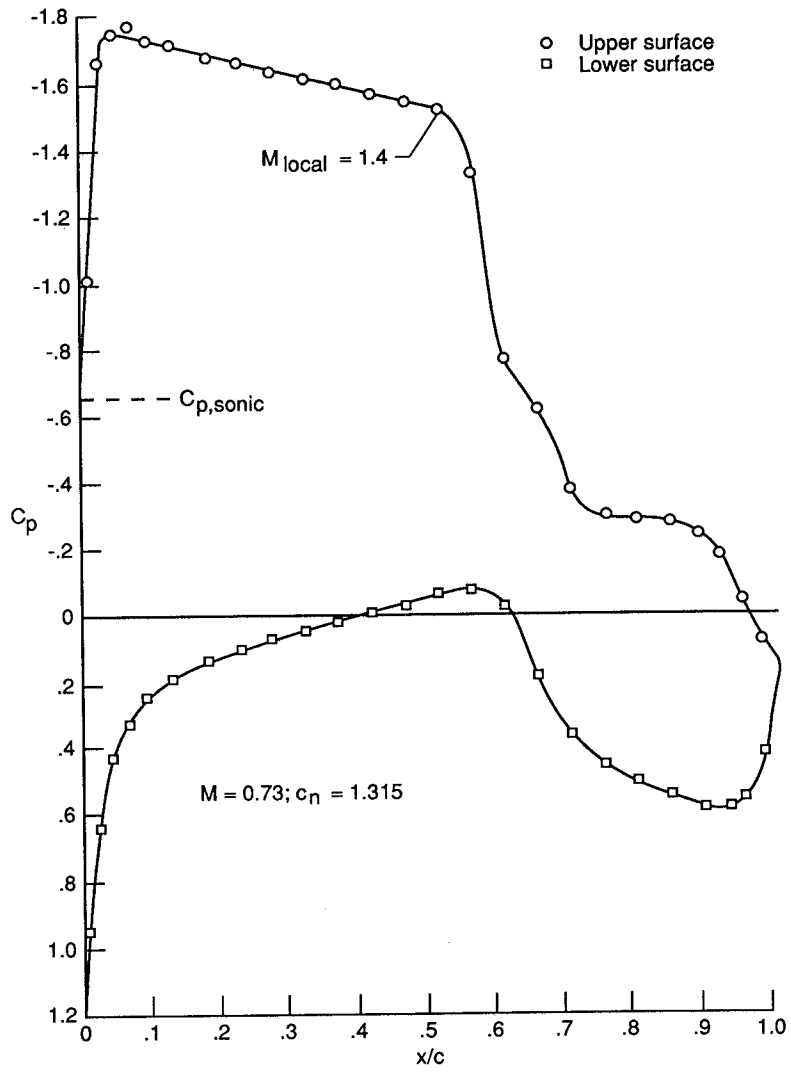
(d) High-lift conditions.

Figure 7. Concluded.
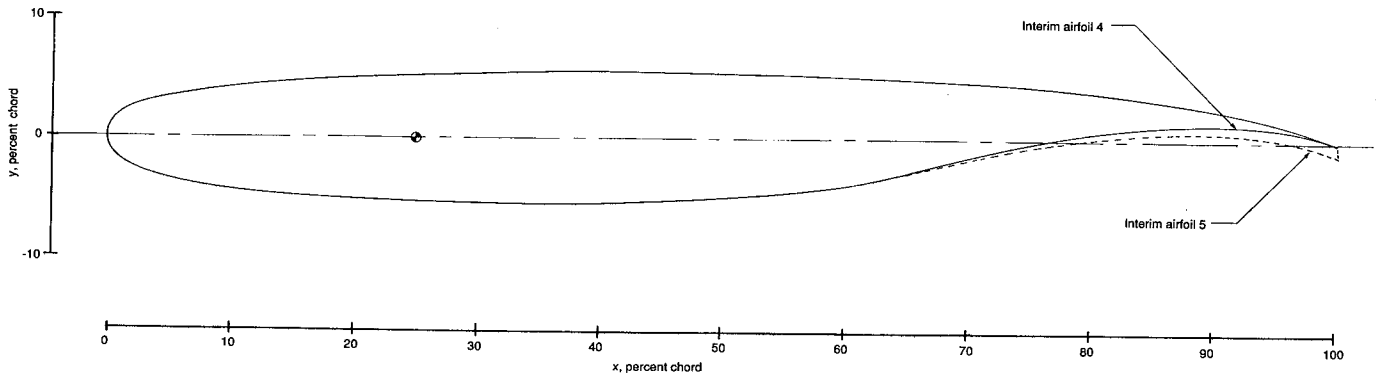
Figure 8. Sketches of 11-percent-thick interim supercritical airfoils showing sharp and blunt trailing edges.
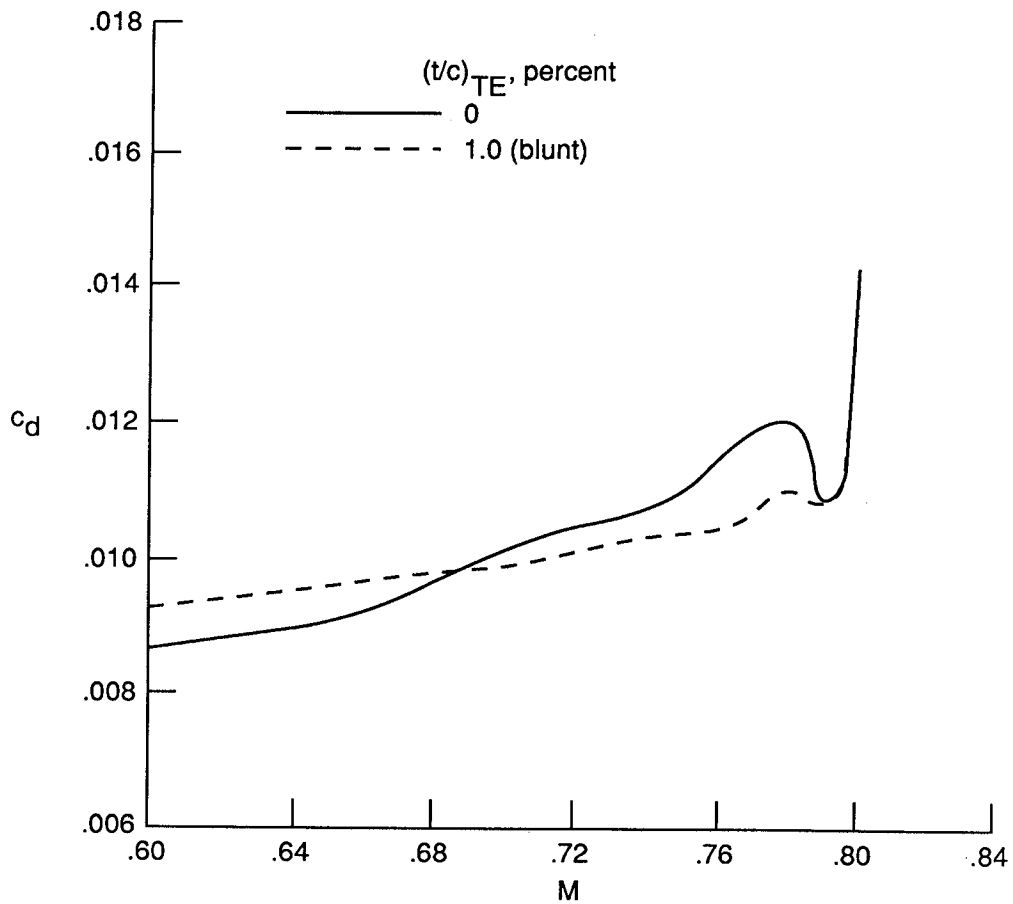
Figure 9. Variation of section drag coefficient with Mach number at a normal-force coefficient of 0.7 for the 11-percent-thick interim supercritical airfoils with sharp and blunt trailing edges.

c = 63.5 cm (25 in.)

0.010c

Supercritical airfoil, $(t/c)_{max} = 0.10$

x/c = 0.692

0.010c

Lower surface
hinge line

1.0-percent-thick blunt trailing edge
(Airfoil 9)

x/c = 0.9915

0.010c

0.020c

1.0-percent-thick trailing edge with cavity

(Airfoil 9a)

0.015c

1.5-percent-thick trailing edge with cavity
(Airfoil 10)

x/c = 1.00

0.007c

0.7-percent-thick trailing edge with cavity
(Airfoil 11)
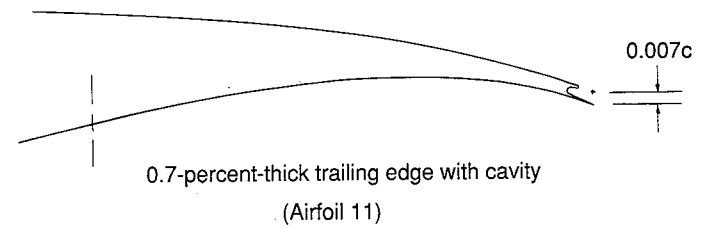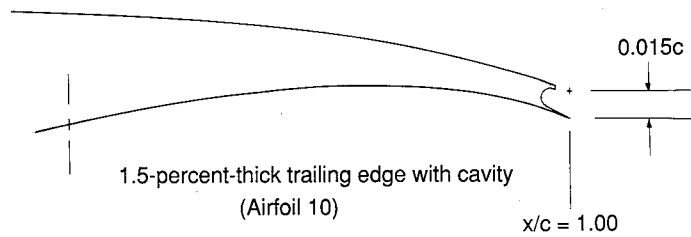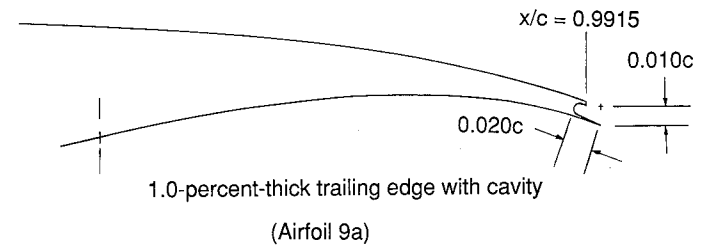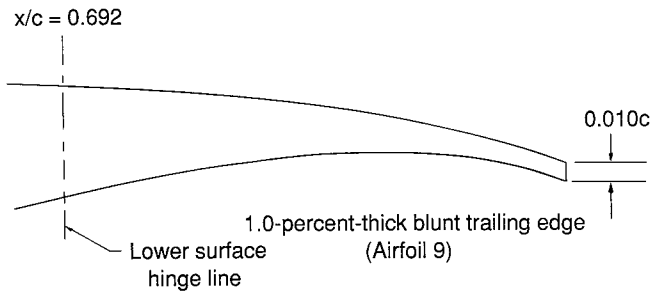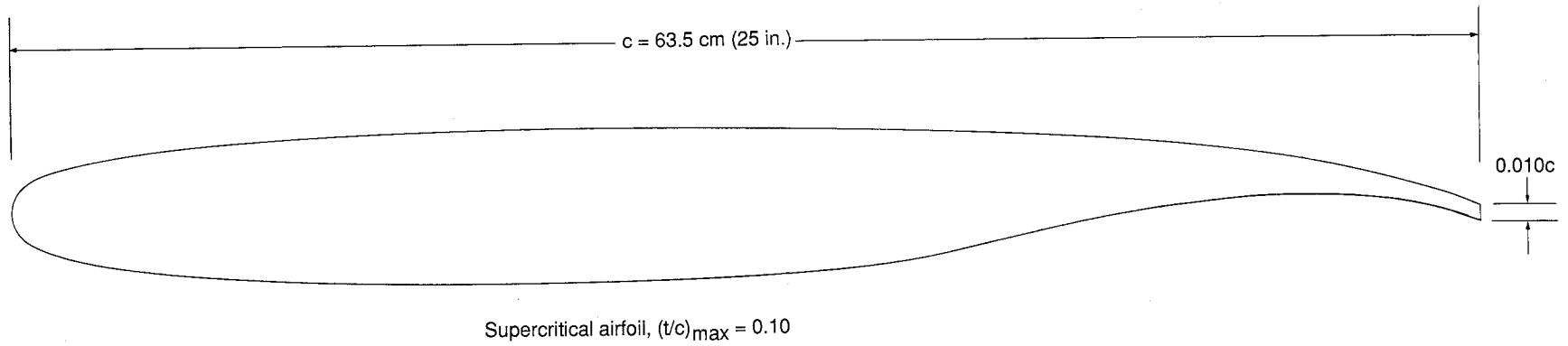
Figure 10. Sketches of refined supercritical airfoil with various trailing-edge geometries.
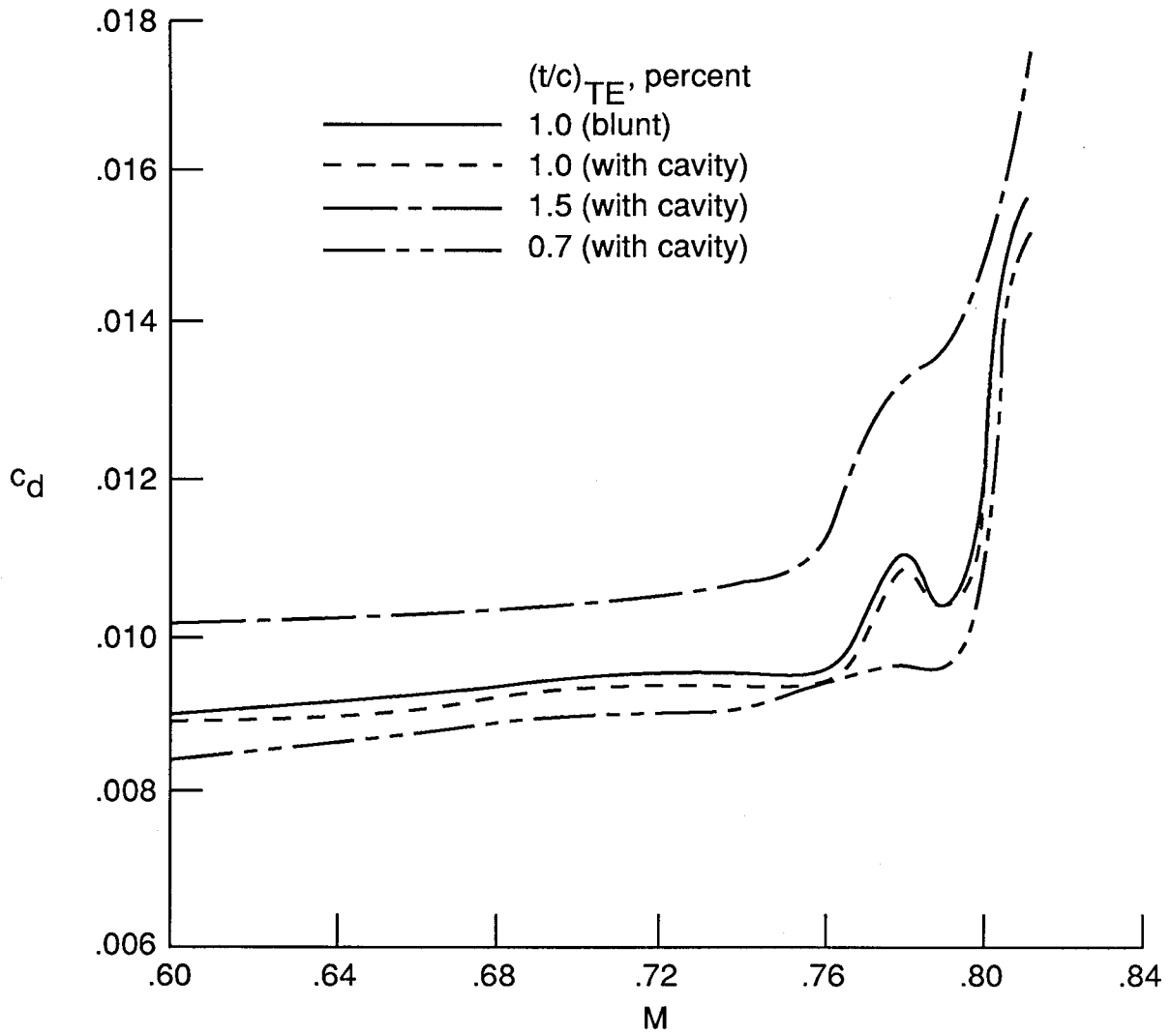
Figure 11. Effect of trailing-edge geometry on variation of section drag coefficient with Mach number at a normal-force coefficient of 0.7 for the 10-percent-thick refined supercritical airfoil.
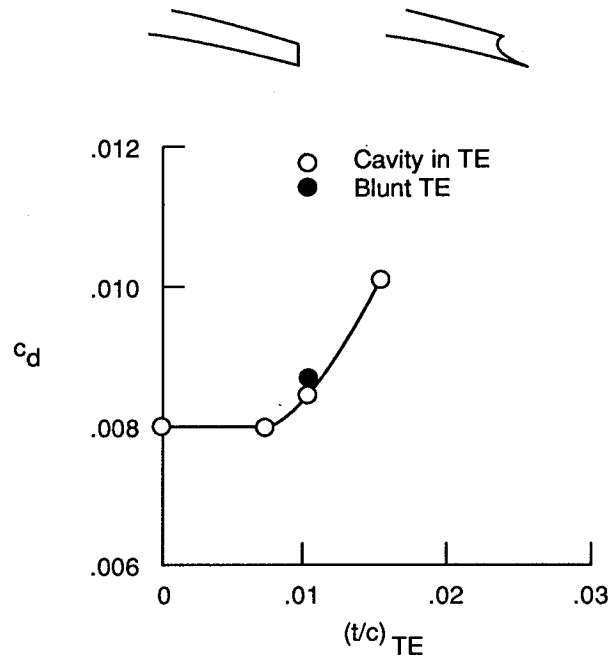
Figure 12.   Effect of trailing-edge thickness on subcritical drag coefficient for 10-percent-thick refined supercritical airfoil. $M = 0.60$, $c_n = 0.60$.
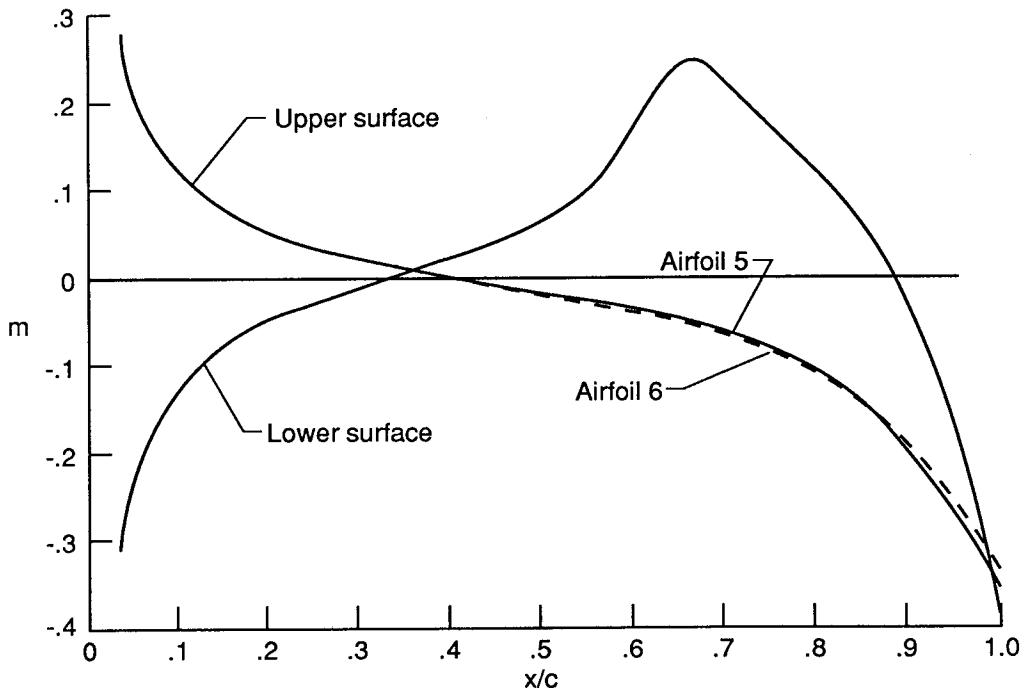
Figure 13. Chordwise distribution of slopes.
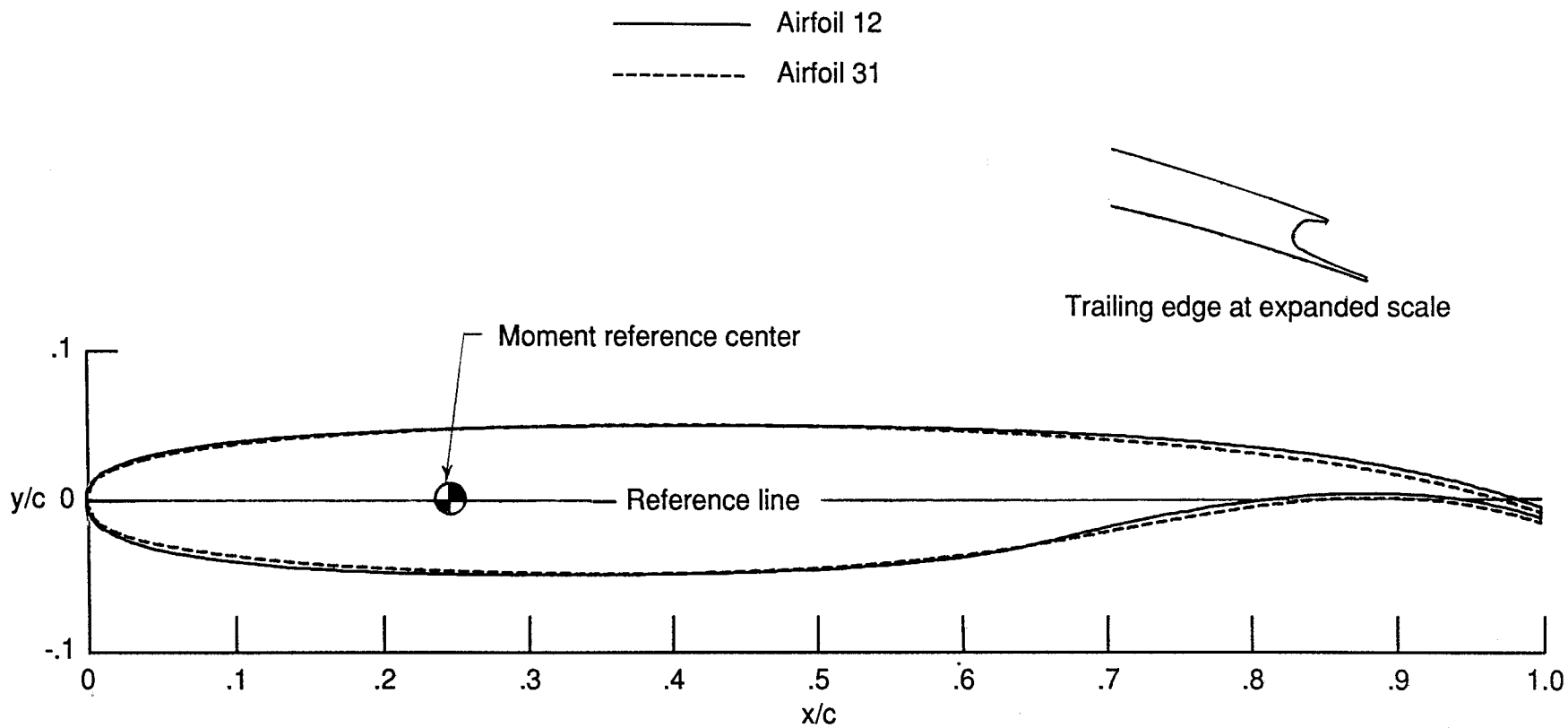
Figure 14. Geometric characteristics of supercritical airfoils 12 and 31.
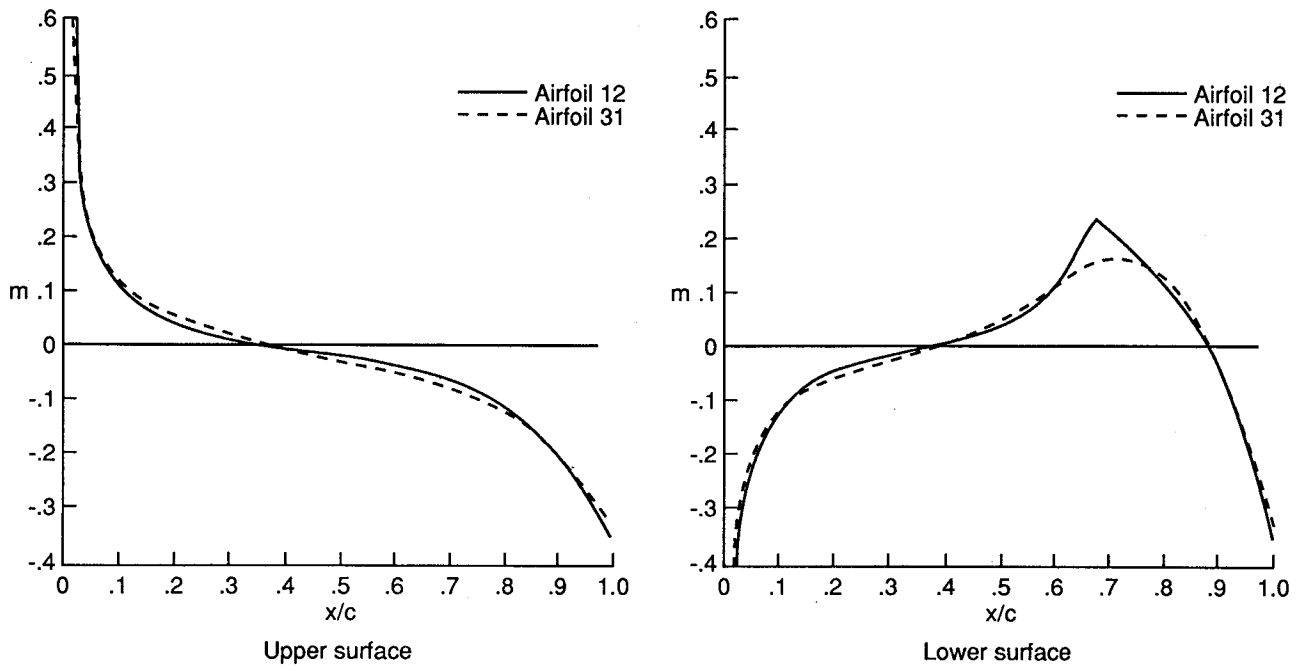
(b) Chordwise distribution of airfoil surface slopes.
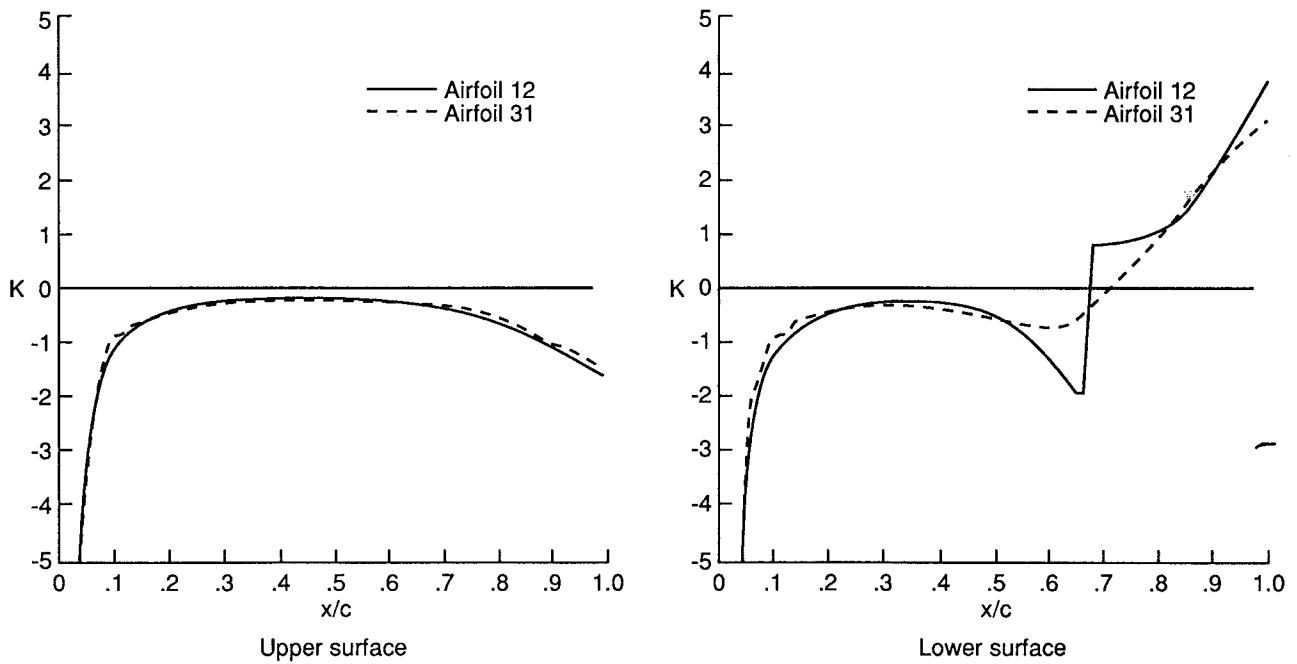
(c) Chordwise distribution of airfoil surface curvatures.

Figure 14. Concluded.
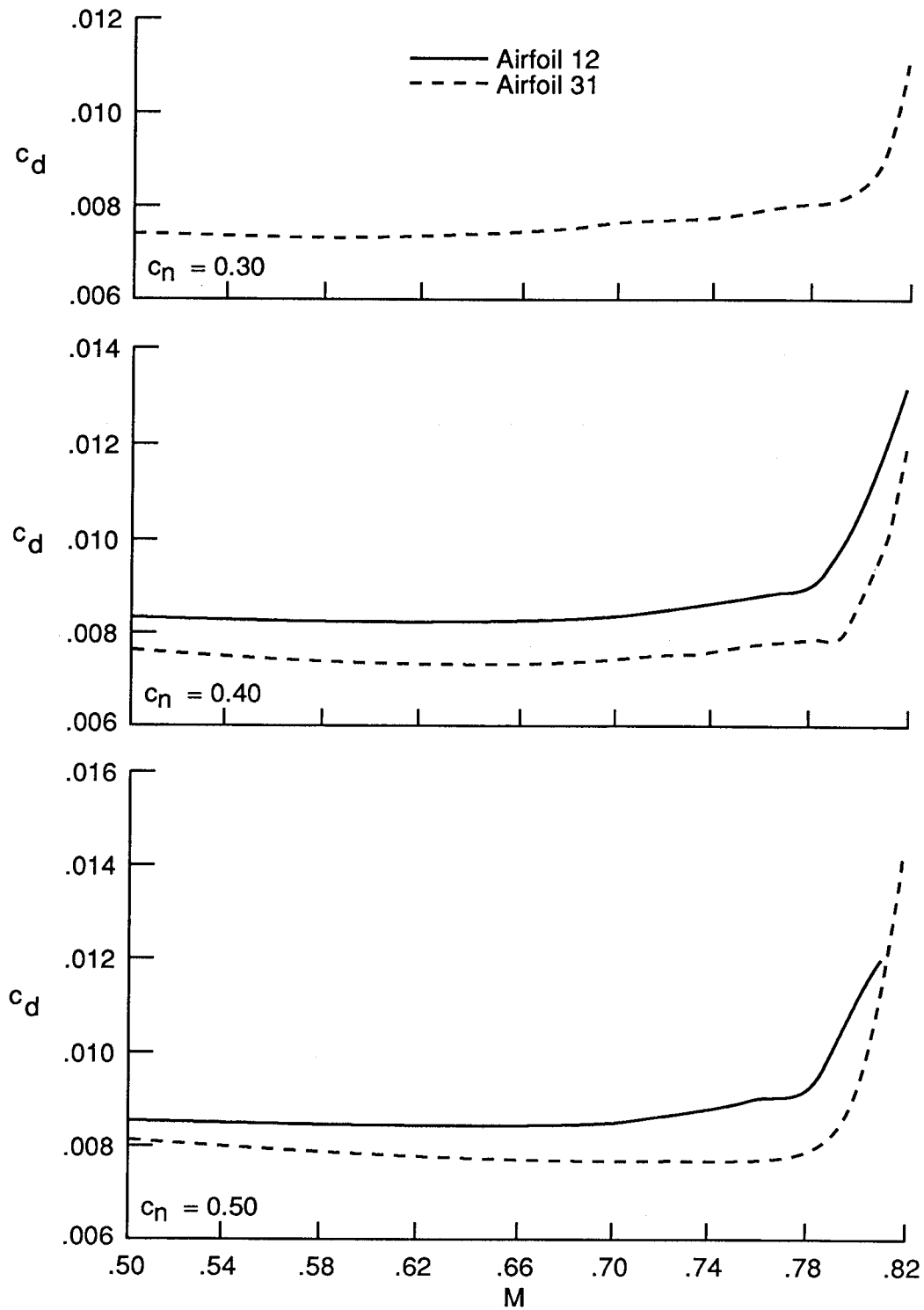
Figure 15. Variation of section drag coefficient with Mach number of supercritical airfoils 12 and 31 at various normal-force coefficients.
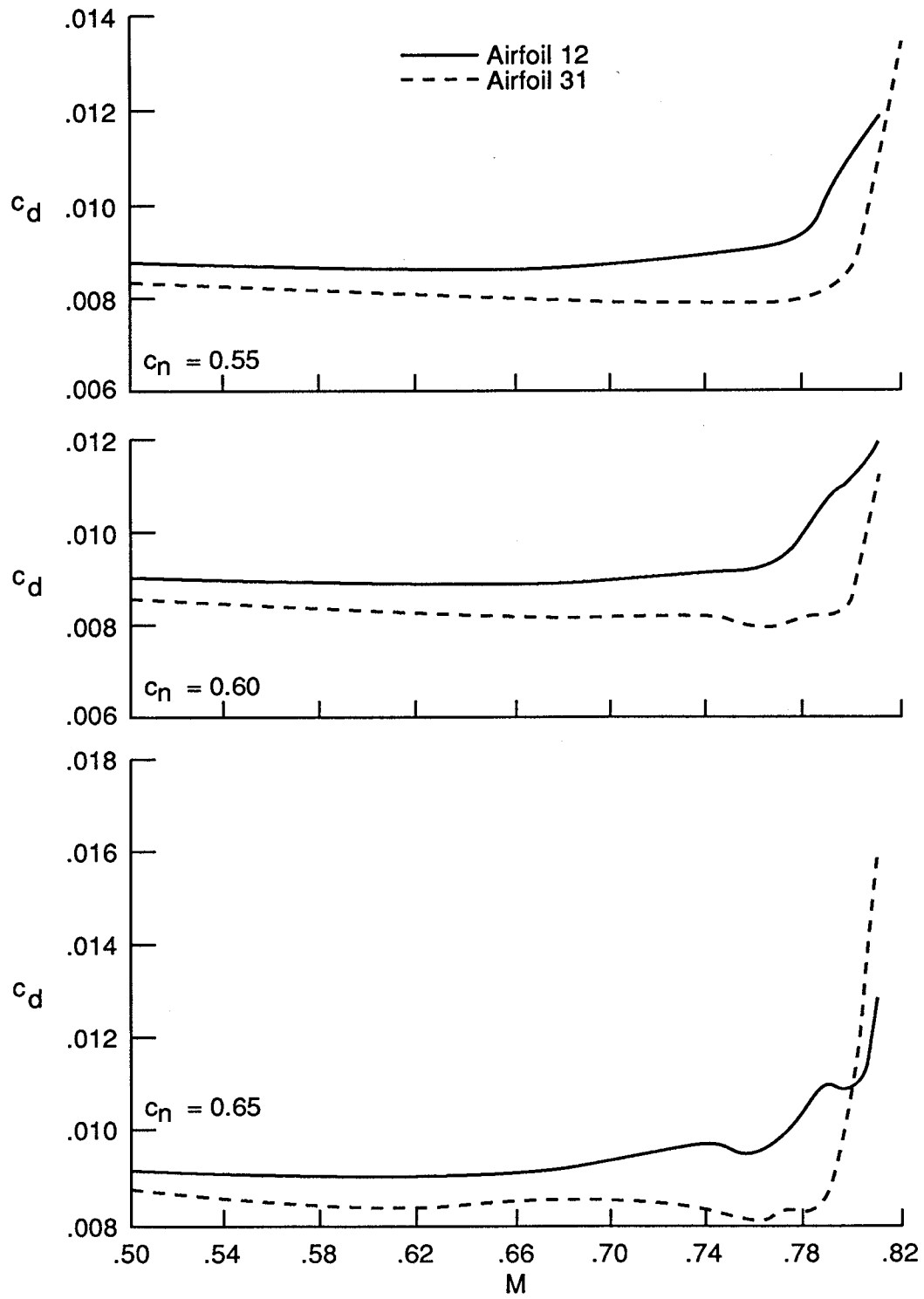
Figure 15. Continued.
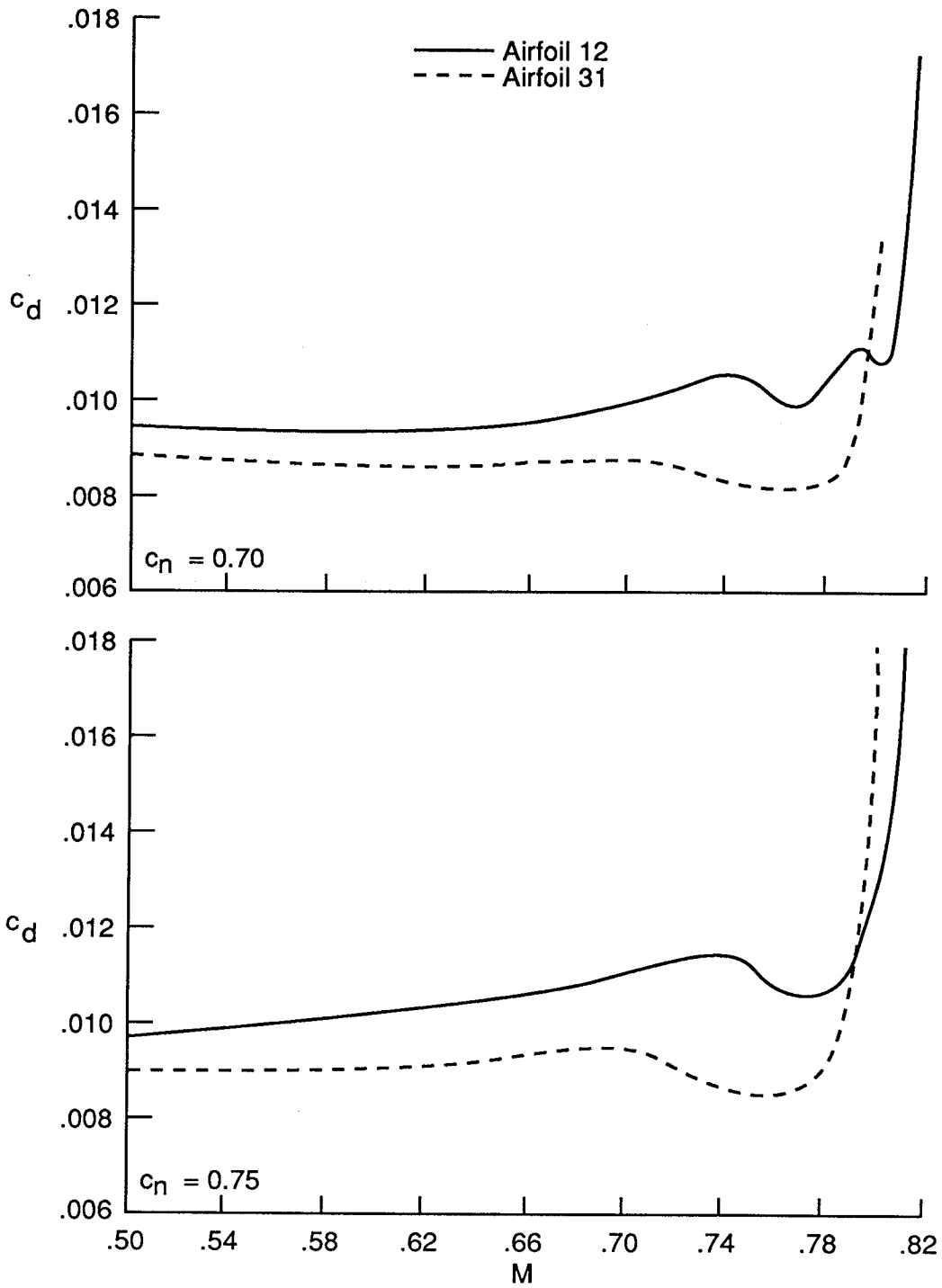
Figure 15. Continued.
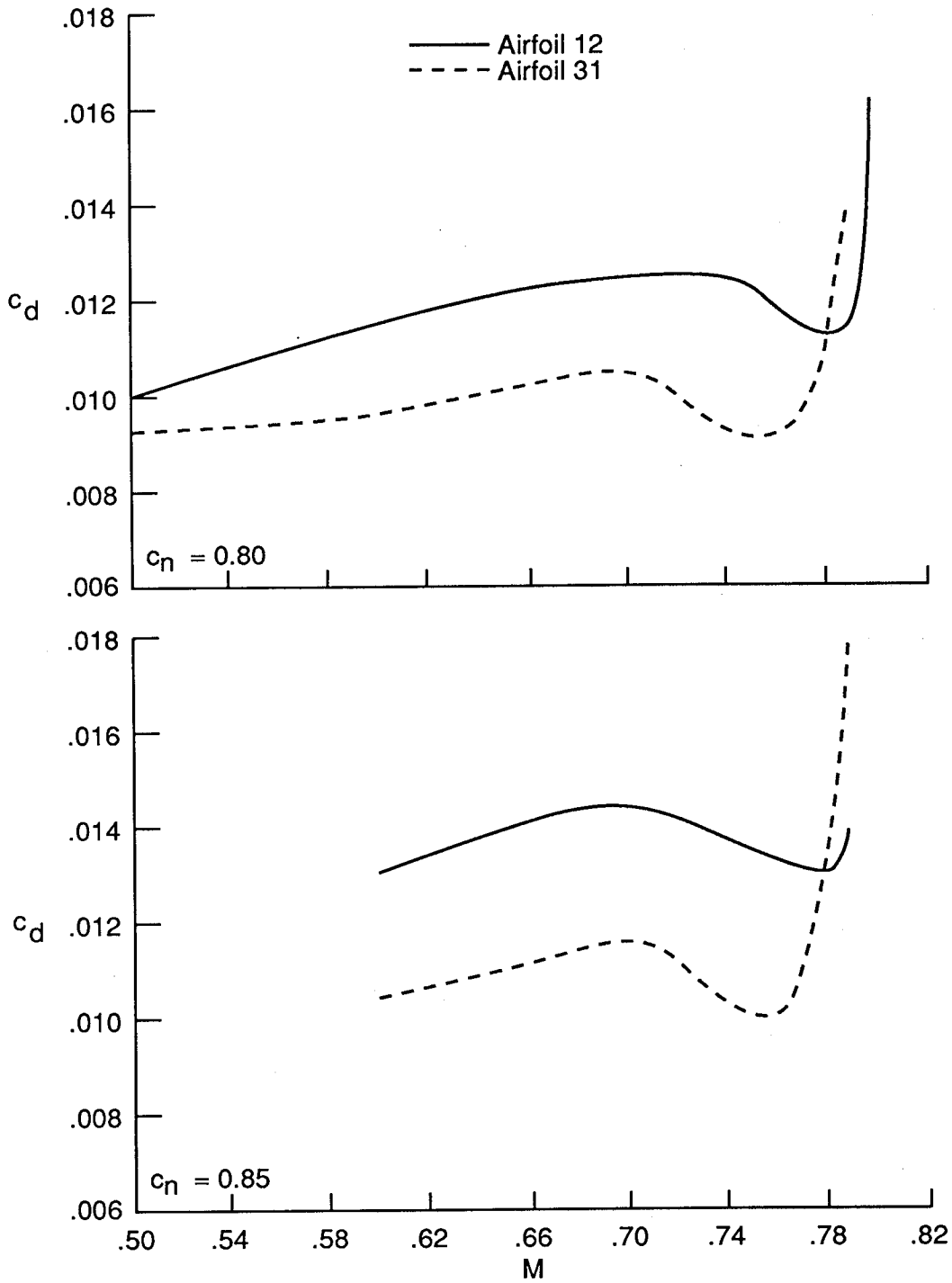
Figure 15. Continued.
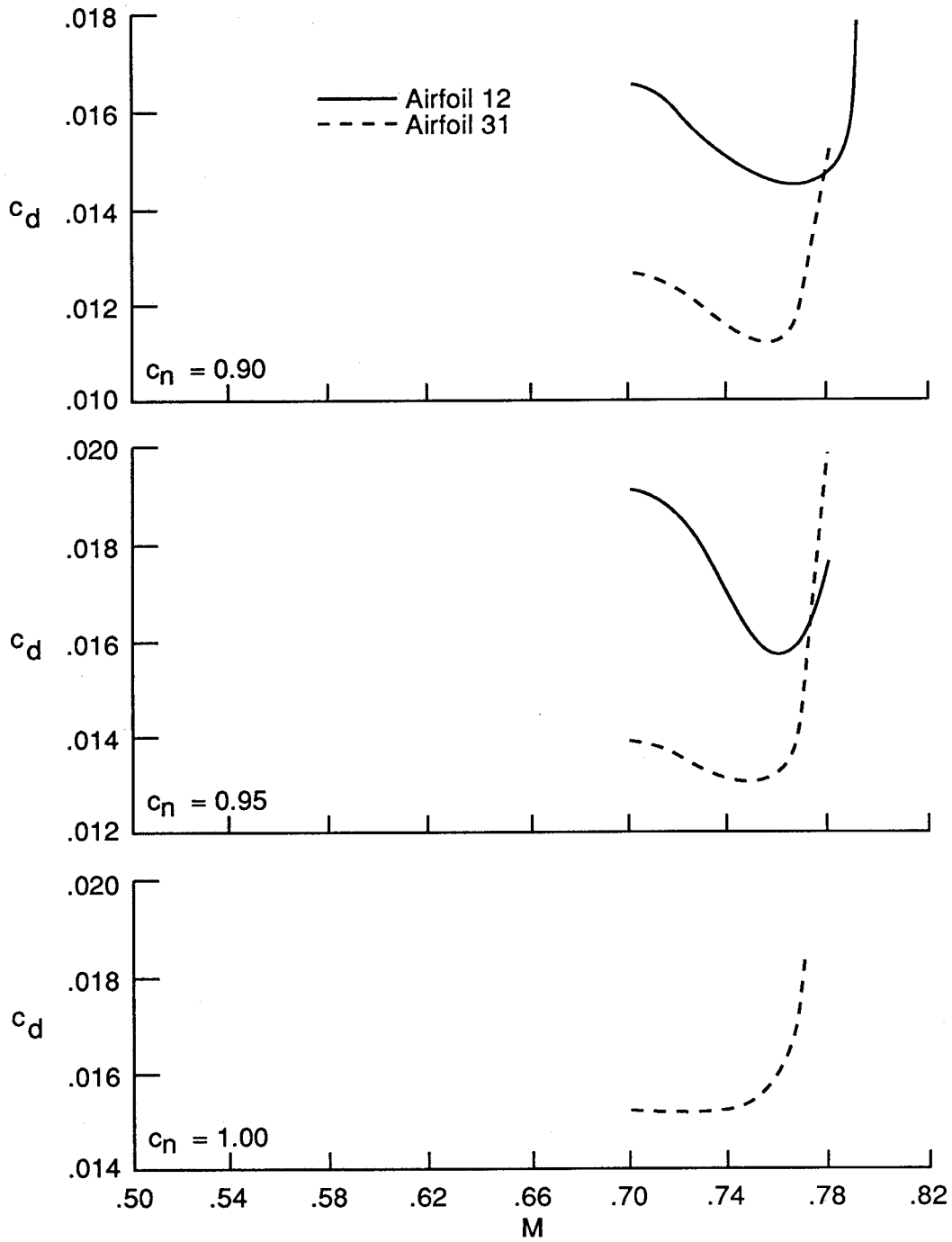
Figure 15. Concluded.
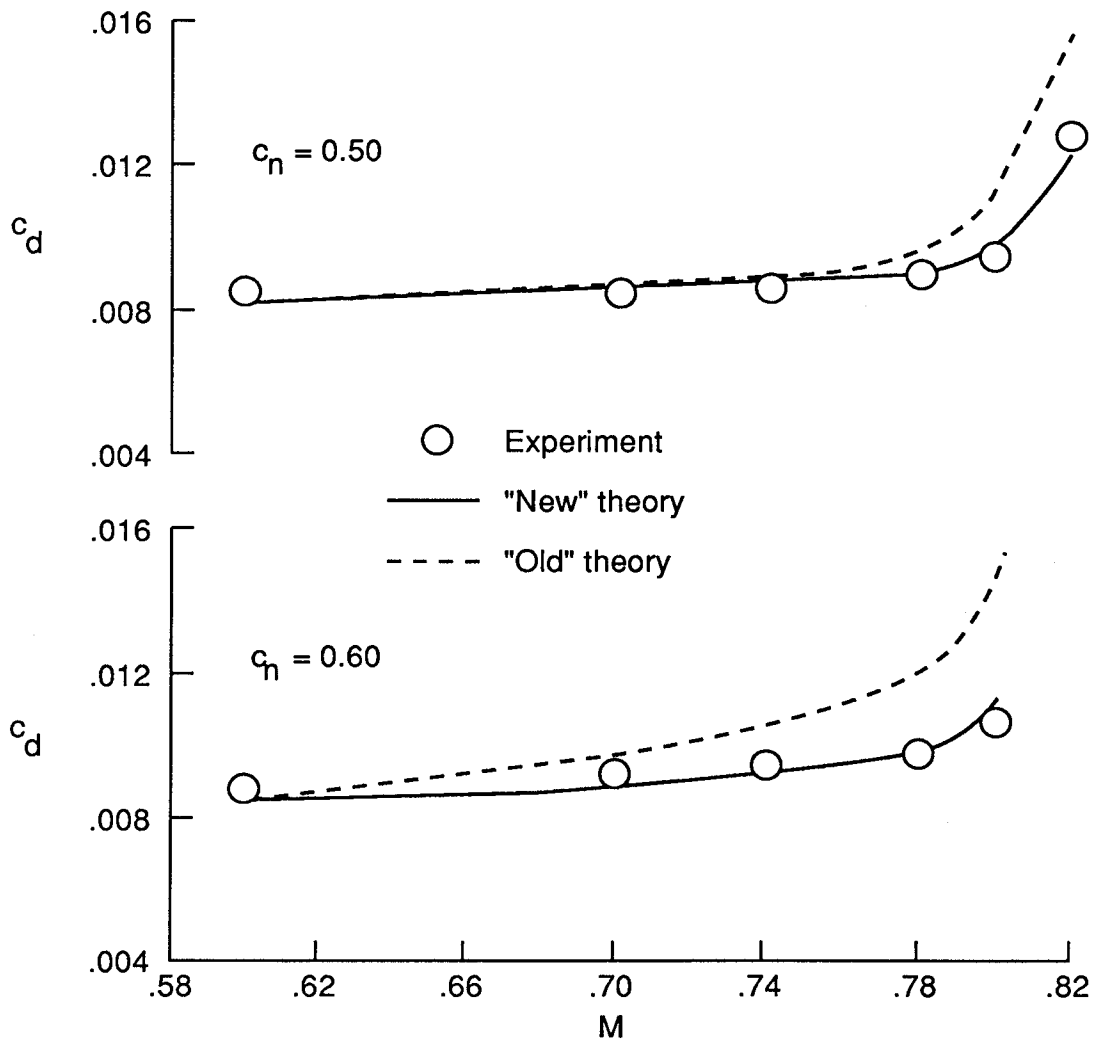
Figure 16. Comparison of experimental and analytical drag characteristics for supercritical airfoil 27. $R_c = 11 \times 10^6$.
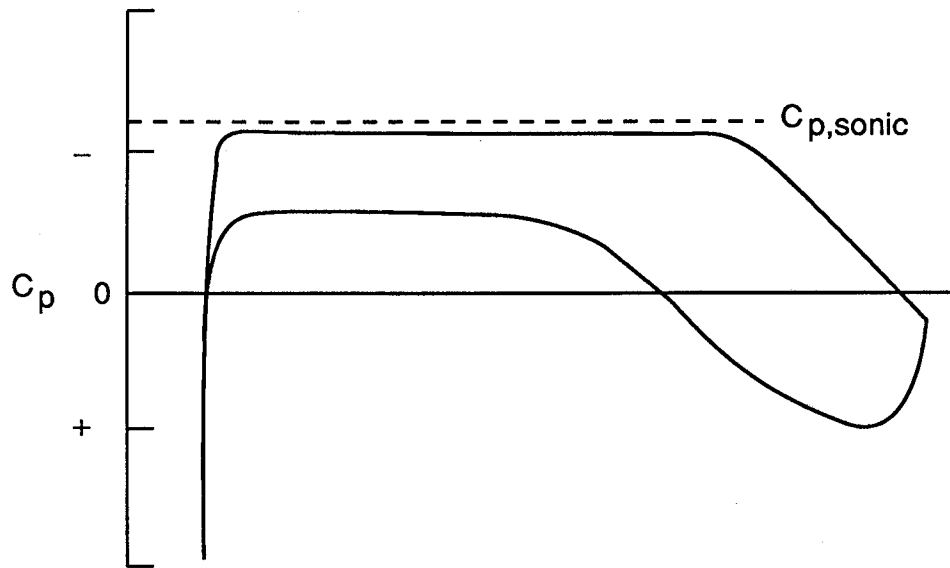
Figure 17. Generalized sonic-plateau pressure distribution.
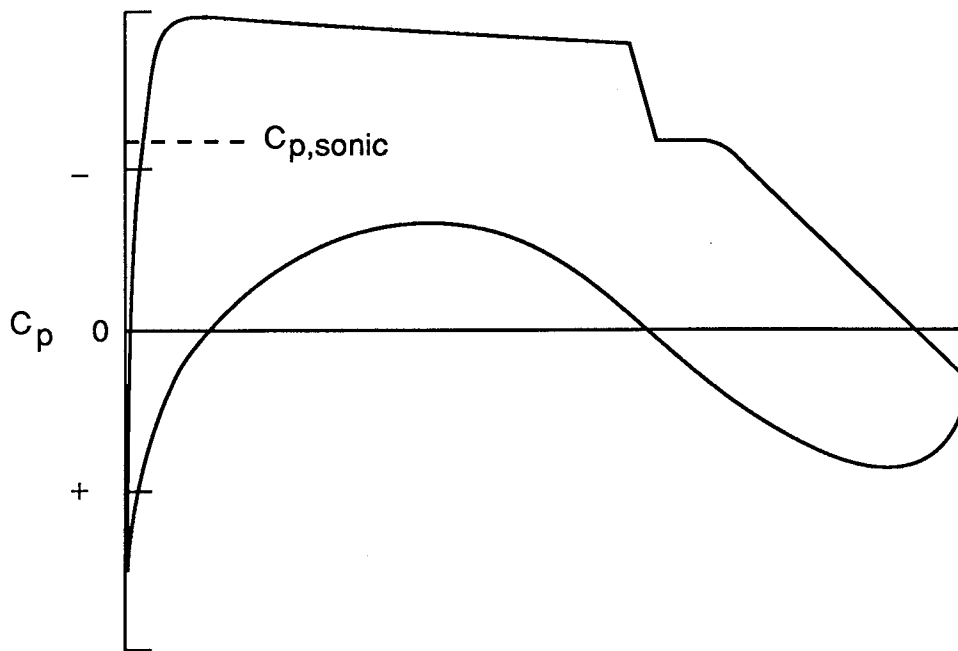
Figure 18. Generalized design pressure distribution.
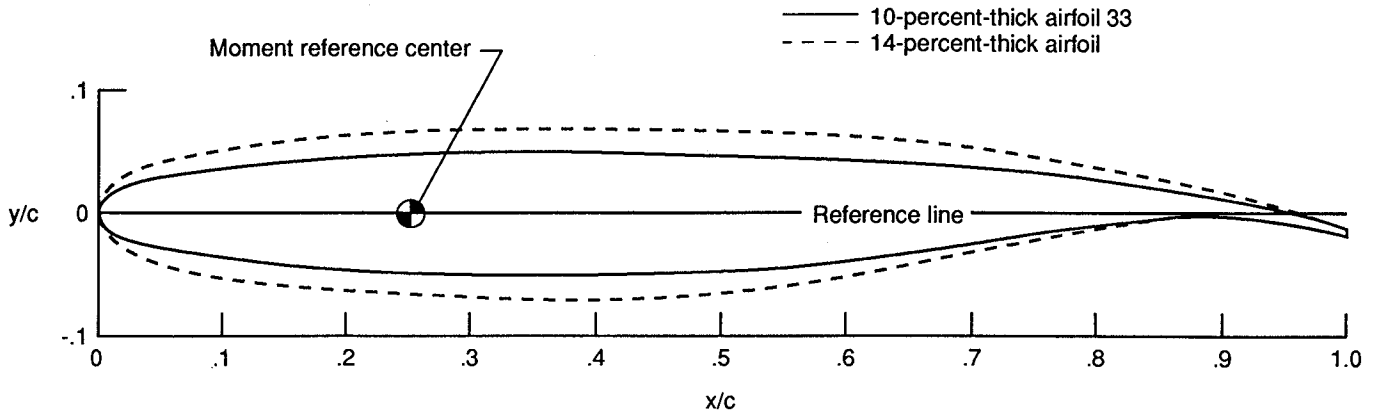
Figure 19. Comparison of 14-percent-thick airfoil with 10-percent-thick airfoil 33.
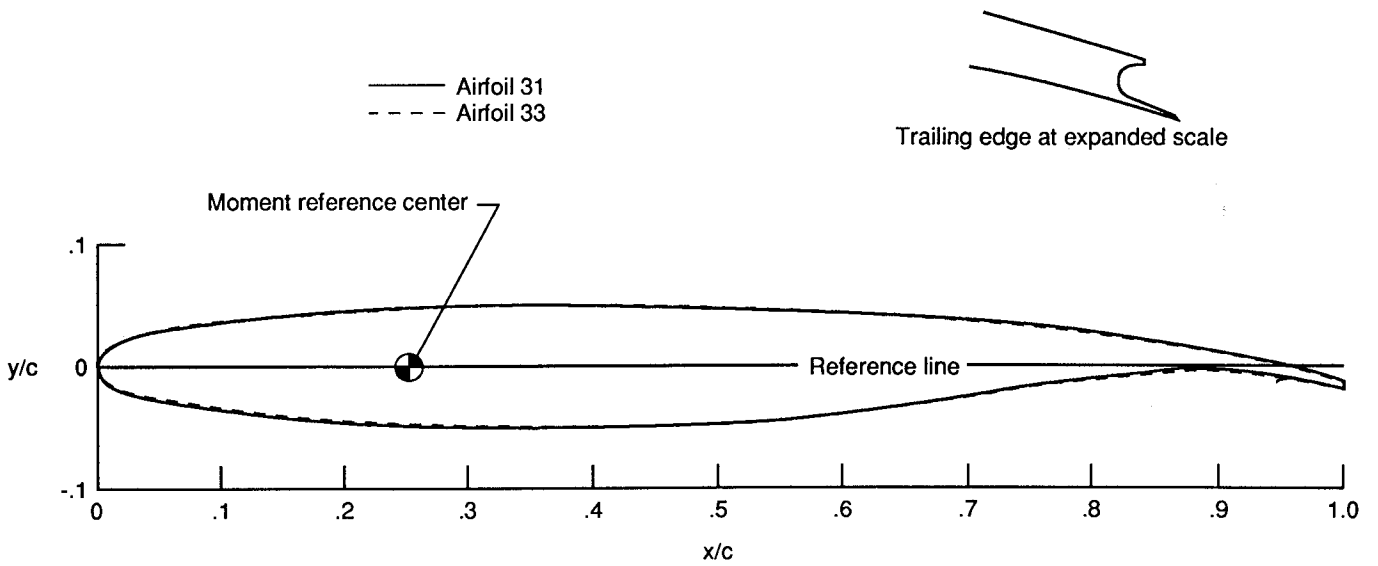
Figure 20. Sketches of 10-percent-thick supercritical airfoils 31 and 33.

60
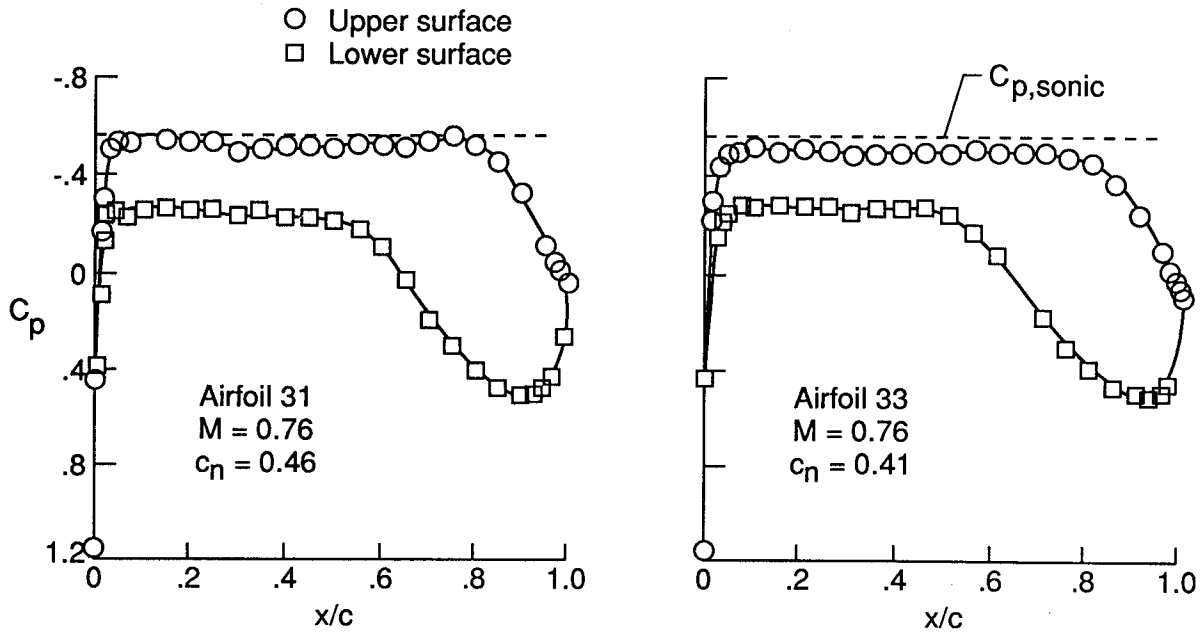
Figure 21. Experimental sonic-plateau pressure distributions for supercritical airfoils 31 and 33.
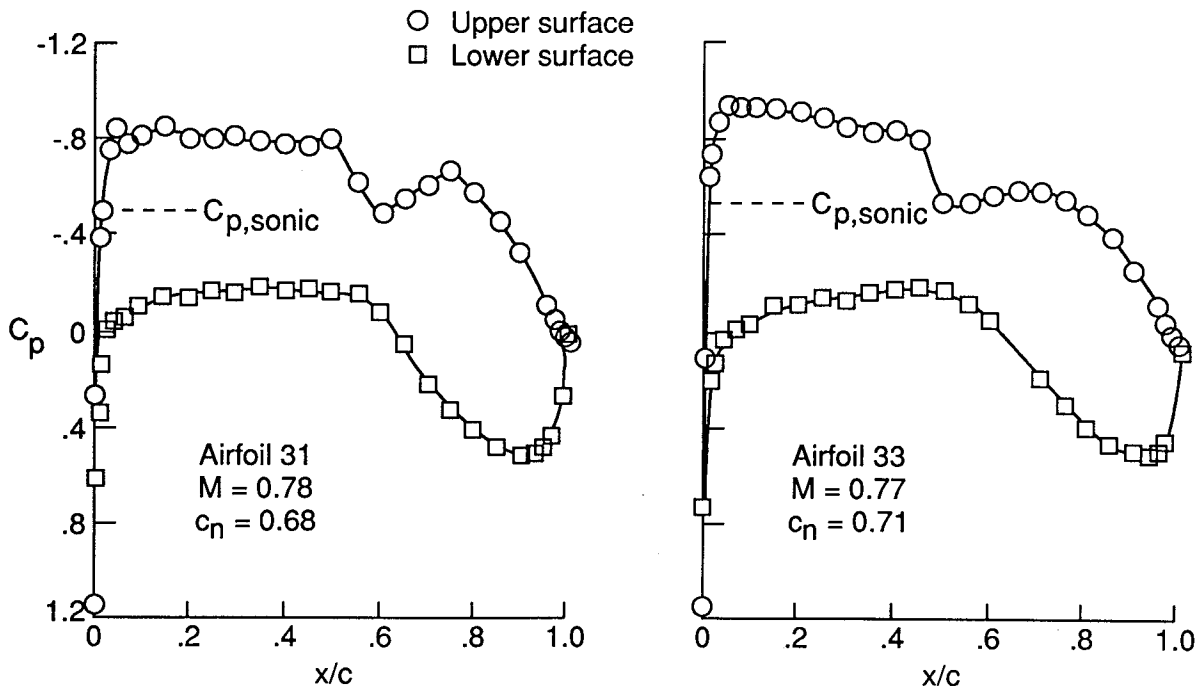
Figure 22. Experimental near-design pressure distributions for supercritical airfoils 31 and 33.

61
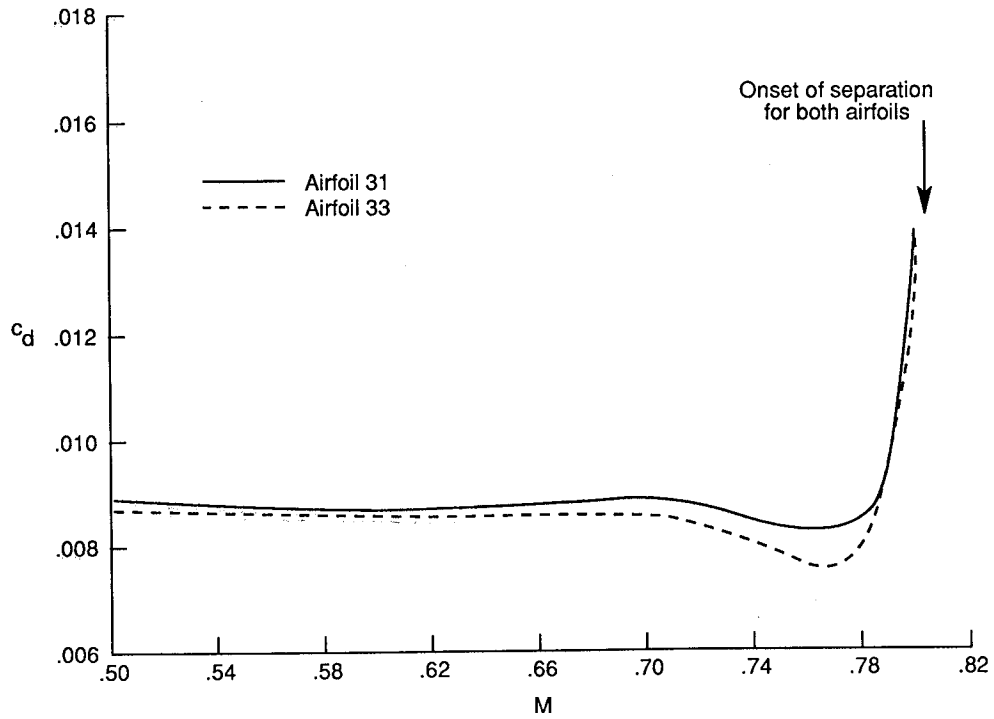
Figure 23. Experimental drag characteristics for supercritical airfoils 31 and 33.
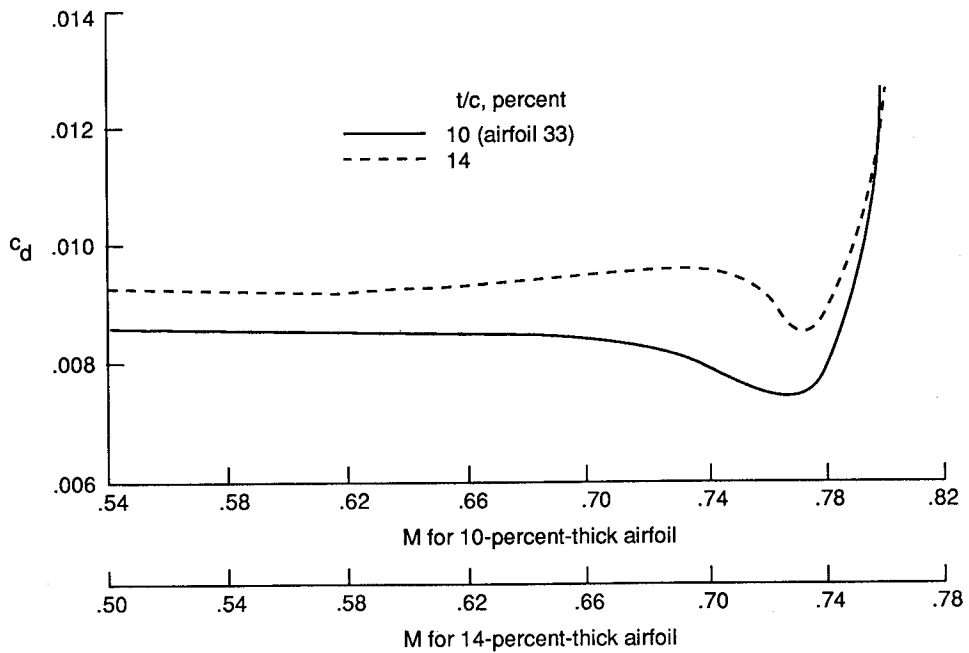
Figure 24. Experimental drag characteristics for 10-percent-thick supercritical airfoil 33 and 14-percent-thick supercritical airfoil. $c_n = 0.70$.
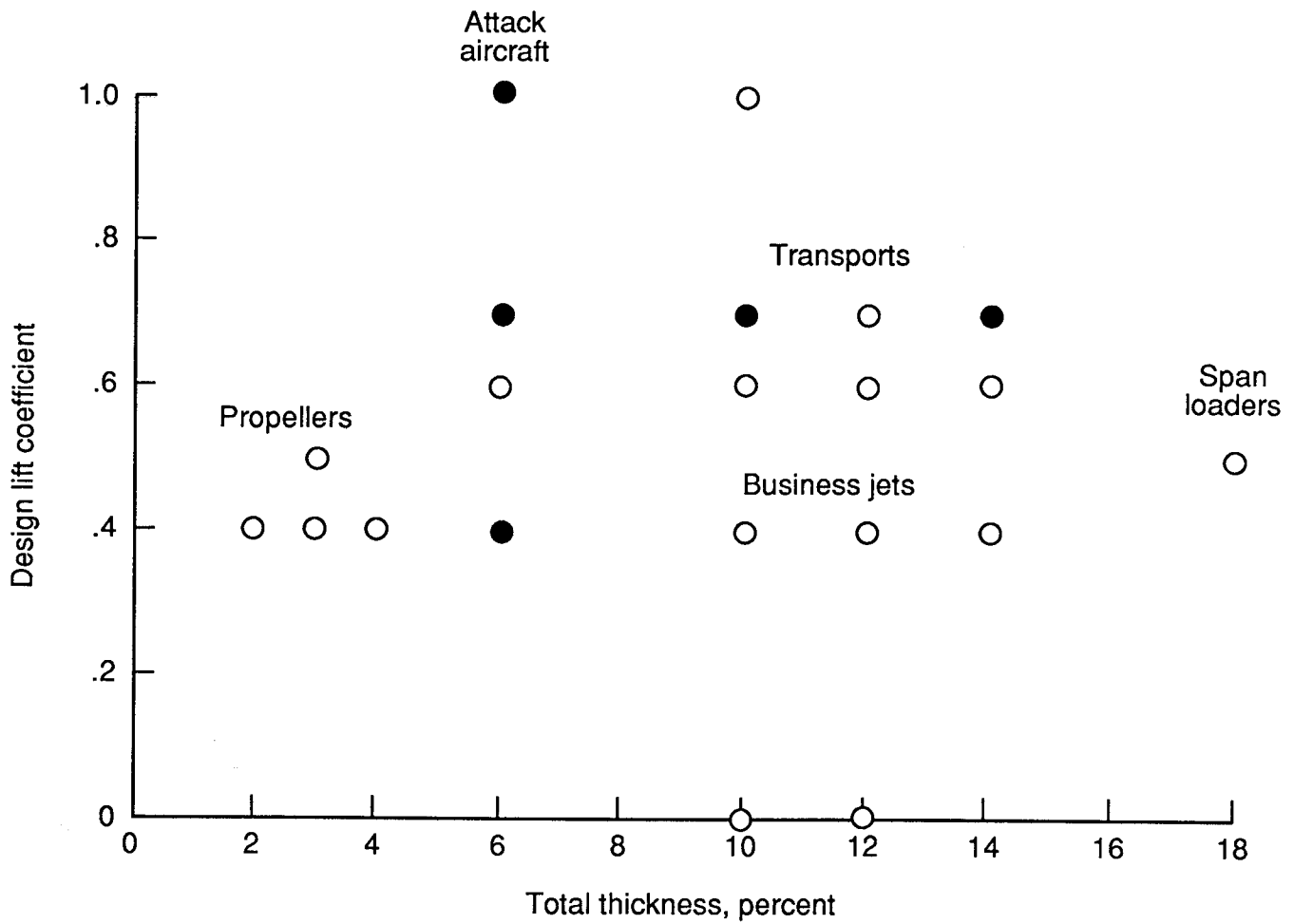
Figure 25. Matrix of phase 2 supercritical airfoils.

SC(2)-0402

0403

0503

0404

0406

0606

0706

1006

0010

0410

0610

0710

1010

0412

0612

0712

0414

0614

0714

(05)(18)

Design c_l x 10 ─┘ └─ t/c, percent
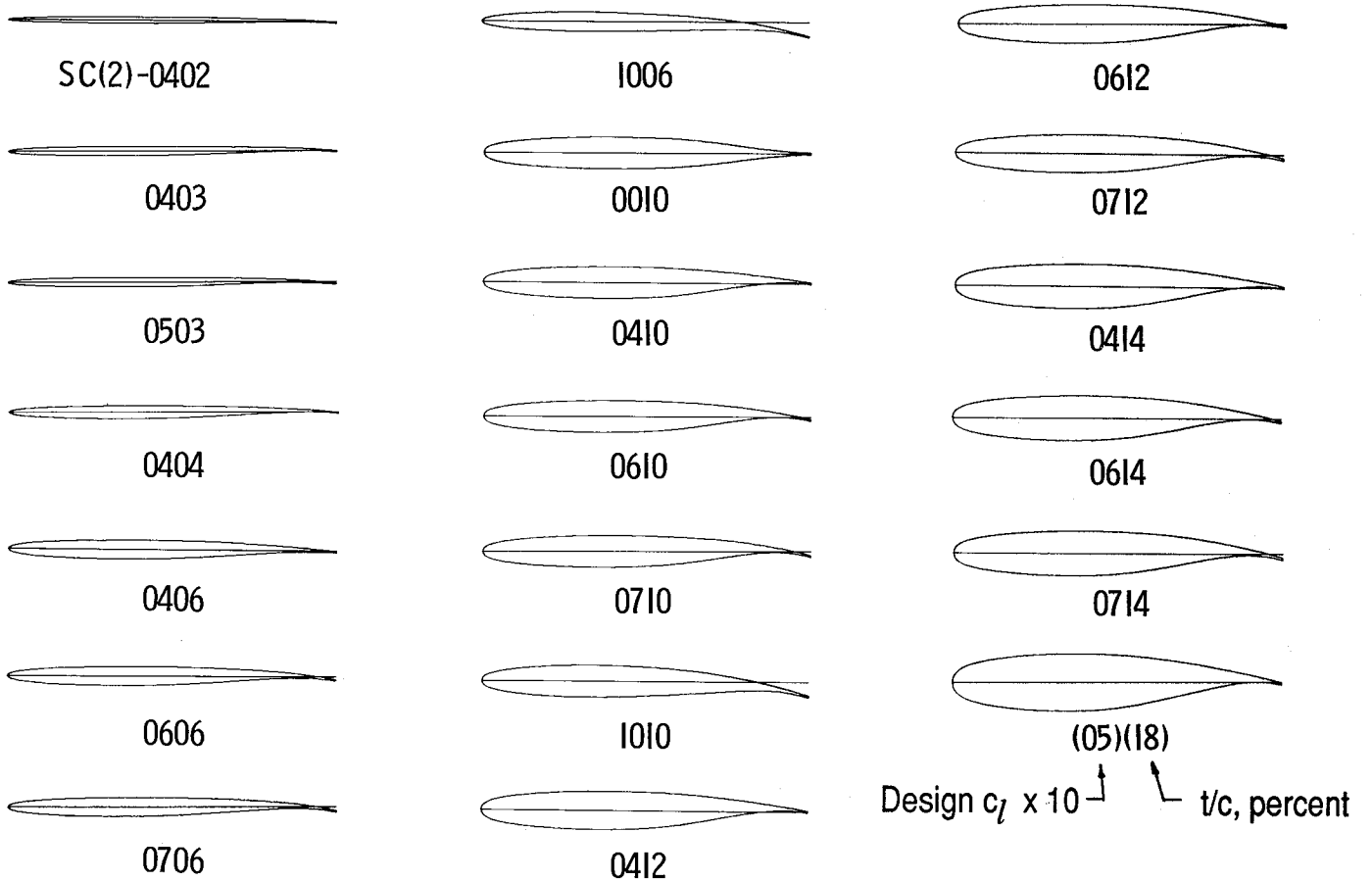
Figure 26. Sketches of airfoils in phase 2 supercritical airfoil matrix.
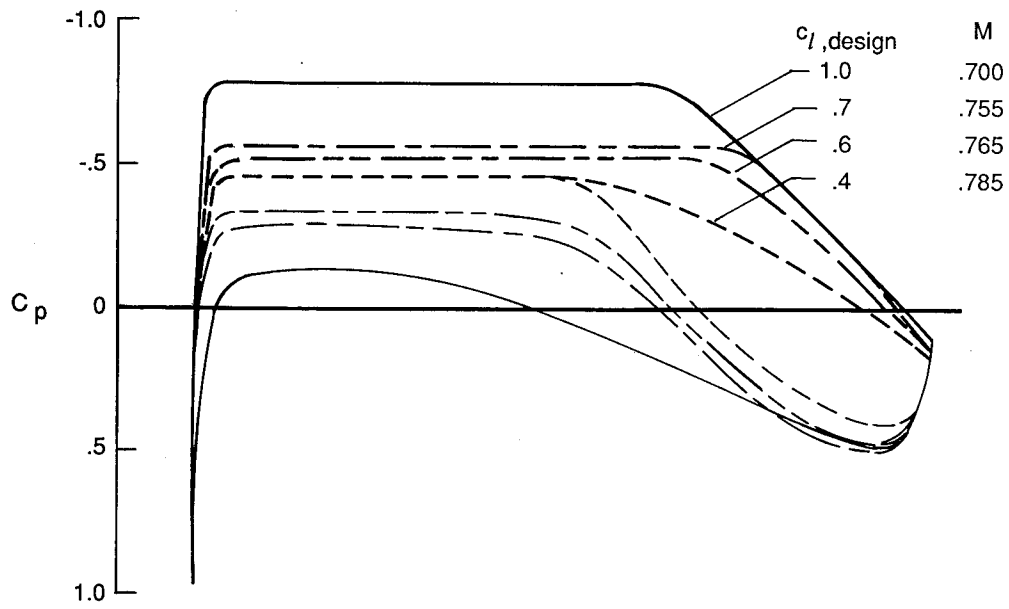
Figure 27. Effect of design lift coefficient on analytical sonic-plateau pressure distribution for 10-percent-thick supercritical airfoils.
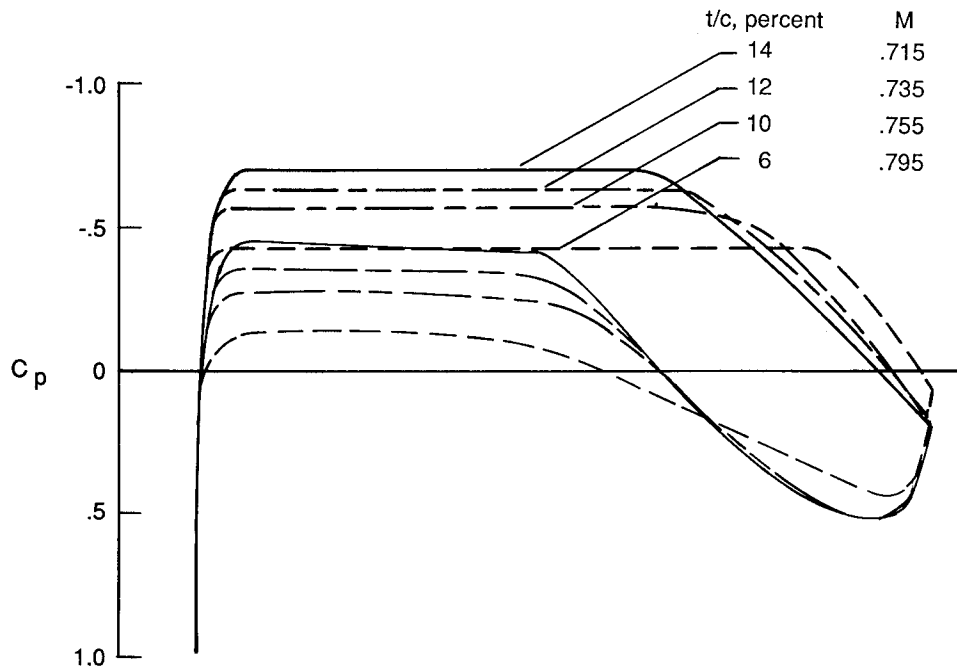
Figure 28. Effect of thickness on analytical sonic-plateau pressure distribution for design lift coefficient of 0.70.

65
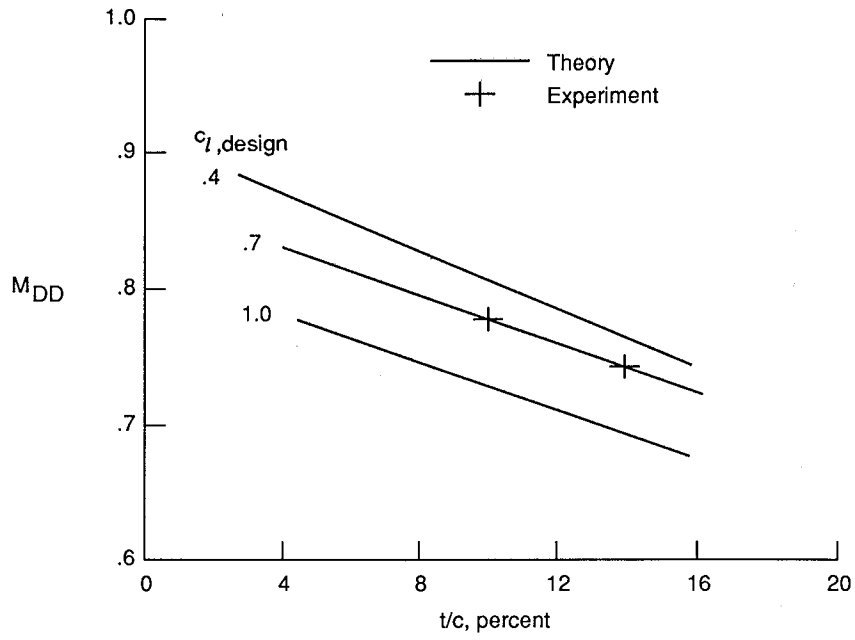
Figure 29. Analytical drag divergence Mach numbers for phase 2 supercritical airfoils.
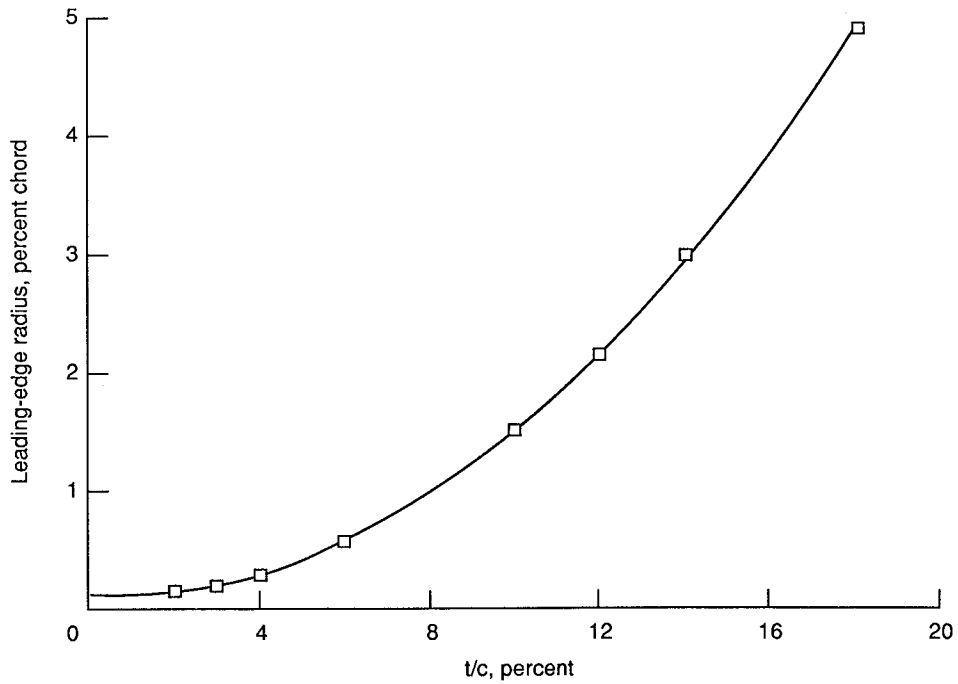
Figure 30. Variation of leading-edge radius with maximum thickness for phase 2 supercritical airfoils.

Figure 31.   Sketches of 12-percent-thick supercritical airfoil with and without forward lower-surface undercutting.
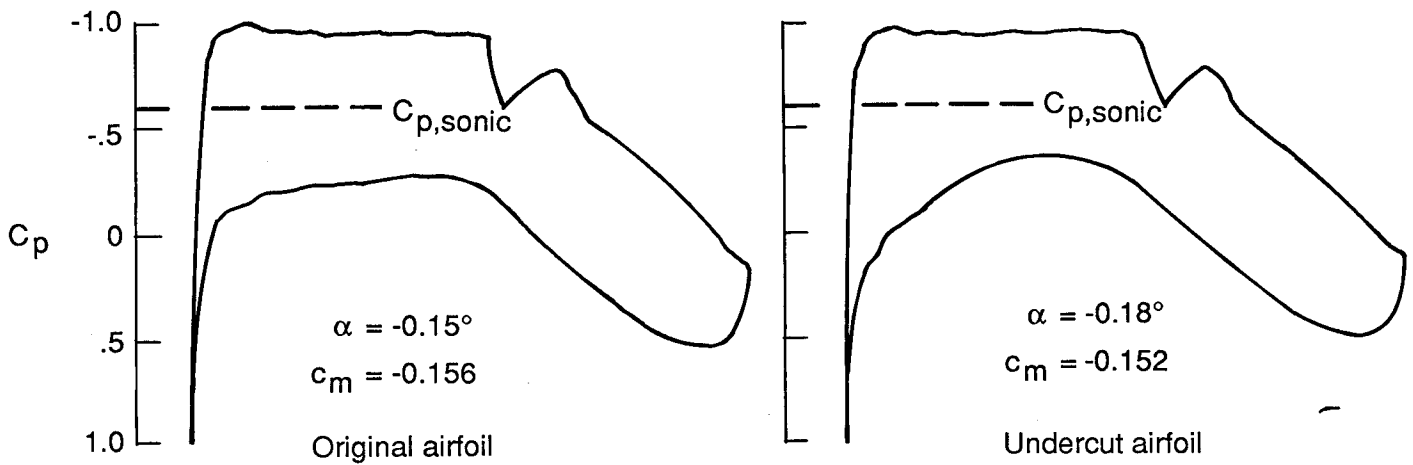
Figure 32. Effect on analytical design pressure distribution of undercutting forward lower surface on 12-percent-thick supercritical airfoil. $M = 0.75$, $c_l = 0.70$; $R_c = 30 \times 10^6$.
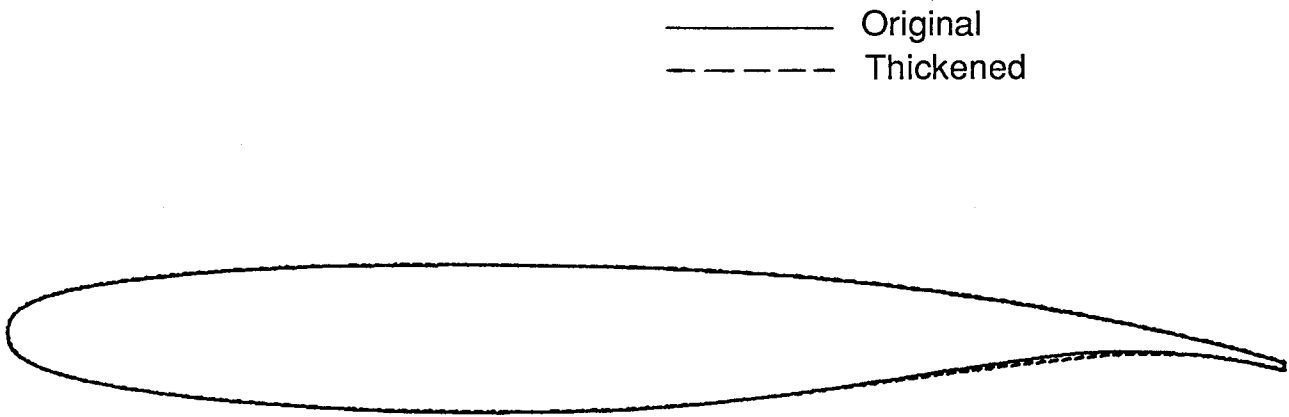
Figure 33. Sketches of 12-percent-thick supercritical airfoil with and without thickening at 80 percent chord.
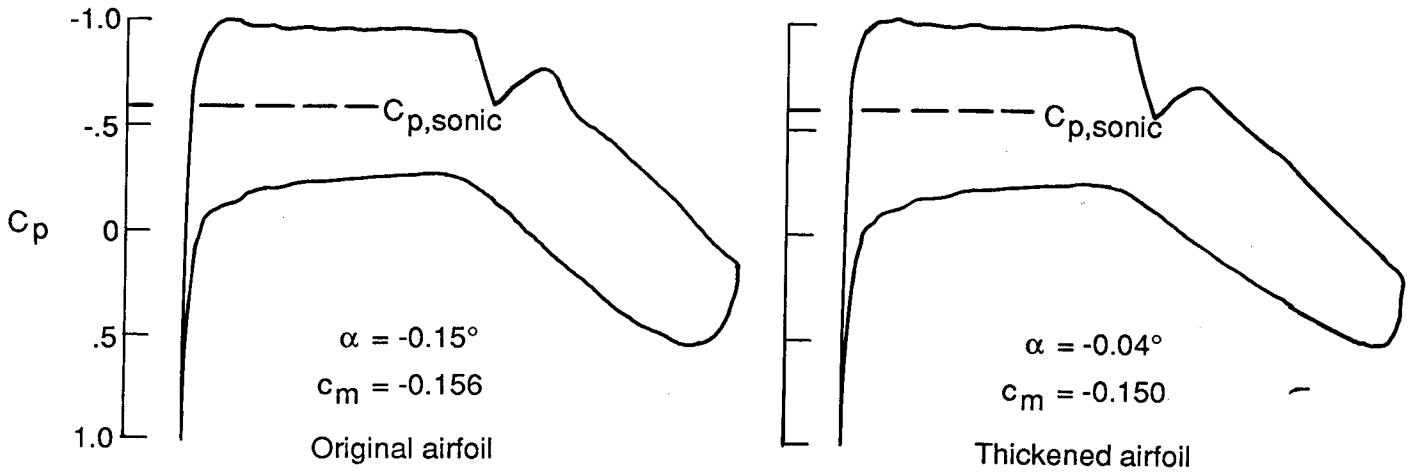
Figure 34. Effect on analytical design pressure distribution of thickening 12-percent-thick supercritical airfoil at 80 percent chord. $M = 0.75$; $c_l = 0.70$; $R_c = 30 \times 10^6$.
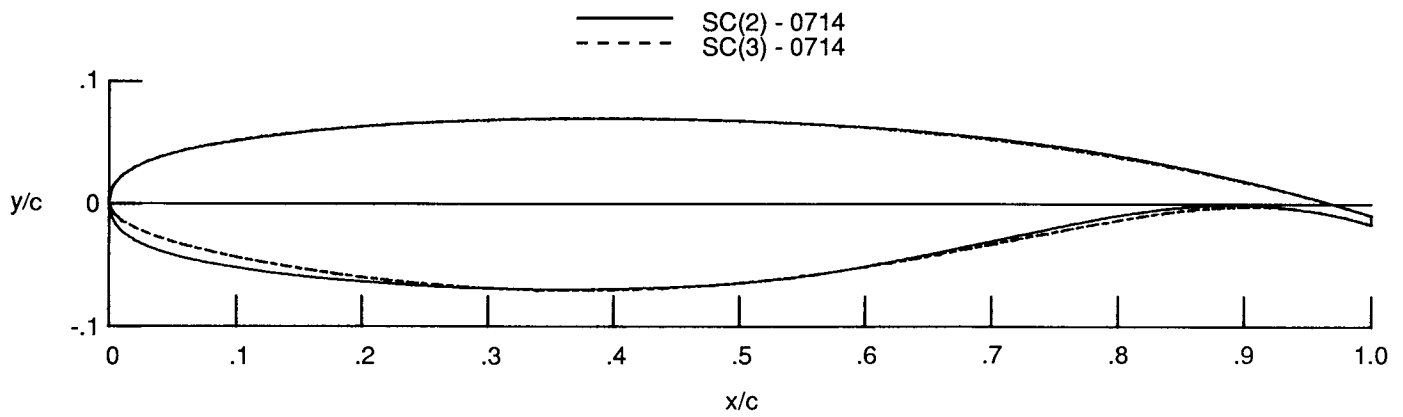
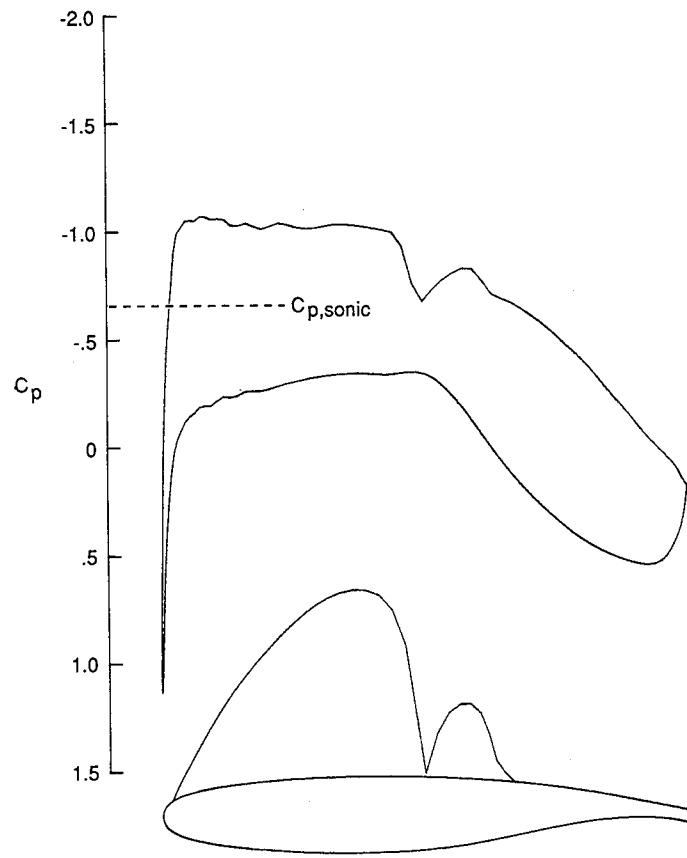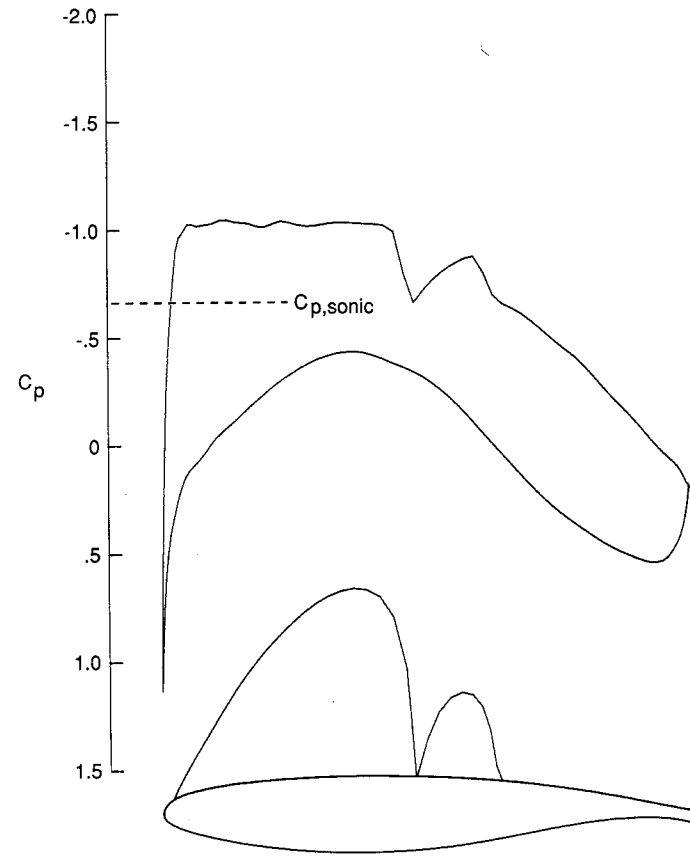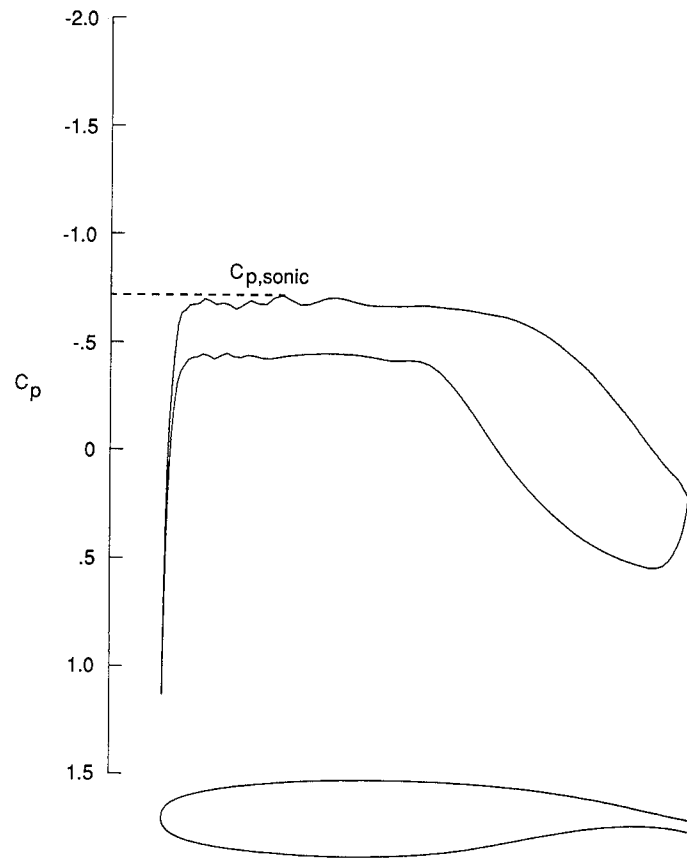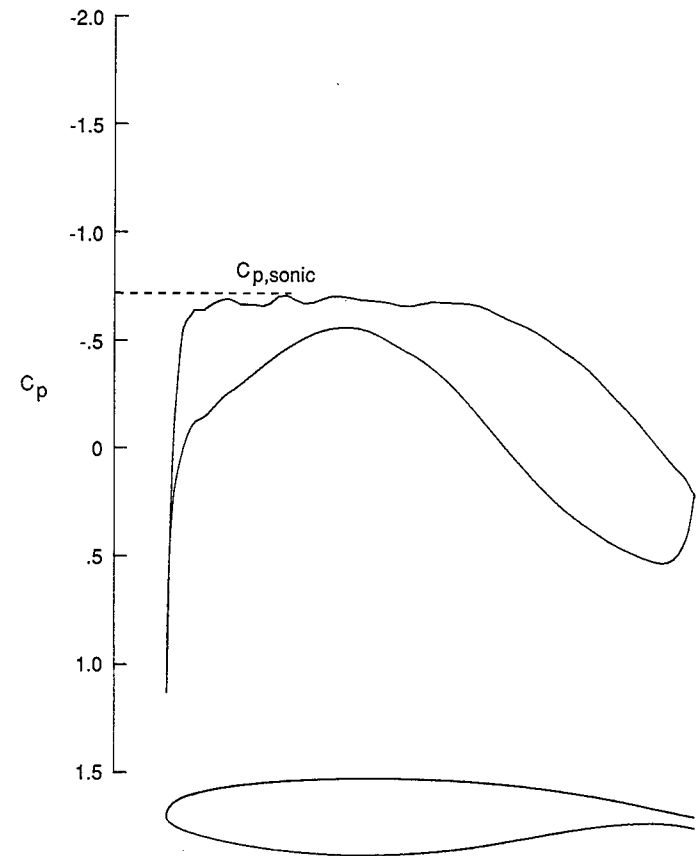Figure 35. Sketches of 14-percent-thick phase 2 and phase 3 supercritical airfoils.

(a) Phase 2; $\alpha = -0.06°$.

(b) Phase 3; $\alpha = 0.03°$.

Figure 36. Analytical design pressure distributions for 14-percent-thick phase 2 and phase 3 supercritical airfoils. $M = 0.730$; $c_l = 0.70$; $R_c = 30 \times 10^6$.

(a) Phase 2; $\alpha = -1.33°$.

(b) Phase 3; $\alpha = -1.26°$.

Figure 37. Analytical sonic-plateau pressure distributions for 14-percent-thick phase 2 and phase 3 supercritical airfoils. $M = 0.715$; $c_l = 0.42$; $R_c = 30 \times 10^6$.

NASA National Aeronautics and Space Administration	Report Documentation Page	
1. Report No. NASA TP-2969	2. Government Accession No.	3. Recipient's Catalog No.
4. Title and Subtitle NASA Supercritical Airfoils *A Matrix of Family-Related Airfoils*		5. Report Date March 1990
		6. Performing Organization Code
7. Author(s) Charles D. Harris		8. Performing Organization Report No. L-16625
9. Performing Organization Name and Address NASA Langley Research Center Hampton, VA 23665-5225		10. Work Unit No. 505-61-21-03
		11. Contract or Grant No.
12. Sponsoring Agency Name and Address National Aeronautics and Space Administration Washington, DC 20546-0001		13. Type of Report and Period Covered Technical Paper
		14. Sponsoring Agency Code

15. Supplementary Notes

16. Abstract

This report summarizes the NASA supercritical airfoil development program in a chronological fashion, discusses some of the airfoil design guidelines, and presents coordinates of a matrix of family-related supercritical airfoils with thicknesses from 2 to 18 percent and design lift coefficients from 0 to 1.0.

17. Key Words (Suggested by Authors(s)) Airfoil Supercritical aerodynamics Transonic aerodynamics	18. Distribution Statement Unclassified—Unlimited Subject Category 02	
19. Security Classif. (of this report) Unclassified	20. Security Classif. (of this page) Unclassified	21. No. of Pages 22. Price 72 A04